学位申請論文

新井場公徳

主論文

A study on the variation of displacement and internal earth pressure in creeping landslides

Thesis submitted to Graduate School of Science
in partial fulfillment of the requirements of the degree
Doctor of Science
in the Division of Earth and Planetary Sciences
Graduate School of Science
Kyoto University

Kiminori Araiba

January 1998

Contents

Abstract

Variations in displacement and internal earth pressure in two creeping landslides were investigated by means of direct observation and finite element method. Test sites were a landslide at Todoroki in Awaji Island, Hyogo Prefecture, and a landslide at Nishi-Ikawa, Tokushima Prefecture.

Characteristics of the Todoroki landslide were studied by means of extensometers, portable cone-penetration tests and ring-shear tests. The results of these studies revealed that landslide movement was of two types: block movement and compressive creeping. The compressive creeping was found to be caused by creeping of surficial soil and movement of a large block that was delineated by cracks. The creeping of this large block caused a non-uniform distribution of displacement along the slope. This non-uniform distribution was considered to have been caused by the shape of the slip surface(s). Propagation of the area of active movement was observed by an extensometer mounted on the large block. The strain that accumulated during movement was released by the propagation of the active area. This propagation was considered to have been caused by stress changes in the curved shear zone or in the contact area between two blocks where kinematic continuity was strong.

The internal horizontal earth pressure was measured *in-situ* in boreholes placed in the Nishi-Ikawa landslide. The horizontal components of earth pressure in the direction of slip and in the transverse direction were measured. Shear displacement and pore pressure were measured at the slip surface.

Variations in the effective horizontal earth pressure (calculated from the measured horizontal earth pressure and pore pressure) above the slip surface were noted. The characteristics of the effective horizontal earth pressure can be summarized as follows: The effective earth pressure at the initiation of movement increased in the middle part of the landslide and decreased in the lower part. Anisotropic variation, the difference between the variation of earth pressure in the direction of slip and that in the transverse direction, occurred during movement. The monitoring showed that, at the end of the

period of movement, the effective earth pressure in the direction of slip increased rapidly ("stopping phase") at most monitored locations. The anisotropic variation was released after the stopping phase. The difference in effective earth pressure before and after the movement was small.

These results are considered to be related to the difference in mechanism of formation of internal earth pressure from the moving condition to that in the static condition. The stopping phase is considered to represent a shift from the moving condition to the static one. According to measurements, this shift in earth pressure state was rapid compared to pore pressure dissipation and the deceleration of displacement measured.

FEM analysis for the onset of movement in the Nishi-Ikawa landslide was performed in order to examine the observed variation in the effective earth pressure. In this analysis, the slip surface was represented by a series of joint elements. The effects of ground water were represented by nodal forces. The results of the FEM analysis provided good agreement with the observed distribution of variations in effective earth pressure in the initial stages of movement. Whether the earth pressure at a certain position increased or decreased was considered to be determined mainly by the shape of slip surface (kinematic constraint) and distribution of pore pressure at the slip surface (stress condition).

1. Introduction

1.1. Creeping landslide

Landslides can be classified in many ways (Furuya, 1996). In this study, they are divided into two types: "creeping landslides" and "slope collapses" by means of displacement rate and amount of geometry changes of the moving mass. "Creeping landslides" are characterized by slow movement of the soil mass without large changes in geometry, and "slope collapses" move rapidly with marked geometric changes. A "creeping landslide" is often transformed into a "slope collapse"; thus, this classification is flexible.

In "creeping landslides", two deformation models are involved:

1) intermittent sliding of the soil mass on a continuous slip surface

2) deformation of the slope without a continuous slip surface

The difference is whether the shear strain concentrates along the slip surface (1), or it is distributed at depth (2). The slip surface is considered to be a significant heterogeneous element in the soil structure, and "creeping landslide" as used in this study involves both models. Hereafter, "the shear zone" is also referred to as "the slip surface"

1.2. Displacement and internal earth pressure in a creeping landslide

The failure process in soil structure is considered to be progressive: i.e., the stress along the entire slip surface (or potential slip surface) does not instantaneously reach the failure condition. In this thesis, this phenomenon is expressed as "enlargement of the failed area" in spite of the widespread use "progressive failure", which has many meanings (Chowdhury, 1978). During enlargement of the failed area, a non-uniform distribution of displacement is likely to occur and it may vary with time. In a study of the progressive failure caused by a deep excavation in Oxford Clay in the United Kingdom, Burland *et al.* (1977) monitored surface displacement by surveying, extensometers, and inclinometers. They explained the observed distribution of surface displacement and its changes with advance of the excavating face by as being caused shear-band propagation.

The enlargement of the failed area in slopes has been investigated for delayed collapse of slopes consisting of over-consolidated clays (e.g. Skempton, 1964). In such a collapse, the

strain-softening character of the clay and high horizontal earth pressures are considered to be important factors (Bjerumm, 1967, Potts *et al.*, 1997). In their research, the process of delayed collapse was illustrated as follows: 1) The initial stress condition in the slope is close to the failure condition because of high horizontal earth pressure. 2) Strain-softening (failure) in a local area changes the stress. 3) The changed stress induces failure in adjacent areas.

Recently, the mechanism of a creeping landslide prior to the collapse of a slope was investigated for the purpose of collapse-time prediction. Tsuchiya and Ohmura (1988) assumed that the rate of enlargement of the slip surface is a function of the size of the previously failed area. They succeeded in producing a so-called "creep curve" (variation in displacement with time before collapse) on this assumption. Kamai (1993) monitored underground displacement in the Yonaihata landslide, a landslide composed of Tertiary mudstone in Japan. He found enlargement of the slip surface prior to catastrophic collapse. He also reproduced this phenomenon using a ring-shear apparatus. These researchers interpreted the mechanism of creeping prior to a collapse of slope as an enlargement process of the slip surface.

In the case of a creeping landslide with a pre-existing slip surface, the enlargement is considered to occur along the slip surface. Suemine (1983) investigated landslides in crystalline schists in detail by monitoring surface displacement and shear displacement along the slip surface. He found that the onset time of displacement differed with positions in the landslide. The difference was considered to be due to the enlargement along the slip surface.

Thus, enlargement of the failed area in the soil mass is considered to be an important process in movement of creeping landslides. Previous research (Suemine, 1983, and Kamai, 1993) focused on distribution of displacement in a landslide. Chowdhury (1978) speculated on the importance of variations in the internal earth pressure during this enlargement. However, it has rarely been investigated in a real landslide.

1.3. Review of previous works on earth pressure

Since Coulomb first established his theory on earth pressure, there have been many studies of theoretical and practical aspects of earth pressures acting on retaining walls. Earth pressures acting on stabilization piles (Fukumoto, 1972) and water catchment wells (Yamagata Prefecture, 1993) have been investigated in relation to landslide prevention works. These researchers have focused on pressures acting on a rigid structure because their main interests have been

concentrated on design problems. The pressure inside a sliding soil mass, however, has received little attention. Fukuoka (1984) considered internal earth pressures as inter-slice forces whose determination is not clear now.

Measurements of internal earth pressures during soil movement have been performed in the laboratory (e.g., Fukuoka *et al.*, 1985) but, mainly because of technical difficulties, few attempts have been made to measure these pressures *in-situ*. Hada *et al.* (1988) used an especially designed transducer to measure the static internal earth pressure in the Takada landslide, a landslide in a geologic unit that contained serpentine. They concluded that the measured pressure was appreciably smaller than the value calculated by the slice method. Recently, researchers have come to the opinion that failure of a soil mass is progressive (e.g. Tanaka and Sakai, 1993), whereas the conventional theory of earth pressure is based on static equilibrium, which assumes that the failure condition is achieved at the same time within the entire sliding mass. The enlargement of the failed area may arrest the mobilization of the extreme earth pressures ("active" and "passive" earth pressures in the Rankine state) as discussed by Habib (1988).

These investigations evaluated the static earth pressure. To investigate the earth pressure during failure, it must be measured in a manner that will obtain time-variant data. Fukuzono (1993) conducted dynamic measurements of stresses in large-scale laboratory tests. He obtained interesting results, only some of which agree with results obtained by means of conventional theory. His results suggest the importance of direct measurement of dynamic internal earth pressure.

As yet, no attempt has been made to measure directly the variation in internal earth pressure in a real landslide. In this study, the horizontal internal earth pressure was monitored during the movement of a landslide.

1.4. Aim and major works for this study

Creeping landslides in natural slopes are not simple; many factors affect their initiation and movement. Though internal earth pressure and displacement within a landslide mass obviously are important factors, the understanding of them is limited, because it is not an easy task. The author aimed to achieve this understanding as much as possible by mobilizing all available sources. The major efforts in this study were as follows:

(1) Observation of displacement in landslides

In order to examine the distribution and variation of displacement in landslides, displacements were observed in two creeping landslides. Surface displacements on the Todoroki landslide in the Awaji-Island, Hyogo Prefecture, were measured by extensometers. Shear displacements along the slip surface of the Nishi-Ikawa landslide on Shikoku Island were measured using boreholes for the observations.

(2) Observation of internal horizontal earth pressures during landslide movement

Internal horizontal earth pressures that developed during landslide movement were monitored in the Nishi-Ikawa landslide at two-minute intervals in order to reveal the characteristics of these pressures. To obtain "internal" earth pressures, pressure transducers were installed in boreholes. Because of technical difficulties in the installation, these transducers were installed in two directions: the direction of slip and the transverse direction.

(3) FEM analysis of the variation of earth pressure at the onset of movement

In order to explain the distribution of variations in effective earth pressures observed in the Nishi-Ikawa landslide at the onset of movement, a FEM analysis was performed.

2. Test sites

2.1. The Todoroki landslide

2.1.1. General aspects

The Todoroki landslide is located on the west coast of Awaji Island (Fig. 1). The Nojima Fault appeared at the Hyogoken Nanbu Earthquake (January 17, 1995). The relative displacement of the Fault was about 1m in both horizontal and vertical planes. Large scale open-cracks (with about 0.7 m step, opening 0.1 - 0.2 m) were found in upper-hill a few weeks later than the Earthquake ("Crack" in Fig. 1). After the Earthquake, many cracks on the slope were found in shocked area (Hiramatsu *et al.*, 1996). Some of them developed to collapses of slopes few days after the Earthquake (e.g. Takeuchi *et al.*, 1996), which can be considered as a continual event from the formation of crack by the Earthquake. Enlargement, due to rainfall, of area of collapsed slopes having been induced by the Earthquake was reported by some researchers (Tomita *et al.*, 1996, Hirano and Ishii, 1997). Some of cracks which did not collapse soon after the Earthquake were suspected to develop to collapse by rainfall. To investigate the post-earthquake behavior of such cracks, a slope in Todoroki area was investigated. A part of slope lower than the cracks is expressed as "the Todoroki landslide" in this study.

A part of slope upper than the Fault consists of granodiorite and its ground surface is weathered to be residual soil. The surface material of a part of slope lower than the Fault is debris laying on the bedrock of sand stone (Kobe group). The thickness of debris is about 23 m at "BV" (borehole vertical) in Fig. 1. The surface of slope from the top of survey line to the Nojima Fault is plane and its average inclination is about 35° Slope lower than the Fault has been artificially changed and its average inclination is about 27° The lower end of survey line is 62 m high above the sea level and 200 m distant from the seashore. Land-use of slope upper than EX 5 is forest and that of lower slope is a fruit farm. No permanent spring exists in the forest.

2.1.2. Arrangement of monitoring equipment

Fig. 1 shows arrangement of extensometers ("EX"), portable penetration test points and sampling point of specimen for ring shear tests. EX 1 to EX 10 were set on April 27 and EX 11 to EX 14 were set on May 23, 1995. The arrangement of extensometers in this research was planed before cracks were found on the upper hill. It was designed to observe an open-crack at the Nojima Fault reported by residents. For this reason, ten extensometers were set first, then the survey line was extended to EX 13 after cracks on the upper slope were found, one extensometer was set in EX 14. Therefore, the main survey line did not locate in the center of cracks, unfortunately. In this research, the whole area delineated by cracks is considered as one block because such a large scaled series of cracks might be induced by deformation of deep soil. As will be discussed later, observed slope deformation is considered to be composed of movement of the large block delineated by cracks and local movement (such as, surficial soil creeping and small blocks).

Borehole for observation (34 m deep) was drilled at the position of "BV". Ground water table and pipe strains were measured using a polyvinyl chloride (PVC) pipe with drainage holes on the wall for the whole depth embedded in the borehole. Slight variation in ground water table was observed. Measurements by "insertion-type bending-pipe" (Shima and Takeuchi, 1973) were also done in the borehole (October 1995 and May 1996). According to measurement in pipe strains (sampled every month), 2000 ($\mu\varepsilon$) output of one strain gauge (attached at the depth of boundary of the debris and the sand stone) was recorded in August 1995. However, only one output is unreliable. According to the measurements by the insertion-type bending-pipe, significant bent of pipe was not observed (Fig. 2). Thus, the output of strain gauge is considered as an error. According to residents and ground surface survey, there is no symptom of landslide in the slope lower than the borehole. Therefore, the ground lower than the borehole was assumed to be stable. The part of slope between cracks and the borehole is discussed in this study.

2.1.3. Ground structure

A series of portable penetration tests was performed along the survey line on September 24 - 25, 1996, about 20 months after the Earthquake. The test results of points shown as solid

triangles in Fig. 1 are presented in Fig. 3. The number of blow for 10 cm penetration (Nc_{10}) is shown.

A test was ended by technical reasons when penetration depth by one blow of less than two mm ($Nc_{10} > 50$) was recorded for five blows, or the total depth reached to 3.5 m. Therefore, the results do not deny existence of another layer of $Nc_{10} < 50$ below the limit depth (as stated in later section, slip surface existed below the lower limit of surficial soil, which suggests another layer of low Nc_{10} below the limit).

Many researchers performed portable penetration tests in slopes composed of weathered granite. Many of them determined the upper limit of basement in the means of collapse of slope problem as depth of Nc_{10} reached to 30 (e.g. Ohsaka *et al.*, 1992). However, the threshold value was determined as 50 in this research, because that layer of $Nc_{10} < 30$ was found below the layer of $Nc_{10} > 30$ in many results in this study. Moreover, creeping slope movement is discussed in this research, while interests of former researchers were mainly focused on the collapse of slope. By these reasons, the layer of $Nc_{10} = 50$ is considered as the lower limit of weathered surficial soil. Distribution of the depth and Nc_{10} profiles (Nc_{10} depth curve) for each point are shown in Fig. 4. Nc_{10} does not reach to 50 for points lower than the Nojima Fault. For points on the upper slope, the layer of $Nc_{10} > 50$ was detected, especially, it appeared in the layer shallower than 1 m at both ends of EX 8. At P 8, Nc_{10} reached to 50 at 30 cm, which is omitted in Fig. 3 for the sake of clarity. Another test was done at a point with 3 m distant from P 9 and similar result was obtained Thus, these extremely shallow limits were not error which might have been caused by existence of large gravel.

Fig. 4 shows the result of portable penetration tests near EX 14. Difference in the elevation of ground surface at the crack was about 70 cm and difference in the depth of lower limit of surficial soil was about 80 cm. Therefore, step of the lower limit at the crack can be estimated as 1.5 m.

2.1.4. Soil properties

Ring shear tests (Sassa *et al.*, 1989) were performed on specimen taken from "sampling point" in Fig. 1. An amount of weathered soil of granodiorite was taken from surface of a small failure. The soil was disturbed, air-dried and sieved by 2 mm. Tests were performed

under constant normal stress, constant speed (3 cm / hr) and drained condition. Five tests were performed; three on air-dried normally consolidated (NC) specimen, one on saturated NC specimen and one on air-dried over consolidated (OC, over consolidation ratio = 3) specimen. Their results are summarized in Fig. 5. Peak stress conditions are plotted with solid marks and residual stress conditions are plotted with open marks. Peak strength parameters for air-dried NC specimen were obtained as c=3.9 kPa and ϕ=39° Residual ones were done as c=0 and ϕ=35° There is slight difference between the strengths of air-dried NC and saturated NC specimen. Also a slight difference is seen in NC and OC specimen in the peak strength, but difference in the residual strength is not marked. As a result, residual strength of the granodiorite is independent of water content and OCR (in the range of OCR $\leq$ 3).

Confining pressure is said to affect the strength of weathered soil of granite because of the effect of grain crushing (JSSMFE, 1982), but its effect was not obvious in ring shear tests in this research. A typical change in sample height and that in shear resistance with shear displacement are shown in Fig. 6. The sample height change can be explained as a shrinkage due to increment in the major principal stress, dilatancy towards void ratio mobilizing the peak resistance and shrinkage after the peak. The shrinkage after the peak is considered as a process of development of slip surface mobilizing residual resistance. Amount of displacement to form the slip surface is determined as about 10 cm by the end of sample height change and shear resistance. The amount of 10 cm is smaller than the relative displacement at the crack (1.5 m) found at EX 14. Therefore, the slip surface is likely to be developed at least in the slope near EX 14.

There is no information about degree of weathering in this slope. Boring and standard penetration tests were carried out in neighboring similar slope. Its result showed that the depth of weathered soil was 3 - 4 m and the depth of highly weathered rock (N < 30) was 8 - 12 m.

2.2. The Nishi-Ikawa landslide

2.2.1. General aspects

The Nishi-Ikawa landslide is located in the Sanbagawa metamorphic rocks region of the Shikoku Island, southwest Japan (Fig. 7). The landslide is close to the Median Tectonic Line (MTL), one of the major active fault systems in Japan. Fig. 7 shows the geological map of the

area around the landslide (after Mizuno *et al.*, 1993). In the figure, "landslide scarp" and "landslide deposit" were identified morphologically. The location of Nishi-Ikawa landslide observed in this study is added by the author. An old landslide scarp surrounds the new active Nishi-Ikawa landslide. The crown of the scarp has been partially dissected. The Nishi-Ikawa landslide is taking place in the deposit of the old landslide. There was no sign of landslide activity before November 1973 when an artificial cutting at the toe made active the landslide. Since then, sliding has occurred repeatedly at times of heavy rainfall. The landslide is about 100 m wide and 170 m long. A counterweight fill work using concrete frames and rocks was constructed at the toe (Fig. 8) in November 1974. It succeeded in reducing the landslide activity. The recent average rate of displacement is a few centimeters per year. The average annual precipitation in this region is 1401 mm. Most landslide events occur in the rainy season and the typhoon season.

Suemine (1983) observed the landslide in detail. He maintained the slide to be a progressive failure and estimated the propagation speed along the slip surface to be of the order of 10 (m / hr). Fig. 8 shows the topography and arrangement of the observation equipment. The main head scarp of this active landslide has been confirmed to be at EX 1. Slope upper than EX 1 and that lower than EX 16 are considered to be stable because no symptom of landslide activity has been seen. Thus the main landslide block is considered to be extended from EX 1 to EX 16.

Land-use of the slope upper than EX 1 is forest. The slope lower than it is covered by trees and bushes. No permanent spring exists in the slope but signs of surface water flow can be seen after rainfall in some positions.

2.2.2. Ground structure

Fig. 9 shows results of visual inspection of drilled cores and standard penetration tests. The ground is composed of highly weathered material including fragments of weathered argillaceous schist, green schist and often hard quartz vein. Because this landslide is located in the deposit of ancient landslide, geological structure is not clear. The bed strikes are N74°E to N95°E with the dips of 20°N to 30°N in the areas around this landslide (Suemine, 1983).

The P-wave velocity structure in this landslide was determined by Maeda and Shima (1982) who used a seismic refraction method; the surface layer of Vp = 370 - 450 (m / s) is from 2 - 10

m deep, the second layer of Vp = 1200 - 1500 (m / s) from 20 - 25 m deep and the basement of 3200 (m / s) below that. Fig. 10 shows two cross sections along the survey lines in November 1995. The depth of slip surface at each borehole (Table 1, Fig. 9 and 10), except BV 12, was identified by strain gauges attached on pipes embedded in the landslide area (as stated later) and checked by measurements made on an insertion-type bending-pipe. The depth had been confirmed by long-term investigations (e.g. Shima *et al.*, 1975, Suemine, 1983) and no other slip surface had been found.

2.2.3. Arrangement of monitoring equipment

Two survey lines were constructed as shown in Fig. 8 (BV 12 to BV 9 and BV 4 to BV 6). "BV" indicates position of boreholes (vertical) for observation. Unfortunately, the survey lines are limited from the toe to the middle part of landslide. No information is available for the slope between BV 12 and EX 1. A conventional pen type extensometer was used for EX 1 whose resolutions both in time and in variation of the distance are not sufficient. Obtained data for it were not used in this study.

Internal earth pressures, pore pressures at the slip surface, and pipe strains were measured using these boreholes. The observation equipment used in this study was installed in June 1994 for BV 7 to BV 9 and in June 1995 for BV 4 to BV 6. BV 12 was drilled in May 1997 without earth pressure transducers. The three movement events were observed since the first installation of earth pressure transducers in BV 7 to BV 9. They were designated as Events 1, 2, and 3 in terms of the amount of displacement of sliding mass measured in BV 7. Fig. 11 shows the results of strain measurement (stated later) in BV 7 at depths just above and below the slip surface for the three events. The time origin is the moment of onset of data acquisition for each event. Events 2 and 3 occurred before the installations of BV 4 to BV 6 and Event 1 occurred about one month after their installations. All the events occurred between May and July 1995, almost one year after the installations of BV 7 to BV 9.

3. Methodology

3.1. Observation equipment

3.1.1. Monitoring of displacement on the ground surface by extensometers

The extensometer is well-used equipment in investigation of landslides because it can be easily set and therefore, it is of benefit to observe wide area (e.g. Sassa, 1984). Especially, when some extensometers are set continuously and one end of survey line is fixed to a stable ground, they can provide distribution of deformation of slope projected to the survey line. Extensometer measures one dimensional strain of the ground, though direction of displacement vector is not always parallel to it. Therefore, quantitative analysis of the result is difficult. It is used in the Todoroki landslide in order to clarify the area of deformation on slope and to investigate its time dependent characteristics.

Schematic structure of an extensometer is shown in Fig. 12. A log pile with diameter of about 20 cm was embedded in a hole with depth of about 1 m. A transducer (model 4701 (Oyo-Chishitsu Co.)) which measures variation of distance between one pile and the upper pile using super-invar-wire was set on it. One end of the wire was connected to the transducer and another end was fixed to the next pile. One extensometer was composed of "two piles, wire stretched between them and the transducer set on one of them" As shown in the figure, one pile was shared by two extensometers. Therefore, there was no gap of wire from the bottom to the top of survey line. The sampling interval of extensometers was 15 minutes in summer and 30 minutes in winter in the Todoroki landslide, while in the Nishi-Ikawa landslide it was 30 min. The positive value in the data indicates extension.

3.1.2. Monitoring of internal horizontal earth pressure

Monitoring of earth pressure is very difficult because many factors are considered to affect it (Hariu, 1984). Brackley and Sanders (1992) made *in-situ* measurements of the horizontal internal earth pressure in a flat land composed of expansive clay. They made *in-situ* tests to check the validity of their measurements and obtained acceptable results. Their works showed that it is possible to measure the *in-situ* earth pressure accurately when there is careful

instrumentation and favorable field conditions (flatness, fine material, uniform geology). Purpose of measurement in this study was to observe the earth pressure at various depths and in many boreholes to determine the earth pressure both at one point and its distribution within an actual landslide. Therefore, it was impossible to have careful instrumentation like that of Brackley and Sanders.

Fig. 13 shows the scheme for an observation borehole. Earth pressure transducers and strain gauges (not shown in the figure) were attached to the outer surface of a PVC pipe (outer diameter of 48 mm and wall thickness of 3.6 mm) embedded in the borehole (diameter 142 mm). After insertion, the clearance between the pipe and the original soil was carefully filled with sand to obtain uniform back-filling. In the installation procedure described, there are three questionable factors: 1) the soil in contact with the surface of transducer is sand, 2) the transducer is attached to the PVC pipe which can be strained by changes in stress in the surrounding soil, and 3) the stress field can have been disturbed by the boring and back-filling.

Factor 1 may cause stress concentration and eccentric loading on a transducer. Such effects can be reduced by using fine sand in the back-filling and the choice of a well-designed transducer.

The effect of Factor 2 was tested by changing the pressure inside the pipe. When the water pressure inside the pipe was increased by poring in water from 0 to 78.4 (kPa), the outputs of earth pressure transducers did not change. Strain on the pipe caused by changes in the inner stress in this range is not so large to disturb the measurement of earth pressure. This is not direct evidence that the effect of Factor 2 can be ignored when the pipe is strained by changes in the outside stress, but it favors the assumption.

Another problem is whether the pipe at the depth of transducer is strained by shear displacement along the slip surface. This effect is considered very small. Nakamura and Itagaki (1976) investigated the behavior of a PVC pipe in landslide. According to their results, bending strain and moment which may disturb the "natural" stress field in ground around the pipe is negligible at the depth 1 m distant from the slip surface. Their result is considered to be valid in the Nishi-Ikawa landslide. Fig. 14 shows the difference of maximum and minimum values in outputs of all strain gauges during Event 1 plotted against the distance from the slip surface. Clearly, strain along a pipe attenuates rapidly with the distance, becoming negligible at the distance of 0.8 m in this landslide. Because earth pressure transducers are attached at

least 1.2 m distant from the slip surface, assumption that the earth pressure measurement is not disturbed by the bend of pipe is considered to be acceptable.

Factor 3 indicates a fundamental problem in measuring the "natural" internal earth pressure. This problem can not be solved without using "remote sensing", for which there is no such technology at present. The author tried to reduce this effect by having the installation in boreholes instead of in excavated pits.

The structure of earth pressure transducer used in this work (BE-5KRS4 (Kyowa-Dengyo Co.)) is shown in Fig. 15. This transducer was chosen because its output is not much disturbed by eccentric loading on the first diaphragm, it has high water resistance with good linearity, and its suitable size for installation in a borehole; all qualities necessary to the measurement of internal earth pressure at many depths and points. On the other hand, the diameter dimension and the aspect ratio (height / diameter) were sacrificed. A large diameter and small aspect ratio are considered preferable for accuracy. However, it is difficult to fulfill both these properties as well as the conditions given above.

Earth pressure transducers were installed in six boreholes (BV 4 to BV 9 in Fig. 8). Table 1 shows the installation depths of earth pressure transducers. Two transducers were attached at each depth; one facing in the direction of the maximum slope gradient ("UD"), the other perpendicular to the first transducer ("RL"). A positive value indicates compression. Their outputs were sampled digitally at two-minute intervals. The zero balances of earth pressure transducers might drift during installation, but there was no way to calibrate them after installation. Therefore, variation in output of each transducer on the basis of initial value of the data-acquisition period will be discussed.

3.1.3. Monitoring of shear displacement and pore pressure at the slip surface

Pairs of strain gauges are bonded to the surface of the PVC pipe at various depths in order to observe the distribution of bending strain. At each depth, there are two gauges; one on the up-slope side, the other on the down-slope side, to compensate for the effect of variations in temperature (two-gauge method). The distance between the neighboring pairs is 0.33 m at the depth of slip surface in order to observe the strain distribution near the surface in detail, and the distance is 1 m at depths distant from the slip surface. Results of a calibration test on the strain measurement made in the laboratory are shown in Fig. 16. A pipe with a pair of strain gauges

was bent, and its output (X) plotted against the curvature (R) of pipe. The unit of X is expressed as ($\mu\varepsilon$). It means 10^{-6} strain. The relative displacement (Y (m)) of two ends of pipe obtained geometrically is

$Y = l^2 / R$

where l is the length of pipe and l / R is assumed to be sufficiently small.

The relationship between the outputs of strain gauge and the relative displacement is shown in Fig. 17 for l = 0.33 m. This l value is the same as that for the system used in the field. This relationship is obtained on an assumption that pipe strain is uniform (the radius of curvature is constant) for 0.33 m long. Though the assumption may not be valid near the slip surface in a real landslide, it can be used as an approximation. Both positive (for a strain gauge above the slip surface) and negative (for one below it) strains are seen in the measurement (Fig. 11). Displacement shown in the right axis of Fig. 11 was calculated using the relationship shown in Fig. 17. Shear displacement along the slip surface used in Figs. 41 and 43 was obtained using the relationship with X as sum of absolute values of strains measured at two depths; just above and below the slip surface.

Movement of a landslide is generally controlled by pore pressure acting on the slip surface. Therefore, it must be monitored when the mechanism of landslide is investigated. In order to avoid the effect of pore water in other depths, two bentonite layers (Fig. 13) were placed (0.5 m above and below the slip surface). Low permeability of bentonite is considered to prevent the transmission of pore pressure. There are drainage holes on the PVC pipe at the depth of slip surface through which pore water flows into or out of the pipe. The pressure is balanced by the head height of water inside the pipe. Pore water pressure at the slip surface can thus be measured by a hydro-pressure transducer (model 4597 (Oyo-Chishitsu Co.)) placed inside the pipe. The absolute value of this transducer is reliable because it is calibrated every few months.

Outputs of strain gauges were digitally sampled at two-minute intervals. Data from the pore pressure transducers were recorded by multi-scanning pen-recorders (chart speed = 25 (mm / hr)) in the field, then, digitized manually at thirty-minute intervals in the laboratory.

3.2. Examination of distribution of internal earth pressure at the onset of movement in the Nishi-Ikawa landslide by FEM analysis

3.2.1. General aspects

FEM analysis has been well used in geotechnical problems. In the case of "long-term" condition of landslides (e.g. Potts, 1997), slope was modeled by elasto-plastic or visco-elasto-plastic elements. When the slip surface does not exist in the slope, this model is adequate. Because the slip surface causes strong anisotropy, it must be represented when creeping landslide with pre-existed or developing slip surface is analyzed (Morsy *et al.*, 1994). To represent the slip surface, it is necessary to use especially designed model (e.g. Desai, 1995). However, simple model is preferable for applying the model to real landslides because amount of underground information is generally limited. Suemine (1984) represented the slip surface by a series of joint elements which was developed in rock mechanics (Goodman, 1976). He succeeded in getting acceptable results. In this study also, slip surface was represented by a series of joint elements for analysis. Joint element is formed by two surfaces with four nodes (each surface has two nodes at both ends). Relative movements of these surfaces are classified into parallel slip, separation (or closing) and rotation. This model is considered to be acceptable for representing behavior of real slip surface. As stated later, joint element used in this study has elastic constitution in the slip. This is a simple model, where plastic behavior of real slip surface can not be represented. The behavior of slip surface in real landslides is not well known. Uncertainty in material model and parameters is a fundamental problem in analysis concerning underground phenomena. Complicated model with many parameters could represent precise behavior of ground, however the uncertainty might be major problem in such model. In this study, the simple model was used to reproduce qualitative behavior of internal earth pressure.

3.2.2. Calculation procedure

Static 2-D FEM simulation under plane strain condition was performed using cross section shown in Fig. 18. Though the line curved in the middle part, structure of ground was simplified in a 2-D model. Depths of slip surface at BV 7 to BV 9 in the figure had been

confirmed by long-term observation. The depth at BV 12 was assumed by inspection of bored core, because BV 12 had been constructed recently and the depth had not yet been confirmed by means of measurement. Structure of model is shown in Fig. 19. The upper and lower ends were extended in order to avoid disturbing behavior of the landslide. The lower and bottom ends were fixed and the upper end was left free. Both shapes of slip surface and ground water table were assumed for the slope upper than BV 12. Results of slope between BV 9 and BV 12 will be discussed.

In the analysis, buoyant and seepage forces due to ground water were represented as external nodal force. Simulation was performed as follows;

1) Applying gravity force using wet total unit weight

2) Applying nodal forces representing buoyant and seepage forces induced by initial ground water table

3) Applying nodal forces representing buoyant and seepage forces induced by ground water table at 15 hours by six steps with constant increment

Here, 15 hours was considered as limit of static analysis. It will be stated with residual forces. Variations in shear displacement along the slip surface (joint elements) and internal stress during 3) are discussed in this thesis.

3.2.3. Parameters

Parameters for isoparametric elements

Except for the slip surface, four-noded 2-D isoparametric elements were used. The constitutive law was elasto-plastic, but yielding condition (Table 2) was not achieved. Therefore, all elements remained in elastic domain. Vermeer (1990) analyzed the biaxial test as a slip of elastic mass on a slip surface. The motion of elastic sliding mass on the slip surface was also reproduced in this analysis. Assumed ground structure is shown in Fig. 20 and table 2.

Elastic constants were assumed by boring data in Fig. 9 and seismic survey (Maeda and Shima, 1982). Young's modulus (E) for sliding mass is obtained using standard penetration tests performed in BV 8. The soil divided in three layers as $N < 10$, $= 20$ and > 50. Empirical relationship of $E = 28\ N$ was used (material 1, 2 and 3). Shear stiffness is calculated from E assuming Poisson's ratio as 0.35 to 0.4. The result of seismic survey shows that P wave

velocity of second layer is three times of shallow soil. E of basement (material 5) was determined 10 times (about 3^2) as large as shallow soil (material 3 was chosen as representative). An intermediate layer (material 4) was inserted between the basement and material 3.

Parameters for joint elements

Table 3 shows material property of joint element. The elastic constants (normal and shear stiffness) of joint elements were determined as the same one with material 2. The material 2 (not 3) was chosen in order to illustrate ductile zone around slip surface which is often observed in creeping landslides. Normal stiffness of joint element in rock mechanics is determined by distance of two surfaces which are forming the element to illustrate the change of contact area. However, the normal stiffness is considered to be constant in this study, because the contact area is likely to be almost constant in the case of slip surface in soil. No drop in shear strength after yielding was considered. Such joint element behaves as bi-linear elastic material with stiffness of second spring is zero (because of this reason, the term "yield" is used in this FEM analysis in spit of "failure"). Therefore, there is no hysteresis in shear stress-strain relationship as shown in Fig. 21, in other words, no plastic displacement was reproduced. Shear behavior of real slip surface in soil is likely to have hysteresis which is not represented by this analysis. The omit of hysteresis did not affect the result of this study, because the shear displacement at all joint elements increased monotonously (shear displacement occurred only in the direction of "loading" in the figure). No shear-induced-dilatancy was considered.

Strengths of joint elements were assumed by trial-and-error to make initial safety factor to be about 1.1. First, average inclination from the top to the toe of landslide (17°) was assumed but the lower half of landslide can not be safe for initial ground water table. Then, strength of lower half was increased (material 2) and that of upper half was left 17° (material 1). Inclination of two upper most joint elements was large (thought its assumption is not reliable). Their strength was also increased (material 3) in order to avoid unrealistically large deformation there. Though this assumption was for convenience's sake, it did not much affect the result of BV 9 to BV 12. The residual strength of residual clay of argillaceous schist was determined as 12° to 21° by Yatabe *et al.* (1991). Assumed values were in the range of it. The width of joint element was determined as 0.4 m.

FEM mesh and external force

Fig. 22 shows ground water table in Event 1 which was used for the analysis. Permeability of sliding soil mass was considered to be high and ground water table shown in the figure was calculated from pore pressure at the slip surface measured in BV 7 to BV 9. For BV 12, where measurement was not done at the time of Event 1, the water table was assumed. Fig. 23 shows responses of ground water table to precipitation observed recently. It shows that initial table for BV 7 and BV 12 were almost the same and rising of the table in BV 12 was faster and larger than that in BV 7. The table for BV 12 was determined as; 7.1 m for initial (the same value in BV 7 in Fig. 22) and 3.2m for 15 hours (the highest value in Fig. 23). Soil below the slip surface was considered impermeable. The variation of shape of the table is shown in Fig. 18. This shape can not be explained in this cross section (2-D) and plural source of ground water may exist in 3-D for this landslide. Buoyant and seepage forces were represented by nodal forces. That is;

buoyant force is $\gamma_w \times$ volume in the vertical direction,

seepage force is $(\gamma_w \times \sin \alpha) \times$ volume in the direction parallel to the stream line,

sum of them is $(\gamma_w \times \cos \alpha) \times$ volume in the direction perpendicular to the stream line,

where γ_w denotes unit weight of water and α is the inclination of the stream line.

In this thesis, stream lines were assumed to be parallel to the ground water table inside the sliding mass (isoparametric elements) and to be parallel to the slip surface at the slip surface (joint elements).

3.2.4. Preliminary analysis

A preliminary analysis was performed before the analysis of real landslide.

To simulate bi-axial compression test of soil, structure shown in Fig. 24 was stressed as follows:

1) Applying isotropic pressure (σ_1 and σ_2)

2) σ_1 was increased to make stresses at joints to be near to yielding condition

3) Applying nodal forces to decrease normal stress on joints (representing decrement in effective stress by pore pressure)

Local safety factors (ratio of shear stress acting on each joint and yielding strength) for three joint elements are shown in the figure. Load step 0 indicates the end of 2) (anisotropic stress

condition of σ_1 and σ_2). Pore pressure was applied by eight steps with constant increment. Joint No. 4 was central one and was suffered high pore pressure. Therefore, decreasing rate in local safety factor was larger than those of other joints before it reached to 1 (the joint was yielded). Joint No. 3 was next of No. 4 and decreasing rate in local safety factor increased at the step 3 when joint No. 4 yielded. Similarly, Joint No. 3 yielded at step 5 and decreasing rate of local safety factor of No. 2 increased at that step. Once one joint element yielded, yielding of the neighboring one was promoted because shear stress exceeding the yielding strength was transmitted through post-yielding displacement. In this test, enlargement of yielding area by pore pressure and re-distribution of shear stress was reproduced.

Shear displacement along the slip surface in real creeping landslides does not always occur at once for the whole slip surface and enlargement of the failed area was observed as stated before. In this analysis, such phenomena can be reproduced as increment of number of yielded joints with load step (increase of pore pressure). This analysis was static, therefore, time dependent phenomena were ignored. The joint element was elastic material and static stable stress-strain field was analyzed. It may be achieved as a result of plastic slip at the slip surface in a real landslide. Its time dependence (delay of displacement) was not reproduced in this analysis.

4. Result of observation of slope deformation in the Todoroki landslide

4.1. Data obtained

Fig. 25 shows the result of measurement on extensometers from April 28, 1995 to December 11, 1996 together with daily precipitation. Periods of data-missing, which differed with extensometers, were caused by break of super-invar-wire, cut of electric line by animals, error of recorder, *etc.*. Variation during a missing period caused by break of super-invar-wire was assumed to be zero because there is no way to estimate it. Variation during a missing period caused by other reasons can be estimated because absolute value of output of the transducer was continuous before and after the period. Marked variations are seen at early period of observation. It is probably partially because of large precipitation then and partially because of effect of damage by the Earthquake. Fig. 26 shows distribution of the final value of each extensometer in the cross section along the survey line. Length of data acquisition period is different in different extensometer because of data-missing periods, as mentioned above. The distribution of extension and compression is in disorder, which is likely to be the result of complex soil movement. Marked extensive values are seen in EX 6, EX 9 and EX 13, suggesting that upper boundaries of blocks of moving soil located around these extensometers. Amount of compression is larger than that of extension throughout the survey line. Large compression is seen even in upper slope (EX 11 to EX 12) and amount of extension in EX 13 is small compared to that of compression in lower extensometers. It indicates that slope upper than EX 13 was also moving. These results can not be explained by a simple landslide model. It is likely that deformation observed was caused by different types of soil movement.

4.2. Relationship between precipitation and slope deformation

Relationship between precipitation and variations in records of extensometers is discussed in this section in order to separate different types of soil movement. Data obtained from EX 6, which was less noisy throughout the observation period, shows characteristic relationship with pattern of rainfall. Fig. 27 shows data obtained for EX 6 in three distinct periods (length = 10 days) with hourly precipitation. Time origin in each figure is 0:00 of the date written in it.

"Short but intense" rainfall was observed both in Period (A) and (B). Precipitation of 140 mm in three days had been observed two weeks prior to (A), while no precipitation had been observed for about two months previous to (B). Step-type variation towards extension appeared about one day after intense rainfall in (A) and lasted for about 3 days. On the other hand, only rapid compressive variation at the moment of rainfall is seen in (B). "Gentle but long" rainfall was observed in Period (C). Step-type extensive variation appeared about one day after the initiation of rainfall.

Thus, extensive variation in the record of EX 6 is considered to correlate to long-term condition of ground water and began about one day after the rainfall. On the other hand, compressive variation took place in short-term one. The compressive variation has been seldom observed in EX 6, but it has been frequently observed in other extensometers, especially in the upper part of survey line. Compressive creeping in upper slope has two characteristics. One is that the variation appears soon after the rainfall as seen in EX 6 in the figure Another is that it lasted for long after rainfall stopped which is not seen in EX 6. These characteristics will be shown later.

4.3. Separation of two types of movement and their characteristics

An attempt to separate two types of soil movement was done in this section. Data used for this analysis was obtained May 11 - 20, 1995, when the largest variations were observed. EX 1 to EX 10 were working during this period. Fig. 28 shows variations in records of extensometers. Time origin is May 11 0:00. Step-type extensive variations began about one day after the initiation of rainfall in EX 6 and EX 9. On the other hand, compressive variations began soon after the rainfall began and lasted for long after the end of rainfall.

By summing output of each extensometer at each sampling time from EX 1 to EX 10, variation of distance from the lower end to each log pile along the survey line can be obtained. The lower end of survey line is assumed stable. Though relative displacement (in 3-D) of each pile to the lower end is not always parallel to the direction of survey line, it is assumed to be parallel as an approximation. The result is shown in Fig. 29. Log piles are numbered from the lower end as Pile 0 to the top end as Pile 10. Pile 0 is origin. Negative variation indicates shortening of the distance from the lower end to each pile (the pile goes downwards). The permanent change in the distance from the lower end to the upper end is about 8 mm. The

amount of permanent change of each pile does not increase monotonously with number of pile. It suggests that several blocks of soil movement existed. To illustrate the individual movement of blocks, change in the distance of each pile at 1.5 days (the end of intense rainfall) and that at 10 days are plotted against the distance (the upper diagram in Fig. 30). Two figures in the lower part of figure show definitions of "Block" movement and "Compressive creeping" in the upper diagram. At the top of Fig. 31, schematic model of soil block movement and its result in the variation in the distance are shown. Relative movement appears on the surface at the upper and the lower tips of block if soil moves as one body ("Block movement"). "Compressive creeping" can not be explained by this simple model.

Moving block is clearly seen in the range of Pile 3 to 6 in Fig. 30, especially in 10 days. It indicates that block movement was activated after 1.5 days. The curve upper than Pile 6 can be explained by superimposing a block in the range of Pile 6 to 9 and compressive creeping upper than Pile 6. Also block movement was activated after 1.5 days here.

4.4. Strain on the ground surface induced by compressive creeping

Compressive creeping, which is not explained by movement of simple soil block, indicates that large part of slope is compressed in the direction of survey line. An extensometer measures relative displacement of two piles in the direction of survey line. However, it is not always parallel to the direction of displacement. In the lower part of Fig. 31, two models explaining the compressive creeping are shown. The upper one explains the creeping by difference in the direction of displacement vector at each point. The lower model explains the creeping by difference in the length of displacement vector (this model is not realistic in the case of usual soil. This is valid in special case in which large change in volume is permitted (surficial soil creeping, underground erosion (Sassa, 1984), *etc.*). Therefore, the upper model is considered to be adequate for compressive creeping caused by movement of the large block delineated by cracks. In this model, the strain on the ground surface is considered to be induced by a non-uniform distribution of displacement in the soil mass.

Compressive creeping was active in the upper part of survey line. Fig. 32 shows data obtained from June 30 to July 12, 1995 when data from EX 11 to EX 14 were available. Time origin is June 30 0:00. Precipitation of 6.5 mm was observed 12 days earlier. Data for EX 4 was missed because of a break of super-invar-wire. Marked compressive variations are seen

in EX 10 and EX 12. These variations have good correlation with intensity of rainfall; acceleration and deceleration correspond to amount of hourly precipitation during rainfall, but variations lasted for long period even after rainfall stopped. End of compressive creeping is not so obvious as block movement (EX 6 and EX 9 are also shown). Neglecting slight variation seen in about 1 day, variation in the record of EX 11 began about 4 days towards compression and then changed its tendency towards extension at about 7 days. Before the change, variation in the record of EX 12 was larger than EX 10 and vice versa after it. These results indicate that active movement area propagated downwards. After 11 days, EX 11 did not show variation, which is likely to be a result of parallel movement of piles of two ends. Propagation of the area of active movement is discussed in section 7.1.

EX 13 did not show clear tendency in this period (also throughout the whole observation period (Fig. 25)). It is impossible to discuss about the upper limit of compressive creeping by this result. Variation in the record of EX 14, which is considered to represent displacement of the large block delineated by cracks, began at about 4 days. It is almost the same as that in EX 11 but delayed to those in EX 10 and EX 12 (3.3 days). In the results of portable penetration tests in Fig. 3, a thin layer with low Nc_{10} is seen just above the layer of $Nc_{10} > 50$ for P 11 to 13. The existence of weak layer indicates surficial soil creeping and fast onset of variations in records of EX 10 and EX 12 might be due to it. Variations in records of extensometers on the upper slope were likely to be caused by both the surficial soil creeping and movement of the large block. Though the surficial soil creeping can disturb data for the movement of large block, the disturbance is likely to be small after 4 days, because the surficial soil creeping converged fast (it started 3.3 days and almost converged at 4 days) and amount of variation in the record of EX 14 was large after 4 days. Fast onset of compressive creeping might be due to surficial soil creeping and its long duration might be due to the movement of large block.

Thus, strain on the ground surface induced by compressive creeping during this activity (Fig. 32) can be summarized as follows.

1) Surficial soil creeping inducing some amount of one dimensional compression, especially in early stage.

2) Movement of the large block inducing large amount of strain in EX 12 and EX 10.

3) Strain accumulated in EX 11 during initial stage (4 to 7 days) of movement inducing stress changes, resulting in propagation of the area of active movement.

4.5. Depth of deformation

Two blocks, found by observation of extensometers, are expressed by solid line in Fig. 33 (EX 7 to EX 9 and EX 4 to EX 6). The lower limit of surficial soil is very shallow in EX 7 to EX 9 (Fig. 3). The slip surface of this block (EX 7 to EX 9) is considered to exist deeper than the lower limit. This slip surface may be controlled by joints, because strength of intact rock (even weathered rock) is very high compared to strength of joint. The lower block (EX 4 to EX 6) crosses the Fault. As shown in P 05 and 06 in Fig. 3, surface layer is thick near the Fault. The marked turbulence in Nc_{10} profile, whose existence is expected because block movement of EX 4 to EX 6 is active, is not seen in P 06. The slip surface is considered to exist lower than the surficial soil because the step-type characteristic of movement is the same as the upper block. However, the possibility can not be fully denied that the slip surface exists in the surficial soil but the turbulence can not be seen because the layer is soft.

The slip surface of large block delineated by cracks is considered to exist deep soil because of the scale of cracks and the result shown in Fig. 4. It is not clear whether continual slip surface existed from cracks to the lower end of the block or not. The lower end was not detected clearly by extensometers because of compressive creeping but it is likely to exist in the span of EX 10 because of large compression in its records.

The author considers that shear strain is localized in a (some) zone(s) with a certain depth because of the existence of part of slip surface (continued from cracks) and large observed deformation. The zone(s) can be expressed as "shear zone(s)" The differences of characteristics between compressive creeping due to the large block movement and step-type movement of two small blocks are mainly due to the size of moving mass and shape of slip surface (or shear zones).

5. Result of *in-situ* monitoring of internal horizontal earth pressure in the Nishi-Ikawa landslide

5.1. Data obtained

Internal horizontal earth pressures measured in BV 4 during Event 1 are shown in Fig. 34 as an example of recorded earth pressure data (data for other boreholes are shown in Appendix 1). These pressures were calculated using the initial imbalance of each transducer. The initial imbalance was measured in the laboratory before field-installation. As stated, the zero balance of an earth pressure transducer may drift during installation. There is a marked difference between the values measured for 13.25 m UD and RL, but their variations are very similar. This difference is considered to have been caused by the drift of zero balance of one (or both) transducer(s) occurred during installation. Hereafter, variation of earth pressure from initial value of this period is discussed.

Values measured at the depth of 18.25 m (both directions) are very low and their variations are small. If this measurement was correct, two possible causes can be considered; one is that "earth pressure coefficient" (horizontal earth pressure / vertical one) is small at the depth, and the other is the absence of ground water (absence of isotropic pressure). However, an error of measurement caused by arching effect is also possible in deep and stiff ground.

In order to discuss about deformation of soil, "effective stress" concept must be employed. Fig. 35 shows the pore water pressure at the slip surface measured in BV 4 to BV 9 during Event 1. The pore water pressure at the depth of each earth pressure transducer was calculated from this result with an assumption that ground water is present as free water. The assumption is made because the sliding soil mass is composed mainly of loose sandy material, which is considered permeable. Fig. 36 shows the calculated highest and lowest table of ground water during Event 1. Ponds were seen around BV 5 after Event 1 and the highest table is almost same with the ground surface there. Though "perfectly permeable" can not exist in nature, the assumption is acceptable as an approximation. It is possible to obtain the effective earth pressure by subtracting the calculated pore pressure from the measured earth pressure:

$EP_{efc} = EP_{obs} - (PP_{obs} - dH \times 9.8)$ (for the case that $(PP_{obs} - dH \times 9.8)$ is positive)

$EP_{efc} = EP_{obs}$ (for the case that $(PP_{obs} - dH \times 9.8)$ is negative)

where EP_{efc}; effective earth pressure (kPa), EP_{obs}; measured earth pressure (kPa), PP_{obs}; pore pressure measured at slip surface (kPa), dH; difference of depth of earth pressure transducer and that of slip surface (m).

Fig. 37 shows variations in calculated effective earth pressure and measured pore pressure at the slip surface in BV 4 during Event 1 (for other boreholes, see Appendix 2). There is marked variation in 3.25 m RL compared to UD direction. Small variations are generally observed for transducers at shallow depths but this transducer (3.25m RL in BV 4) is an exception, which reason is not clear. Rapid increment in pressures is seen in 8.25 m, while its decrement is seen in 13.25 m. Calculated effective earth pressures for 18.25 m behave almost reversely to the pore pressure at slip surface because measured earth pressures have slight variations as shown in Fig. 34. The assumption of free water is likely to be inadequate for soil blow the slip surface. It is often observed that head height of ground water in the sliding soil mass and that in soil below the slip surface are different. The author considers that the effective earth pressures obtained for 18.25 m are not correct.

To discuss variation in the internal horizontal earth pressures of sliding soil mass, outputs of the earth pressure transducers installed at the nearest depth above the slip surface in each borehole (underlined transducers in Table 1) are used in this study. Hereafter, their depths are not mentioned.

5.2. Comparison of monitored earth pressures in boreholes at various points

Fig. 38 shows variations in the effective earth pressure in the UD direction during Event 1. As an index of displacement of sliding soil mass, the pipe strain at the slip surface in BV 7 is shown at the bottom. In BV 4 and BV 7, there is a rapid increment in the pressure at first, then a gradual decrement was observed while the soil mass was moving and another increment appeared at the end movement. BV 5 and BV 8 show a sudden drop in the pressure first and a jump-up at the end. Pattern of these variations seems to correspond to longitudinal positions of boreholes. BV 6 in Fig. 38 shows a slight compression. The variation in the pressure at the toe was relatively small compared to variations in uphill boreholes (the pressure below the slip surface in BV 9 also shows slight variation (Appendix 2)).

Fig. 39 shows results of extensometer measurement. Marked compression is seen in EX 12 and marked extension is seen in EX 13. EX 13 is beside BV 8 and its extensive variation

agrees with the decrement of the effective earth pressure in BV 8. EX 12 is not just beside BV 7 but is close to it. Its compressive variation agrees with the increment in the effective earth pressure in BV 7. Though the direction of extensometer survey line is much different from that of cross section of slip surface (Fig. 10), distribution of deformation mode observed in the effective earth pressure measurement is supported by the extensometer measurement.

Variation in the effective earth pressure differs markedly depending on position. It indicates that the sliding soil mass did not move as one block. The mechanism of movement of soil with a developed slip surface is explained as the slip of an elastic body on the surface rather than failure of the entire mass. Soil around the slip surface is in, or very near to, the stress condition of failure (plastic state), whereas other parts of the sliding soil mass remain elastic. If displacement were uniform along the slip surface, there would be no strain inside (parallel movement does not cause strain inside a sliding mass, whereas there must be shear strain between the sliding mass and the stable basement), so there would be no earth pressure variation. Contrary to this, variations in the effective earth pressure are founded. It indicates that displacement along the slip surface was not uniform, thereby causing strain inside the sliding mass.

5.3. Variation in the effective horizontal earth pressure at the onset of failure

Earth pressure variations in the UD direction at about the onset of landslide movement are shown in Fig. 40. The pipe strain near the slip surface at BV 7 (the bottom diagram) indicates that the shear displacement along the slip surface began at a time between 10 to 10.5 hours at BV 7. There is no variation in the earth pressure in BV 4 or BV 7 before that, whereas BV 6 and BV 8 show similar variations at that time, and BV 5 shows a slight one. Although small, these variations (BV 5, BV 6, and BV 8) seem to be physically associated with the onset of failure because they occurred at different depths and boreholes at the same time. The first onset of failure appears to have been a relatively small event in terms of earth pressure. It might be the result of its being local (failure did not occur along the entire slip surface at once).

Large variations in the effective earth pressure first appeared after a considerable amount of displacement of the sliding mass. Fig. 41 shows the relationship between the effective earth pressure and shear displacement along the slip surface in each borehole. Variation in the effective earth pressure appears after displacement of about 10^{-2} cm, displacement apparently

preceding stress. The failure of limited area then might enlarge along the slip surface. The soil mass above the surface might loose uniformity, thereby inducing larger variation in the effective earth pressure.

5.4. Variation in the effective horizontal earth pressure at the end of the period of movement

As pore pressures dissipated after rainfall stopped, the rate of pipe strain decreased. In this stage, the effective earth pressures increased in many boreholes, though variations in those located in the foot of landslide were relatively small (BV 6). Fig. 42 shows the phenomena observed during Event 1. The increment first appears at BV 5 and BV 8 (in every event) and "hesitant" behavior is seen as pointed out by open arrows. The last increment, which is pointed out by solid arrows, is expressed as "stopping phase" in this thesis . As shown in Fig. 38, the effective earth pressure returned to almost same level as that before sliding in BV 5 and BV 8 after the stopping phase. The pressure in BV 7 was still higher than the initial value at the end of period in Fig. 38 (150 hours), but it gradually decreased becoming almost the initial value at about 300 hours. The difference in the effective earth pressure before and after movement is small, which would facilitate the repetition of movement. The rate of increment in the effective earth pressure at the stopping phase is high nevertheless there was no change in rate of pore pressure dissipation at that time (pore pressure at the slip surface in BV 7 is shown at the bottom of Fig. 42). The end of landslide movement can be indicated by the rapid increment in the effective earth pressure, whereas it is not clearly detected by pipe strain (Figs. 38 and 55).

5.5. Internal earth pressure during motion

Fig. 43 shows rate of shear displacement in each borehole calculated at the interval of 30 minutes. Comparing it to Fig. 38, major variations in the effective horizontal earth pressure were observed before the peak of slip rate and at the decelerating stage. Slip rate during 50 - 80 hours shows relatively small variation and the effective earth pressure shows relatively small variation. During that period, variations induced at the initiation of movement were maintained except in BV 4 where it was gradually released. Fig. 44 shows the difference between the

measured variations in the UD and RL directions (UD RL). By examining these data, elimination of the effect of pore pressure is achieved without making any assumption about it, and their comparison is possible. Clearly, there is a marked difference during motion (hatched in the figure), which becomes small after the stopping phase. The values in BV 4 and BV 7 are small at the initiation of movement and increase up to the stopping phase. In BV 5 and BV 8, the difference was caused by the drop of effective earth pressure in UD direction and vanished by jump-up in it. Although more detailed discussion about the stress condition is impossible, because measurements are limited in two directions, the difference can be seen as an index of anisotropy of earth pressure. Fig. 44 indicates that anisotropic earth pressure was induced during motion.

5.6. Comparison of events

Figs. 45 and 46 show variations in effective earth pressure and pore pressure at the slip surface for three events, respectively. Measurement of pore pressure failed after 35 hours in Event 3. Clearly, as displacement during each event increases (Event 3 to 1, Fig. 11), the amount of and duration of decrement in the effective earth pressure in BV8 becomes large. On the other hand, the effective earth pressure in BV 7 does not show such a clear tendency. The fact that the variation in the pressure in BV 7 for Event 2 is smaller than that for Event 3 may correspond to that the initial pore pressure. The initial pore pressure was the highest in these three events, because this event occurred after considerable amount of rainfall before it. Event 3 is not a clear "event" because pipe strain in Fig. 11 is small. The effective earth pressure shows a clear variation in BV 7 but does not in BV 8.

According to the traditional theory, the earth pressure at the moment of failure of soil mass is a constant determined by the soil strength and mode of deformation (passive / active). In the active region, it decreases down to the "active earth pressure" value, whereas in the passive region, it increases up to the "passive" one. Both extreme pressures are determined only by the internal friction angle of soil. This theory bases on the assumption of simultaneous failure of the whole sliding soil mass. However it is, generally, not valid in real landslides. In real landslides, two major points are different from this assumption; one is the existence of slip surface and the other is that failure in real landslide is progressive. These points may arrest the

mobilization of peak stress condition in sliding soil mass. Thus, two extreme pressures can not always be observed.

As stated, measurement of the earth pressures in BV 7 and BV 8 during three events were succeeded. The larger the amount of displacement, the higher the pore pressure at the slip surface. The "effective" earth pressure is used to compare the data obtained for these events. Fig. 47 shows the maximum and minimum values and the variation range (difference of those two values) of effective earth pressure at BV 7 and BV 8 during movement of the landslide. For this plot, zero balance of each transducer measured before the field installation was used for the sake of comparison of events. Because these three events occurred between May and July 1995, possibility of drift of the zero balance during this period is considered to be little. Plotted values with "?" for BV 8 in the Event 3 were obtained from 0 to 35 hours. At BV 7, where the soil was deformed in the passive mode, the maximum value is nearly constant regardless of differences in the amount of displacement and pore pressure at the slip surface. This value seems to correspond to the extreme earth pressure. In other words, the soil around this borehole was under almost constant pressure at failure, which agrees with the traditional theory ("passive earth pressure"). There is no such a tendency at BV 8 for either the maximum or minimum value, but there is a positive correlation between the variation range and the amount of pore pressure and displacement. "Active earth pressure" was not detected in this borehole, which could be due to the effect of enlargement of the failed area, the existence of a developed slip surface, or both.

6. Result of FEM analysis on the earth pressure in the Nishi-Ikawa landslide at the onset of movement

6.1. Residual forces

Nodal forces representing ground water table at the 15 hours were applied by six load steps with constant increment. The condition of "constant increment" means that detailed change of ground water table was not reproduced. This condition was determined because the rate of rising of ground water table (Fig. 22) was too high to reproduce its detailed change in the calculation. Fig. 48 shows maximum residual force after calculation of each step. These residual forces mainly existed in nodes of yielded joint elements. Approximate length of a joint element was 10 m and residual force was about 10 (kN), thus, residual stress was about 1 (kPa). Though this value can be negligible, marked increment is seen at step 5 to 6. This increment is a result of yielding of large number of joint elements. Landslide movement was already observed at 15 hours. It suggests that soil mass was not in static safe condition then. The increment of maximum residual force in step 6 (Fig. 48) is considered to correspond to the movement. Time dependent effects (rate of displacement, energy loss by viscosity, etc.) are necessary to be considered in order to extend the analysis after 15 hours.

6.2. Enlargement of the failed area and relative displacement at joint elements

Fig. 49 shows decrement of local safety factor with load step (rising of ground water table). Initial local safety factors of joint elements at the toe were relatively small. Yielding of joint elements occurred there first, and yielded area enlarged upwards. In upper parts, local safety factors were initially high but it decreased markedly with load step because of large rising of ground water table. Most of joint elements were yielded at step 5 and residual force (Fig. 48) began to increase from that step. Joint No. 9 yielded at step 6. As a result, the whole slip surface yielded and the structure became unstable. Thus initiation of local yielding in this model was occurred in two areas; one was at the toe where stress ratio is initially large and another is the area where rising of ground water table was large.

At the last load step, Joint No. 9 yielded. This joint element behaved as a "barrier" in this landslide because direction of slip surface is changed markedly there. Its local safety factor

decreased by re-distribution of exceeding shear stress from both sides. As a result, the rate of its decrement increased with load step. Fig. 50 shows distribution of shear displacement at joint elements. Relatively small displacement is seen at the central part. Marked change in the direction of slip surface hinders smooth transmission of shear displacement (also shear force) at a joint element to the next one. Thus, the shape of slip surface affected the distribution of shear displacement. Fig. 51 shows variations in pipe strain observed during initial period of Event 1. Initiation of soil movement can be seen about 10 to 10.5 hours in BV 7 and BV 9. It is not clear in BV 8 and absolute value of displacement in BV 8 is smaller than other two boreholes. Qualitatively, the observed distribution was reproduced in Fig. 50.

6.3. Variation in earth pressure

Fig. 52 shows the distribution of difference in earth pressure coefficient (ratio of vertical and horizontal earth pressure) in isoparametric elements between the initial condition and the end of loading. Elements where change of the stress ratio was larger than 4 % (both increment and decrement) are illustrated. The maximum change was about 10 %. The creeping landslide is close to critical to move at the initial condition, hence the stress change is not so large. Marked change is seen in elements just above the slip surface and change in elements distant from the slip surface was relatively small.

Elements on the ground surface around BV 8 are in active mode deformation (the ratio in the element at the ground surface of BV 8 decreased about 3 %). Those around BV 9 and BV 7 are in passive mode one. This distribution is in good agreement with result of extensometer measurement shown in Fig. 39. This distribution can be explained by the non-uniform distribution of shear displacement at joint elements (Fig. 50). Passive mode deformation around BV 7 is explained to be caused by large shear displacement around BV 12 (Fig. 50) and small displacement around the "barrier". Active mode deformation around BV 8 is explained to be caused by large shear displacement around BV 9 (Fig. 50) and small displacement around the "barrier".

Fig. 53 shows variation in horizontal earth pressure. Those in elements 85 87 decreased with load step due both to decrement in vertical earth pressure by buoyant force and to displacement of lower elements. Those in elements 88 90 first decreased and changed their tendency to increase. The first decrement was caused by buoyant force and next increment can

be explained by large slip in upper elements. Qualitatively, increment in the effective earth pressure in BV 7 and its decrement in BV 8 observed at the initiation of movement (Fig. 38) were reproduced in Fig. 53.

6.4. Absolute value of displacement and earth pressure compared to *in-situ* monitoring

Results of analysis could not reproduce observed data perfectly. Especially in BV 8, measured variation in effective horizontal earth pressure is larger than calculated one (element 86 in Fig. 53 and BV 8 in Fig. 38) and shear displacement measured there is smaller than calculated one (Fig. 50 and 51). These differences are likely to be partially due to the assumption of static deformation but mainly due to uncertainty in parameters; elastic modulus both in isoparametric elements and joint elements, and precise shape of the slip surface. For example, material parameters for the layer of $N > 50$ were determined with an assumption of $N = 50$. This evaluation might cause underestimate of the elastic modulus in deep soil. It also remains questionable how to estimate and represent "ductile" characteristic of zone around the slip surface. In this analysis constant elastic modulus were assumed for all joint elements nevertheless of their difference in depth.

On the curvature of slip surface, large change in direction of slip surface surely existed between BV 7 and BV 8 because depths of slip surface in both boreholes had been confirmed by the long-term observation. Therefore, the distribution of shear displacement would not be much affected by minor change of the shape. However, its minor change might have affected absolute value of displacement at each node. These parameters needed to be determined precisely in order to reproduce absolute measured values (both displacement and earth pressure) but it is difficult in a real landslide. In such case, the author considered that simple model was preferable as mentioned in Section 3.2.1.

7. Discussion

7.1. Propagation of the area of active movement observed in the Todoroki landslide

Fig. 33 shows two possible models for the Todoroki landslide. Movement of two blocks (below EX 9) and surficial soil creeping are common for both models. In the upper model, compressive creeping caused by the large block delineated by cracks is explained by movement of one block with curved slip surface. In this model, a non-uniform distribution of displacement on the ground surface (the middle model in Fig. 31) is induced by the shape of slip surface. The lower model (Fig. 33) explains the compressive creeping by movements of some blocks. Because of lack of information on the underground deformation, further discussion is impossible.

Downward propagation of the area of active movement was observed in EX 11 (Fig. 32). It suggests that displacement at A (Fig. 33) which had been first superior to that at B was overcome by that at B (in both models). Several changes in tendency of variation (compression and extension) in EX 11 are seen in Fig. 54 as pointed by arrows. These changes indicate that the area of active movement propagated downwards when the variation changed its tendency from compression to extension and upwards (vice versa). They were observed in this extensometer probably because its span was small and / or because of the shape of shear zone (lower model in Fig. 33). The variation in Fig. 54 was limited in the range of ± 2 mm, which value is smaller than those in other extensometers (Fig. 25 and 26). Propagation occurred in both directions (upwards and downwards) and the relatively small final strain was observed in EX 11. These results suggest that soil at A and B did not much loose their continuity. This result supports the upper model in Fig. 33, because continuity of soils at A and B is weak in the lower model.

This propagation suggests large variation in stress in the slope during movement. In Fig. 32, soil at EX 11 had been first in passive mode deformation for earlier 4 days and then became in active mode deformation. Thus, deformation mode of soil in a certain position can often change during creeping, especially in those where the shape of slip surface curved (in the upper model of Fig. 33) and where two blocks are in contact (the lower model).

7.2. Distribution of increment and decrement in internal horizontal effective earth pressure at the onset of movement

The effective earth pressure in the direction of slip at the initiation of movement increased in the middle part of landslide (BV 4 and BV 7) in the Nishi-Ikawa landslide (Fig. 38). It decreased in the lower part (BV 5 and BV 8) and did not show large variation at the toe (BV6). These results indicate that the soil in the middle part of the landslide was in the passive mode deformation and the soil in the lower part was in the active mode deformation. The observed distribution of increment and decrement in the horizontal effective earth pressure was reproduced by the FEM analysis qualitatively (Figs. 38 and 53). The reproduced distribution was explained as a result of strain caused by a non-uniform distribution of shear displacement along the slip surface (Fig. 50) in the FEM analysis. The non-uniform distribution of shear displacement was induced during enlargement of the failed area. The distribution was considered to be determined both by the shape of slip surface and by the shape of ground water table. Consequently, observed distribution of increment and decrement in the horizontal effective earth pressure is considered to be determined mainly by both of these shapes.

The similar situation with initial stage of movement (enlargement of the failed area) can be considered for the end of the period of movement. When pore pressure dissipated, local safety factor increased and shrinkage of the failed area might occur. The stopping phase (Fig. 42) may correspond to it. The facts that "hesitant" behavior was first observed in BV 5 and 8 and that effective earth pressure increased in all boreholes suggest that shrinkage first occurred in the slope below these two boreholes.

7.3. Internal horizontal earth pressure during landslide movement in relation to movement process

In-situ monitoring of internal horizontal effective earth pressure in the Nishi-Ikawa landslide showed slight variation at the onset of failure (Fig. 40). It is considered to be explained by that onset of failure was localized. In the FEM analysis, decrement of local safety factor (Fig. 49) showed that there were two parts of slip surface where yielding condition was achieved earlier than other parts; one is where the initial local safety factor was small (at the toe) and another is where decrement of local safety factor was large due to the large rising of ground water table

(around BV 12). The small variations observed at the onset of displacement in BV 5, BV 6, and BV 8 in Fig. 40, might correspond to a local failure in the former part. The yielded area enlarged because both of the rising of ground water table and of stress re-distribution due to post-yielded displacement at yielded part of slip surface. The post-yielded displacement induced large variation in the stress inside the soil above the slip surface. This inducement continued until the whole slip surface was yielded. The whole slip surface was yielded in the final state (Fig. 50 and 52). Once this state was achieved, sliding soil mass can move plastically on the given slip surface. The final state of the analysis seems to be not much disturbed during movement because variations in the effective earth pressure during the movement were smaller than those at the initiation of movement (BV 5, BV 7 and BV 8 in Fig. 38).

Internal horizontal effective earth pressure showed a clear stopping phase (Figs. 42). After the stopping phase, the effective earth pressure in many boreholes (except BV 7 and BV6) returned to be almost the same value with that before the movement. Anisotropic variation between the direction of slip and the transverse direction was induced during movement and was released at the stopping phase (Fig. 44). These facts suggest that the mechanism of development of internal earth pressure during movement is different from that of static condition.

Thus, variation in the horizontal internal earth pressure is explained as;

1) small variation at the onset of local failure

2) large variation during enlargement of the failed area

3) relatively small variation during the steady slip

4) large variation at the stopping phase probably due to shrinkage of the failed area

The variation of 2) and 3) was anisotropic and the anisotropy was released at 4) except in BV7.

7.4. Stopping phase and residual strain

Appearance of the stopping phase (Fig. 42) and the release of anisotropy (Fig. 44) seem to be sudden, comparing to their variations before and after the phase. On the other hand, rate of dissipation of pore pressure at the slip surface (Fig. 35) and rate of deceleration of pipe strain (Fig. 11) did not show large change (except pore pressure in BV7) at the stopping phase. This

is also seen in Event 2 (Fig. 45 and 46). These facts suggest that state change from movement to stable condition, in terms of internal earth pressure, was rapid compared to the other monitored data (pore pressure and pipe strain).

After the stopping phase, the effective earth pressure (Fig. 38) returned to be almost the same value with that of before the movement except in BV 6 and BV 7. That in BV 7 returned to be almost the same value much later than the stopping phase as stated in 5.4. In the Event 2 (Fig. 45), the return of BV 8 was after the stopping phase and the return of BV 7 delayed, too. The author considers that this delay of BV 7 can be explained by that accumulated strain during motion was not released at the moment of stopping phase but it was released gradually by plastic behavior (for example, stress relaxation) of soil or slip surface.

It is surprising that the difference in the effective earth pressure before and after the movement is small in BV 5 and BV 8 (Figs. 38 and 44) nevertheless marked non-uniform distribution of shear displacement along the slip surface still remained even after the stopping phase (Fig. 55). From the point of displacement, residual strain, caused by the non-uniform distribution, seems exist after the stopping phase but residual earth pressure was not observed. Two possible mechanisms can be considered:

1) Residual strain was released during the stopping phase in the way which could not be observed by the system used (gauges on pipe).

2) Re-distribution of shear stress occurred during stopping phase in order to keep the residual strain inside the sliding mass by the shear stress on the slip surface.

Situation of 1) can be achieved assuming plastic behavior of sliding soil mass (for example, delayed failure at another slip surface (though such slip surface has not been detected by long-term observation)). However, this may not be consistent with facts that stopping phase was rapid. Standing on observational facts, 2) seems preferable. However it leads to a result that distribution of shear stress along the slip surface can not be determined only by the slope structure but it has history dependence (its distributions before and after one event are different). Further discussion is difficult in this study because of the lack of direct evidence. Therefore, measurement of three components of earth pressure in vertical plane in order to measure shear stress is required for further understanding of stress in the landslide.

8. Conclusions

(1) Continuous extensometer measurements for the Todoroki landslide revealed a non-uniform distribution of ground displacement. This non-uniform distribution probably is a result of the shape of slip surface(s). Propagation of the active area of movement was observed in an extensometer. Strain that had been accumulated during movement was released by this propagation, which was considered to be due to stress changes in the curved shear zone or contact area between two blocks that did not move independently.

(2) Direct monitoring of internal horizontal earth pressure was performed in the Nishi-Ikawa landslide. The effective earth pressure was calculated from the measured earth pressure and pore pressure at the slip surface based on the assumption of free ground water. Variations in the effective earth pressure in the direction of slip can be summarized as follows:

2-1) The effective earth pressure at the initiation of movement increased in the middle part of landslide, decreased in the lower part, and did not show large variation at the toe.

2-2) The effective earth pressure at many points in the landslide increased during deceleration of movement (stopping phase). The rate of earth pressure variation at the stopping phase was large; nevertheless there was not a marked change in rate of deceleration of pipe strain and rate of dissipation of pore pressure.

2-3) Differences in effective earth pressure before and after movement were small.

(3) Anisotropic variation (difference between variation in the horizontal earth pressure in the direction of slip and that in the transverse direction) was induced during movement and was released at the stopping phase. Based on the characteristics of 2-1) to 2-3), the mechanism of development of internal horizontal earth pressure during movement is considered to be different from that in the static state. The shift from the moving state to the static one was rapid.

(4) Distribution of variations in effective earth pressure at the initiation of movement was reproduced by FEM analysis. In the analysis, the slip surface was represented by a series of joint elements, and external forces that were induced by ground water were represented by nodal forces. Whether the earth pressure in a certain position of the landslide increased or

decreased was determined mainly by the shape of slip surface (kinematic constraint) and by distribution of pore pressures at the slip surface (stress condition).

Contents of this thesis are based on papers as follows:

1. "On a crack induced on a slope during earthquake ground motion", Proc. of Symp. on Geotechnical Problems in Landslide, Shikoku Branch of Japanese Geotechnical Society, pp. 91-98, 1996, by Araiba, K, and Suemine, A (in Japanese).
2. "Analysis on the Result of Slope Deformation Observation in Todoroki Area, Hokudan-cho, Awaji-Island", Landslides, Jour. of Japan Landslide Society, Vol. 34, No. 2, pp. 17-24, 1997, by Araiba, K., Suemine, A., Sakamoto, T (in Japanese).
3. "In-situ Measurement of Internal Earth Pressure during Landslide Movement", Soils and Foundations, (submitted), by Araiba, K. and Suemine, A.

Acknowledgments

The author is profoundly grateful to Associate Prof. A. Suemine of the Tokushima Landslide Observatory, DPRI, Kyoto Univ. and Prof. K. Sassa of DPRI for their valuable supervising. The author would thank to Prof. Y. Kobayashi, the former professor of the Aso Volcanology Laboratory, Kyoto Univ., Prof. K. Okunishi, Prof. M. Chigira and Associate Prof. H. Fukuoka of DPRI for their helpful advise. Dr. A. Takeuchi, Assistance of DPRI, who gave the author chance to touch real landslides which fascinate him is also acknowledged. Thanks are also due to Mr. T. Konishi and Ms. T. Onoda of the Tokushima Landslide Observatory for their helps in observation and Mr. K. Koketsu (Tech-Gihan Co. Ltd.,) for his technical advise on earth pressure measurement. The author would express sincere gratitude to residents of investigated landslides who gave the author large cooperation. Kind helps and useful discussions given by present and former students of the Landslide Section of DPRI are appreciated.

Reference

1) Bjerrum, L. (1967), "Progressive Failure in Slopes of Overconsolidated Plastic Clay and Clay Shales", Proc. of American Society of Civil Engineering, Vol. 93, No. SM 5, pp. 3-49.

2) Brackley, I. J. A. and Sanders, P. J. (1992): "In situ measurement of total natural horizontal stresses in an expansive clay", Géotechnique, Vol. 42, No. 2, pp. 443-451.

3) Burland, J. B., Longworth, T. I. and Moore, J. F. A. (1977): "A study of ground movement and progressive failure caused by a deep excavation in Oxford Clay", Géotechnique, Vol. 27, No. 4, pp. 557-591.

4) Chowdhury, R. N. (1978), "Slope Analysis", Elsevier Scientific Publishing. Co., pp. 69-77.

5) Desai, C. S., Naresh, C. S. and Vulliet, L. (1995): "Constitutive Modeling and Analysis of Creeping Slopes", Jour. of Geotechnical Engineering, American Society of Civil Engineering, Vol. 121, No. 1, pp. 43-56.

6) Fukumoto, A. (1972): "Study on the Behavior of Stabilization Piles for Landslides", Soils and Foundations, Vol. 12, No. 2, pp. 61-73 (in Japanese).

7) Fukuoka, M. (1984): "Earth Pressure on Walls of Slices in Sliding Soil Mass", Proc. 4th Int. Symp. on Landslides, pp. 137-139.

8) Fukuoka, M., Imano, M. and Hada, M. (1985): "Earth Pressure in the Sliding Soil Mass", Proc. 4th Int. Conf. and Field Workshop on Landslides, pp. 245-250.

9) Fukuzono, K. (1993): "Attempt at and Problems of Measurement of Internal Stresses in Slope Failure", Proc. SABO Workshop on Experimental Research on Landslide Mechanisms, Japan Society of Erosion Control Engineering Publication No. 10, pp. 1-8 (in Japanese).

10) Furuya, T. (1996): "Landslide", Kokin-Shobo, pp. 1-26 (in Japanese).

11) Goodman R., E. (1976): "Methods of Geological Engineering in Discontinuous Rocks", West Publishing Co., pp. 300-368.

12) Habib, P. (1988): "Slip Surface in Soil Mechanics", Rock and Soil Rheology, Lecture Notes in Earth Sciences, Springer-Verlag., pp. 93-116.

13) Hada, M., Fukuoka, M. and A. T. Cristos. (1988): "Earth Pressure during Landslide", Proc. 5th Int. Symp. on Landslides, pp. 175-180.

14) Hariu, K. (1984): "Errors in earth pressure measurements and their correctional procedures", Tsuchi-to-Kiso, Japanese Society of Soil Mechanics and Foundation Engineering, Vol. 32, No. 6, pp. 41-48 (in Japanese).

15) Hiramatsu, S., Mizuyama, T., Ishikawa, Y, Koyamauchi, S and Nishinaka, S. (1996): "Discussion on change in potential of eroded soil production in slope after an earthquake", Proc. of annual meeting of Japan Society of Erosion Control Engineering, pp. 167-168 (in Japanese).

16) Hirano, M. and Ishii, T. (1997): "Characteristics of Slope Failures Induced by 1995 Hyogoken-Nanbu Earthquake in The Rokko Mountain and Their Changes by Subsequent Rainfall", Jour. of Japan Society of Erosion Control Engineering, Vol. 50, No. 1, Ser. No. 210, pp. 23- 32 (in Japanese).

17) JSSMFE (Japanese Society of Soil Mechanics and Foundation Engineering) (1982): "Engineering properties and their application of weathered granite and weathered soil of granite" pp. 205-209 (in Japanese).

18) Kamai. T. (1993): "Failure propagation process in landslide clay", Proc. 7th Int. Conf. and Field Workshop on Landslide, pp. 243-248.

19) Maeda, K. and Shima, M. (1982): "Microseismic Activity in a Landslide Area", Disaster Prevention Research Institute Annuals, DPRI of Kyoto Univ., No.25B1, pp. 115-127 (in Japanese).

20) Mizuno, K., Okada, A., Sangawa, A. and Shimizu, F. (1993): "Strip Map of the Median Tectonic Line Active Fault System in Shikoku", Geological Survey of Japan.

21) Morsy, M. M., Morgenstern, N. R. and Chan, D. H. (1995): "Simulation of creep deformation in the foundation of Tar Island dike", Canadian Geotechnical Journal, Vol. 32, pp. 1002-1023.

22) Nakamura, H. and Itagaki, O. (1976): On gauge interval of strain gauge pipes for detection of slip surface, Landslide, Jour. of Japan Society of Landslides, Vol. 13, No. 2 pp. 21-26, (in Japanese).

23) Ohsaka, O., Tamura, T., Kubota. J. and Tsukamoto, J (1992): "Process Study of the Soil Stratification on Weathered Granite Slopes", Jour. of the Japan Society of Erosion Control Engineering, Vol. 45, No. 3, pp. 3-12 (in Japanese).

24) Potts, D. M. , Kovacevic, N. and Vaughan, P. R. (1997): "Delayed collapse of cut slopes in stiff clay", Géotechnique, Vol. 47, No. 5, pp. 953-982.

25) Sassa, K. (1984): "Monitoring of a Crystalline Schist Landslide Compressive Creep affected by "Underground Erosion"-", Proc. of 4th Int. Symp. on Landslides, Vol. 2, pp. 179-184.

26) Sassa, K., Fukuoka, H. and Shima, M. (1989): "Development of a High-Speed High-Stress Ring Shear Apparatus and Shear Strength Reduction at Rapid Loading in Landslides", Annuals, Disaster Prevention Research Institute, Kyoto Univ. No.32B-1, 165-182 (in Japanese).

27) Shima, M., Furuya, T. and Konishi, T. (1975): "The observation of internal strain at a shattered zone type landslide areas", Annuals, Disaster Prevention Research Institute, Kyoto Univ. No.18B, 253-263 (in Japanese).

28) Shima, M. and Takeuchi, A. (1973): "On a Method of Instrumentation of Underground Deformation", Landslides, Jour. of Japan Landslide Society, Vol. 10, No. 2, pp. 6-17 (in Japanese).

29) Skempton A. W. (1964): "Long-term Stability of Clay Slopes", Géotechnique, Vol. 14, No. 2, pp. 77-100.

30) Suemine, A. (1983): "Observational Study on Landslide Mechanism in the Area of Crystalline Schist (Part 1)", Bull. Disaster Prevention Research Institute of Kyoto Univ., Vol. 33, Part 3, No. 299, pp. 105-127.

31) Suemine, A. (1984): "Observational Study on Landslide Mechanism in the Area of Crystalline Schist (Part 2)", Bull. Disaster Prevention Research Institute of Kyoto Univ., Vol. 37, Part 2, No. 324, pp. 39-58.

32) Tanaka, T. and Sakai, T. (1993): "Progressive Failure and Scale Effect of Trap-door Problems with Granular Materials", Soils and Foundations, Vol. 33, No. 1, pp. 11-22.

33) Takeuchi, A., Fujiwara, J. and Tohyama, S. (1996): "On the characteristics of the Kohtaki landslide, Awaji-Island, induced by the Hyogo-ken Nanbu Earthquake", "The Great Hanshin-Awaji Earthquake Disaster -Effort for study of disaster reduction- ", Disaster Prevention Research Institute of Kyoto University, pp. 236-249 (in Japanese).

34) Tomita, Y., Sakurai, W. and Naka, N. (1996): "Study on the Extension of Collapse Caused by rainfall after the Earthquake in Rokko Mountain Range", Jour. of Japan Society of Erosion Control Engineering, Vol. 48, No. 6, Ser. No. 203, pp. 15- 21 (in Japanese).

35) Tsuchiya, S. and Ohmura, K. (1988): "Forecast Methods for Slope Rupture Time and the Mathematical Analysis of Their Mechanical Properties", Landslide, Jour. of Japan Landslide Society, Vol. 25, No. 2, pp. 2- 8 (in Japanese).

36) Vermeer, P. A. (1990): "The orientation of shear bands in biaxial tests", Géotechnique, Vol. 40, No. 2, pp. 223-236.

37) Yamagata Prefecture (1993): "On the method for back-filling of clearance between drainage well (liner-plate) and original ground", "Landslides controlled by the Forestry Bureau", Japanese Forestry Bureau, pp. 210 - 235 (in Japanese).

38) Yatabe, R., Yagi, N. and Enoki, M. (1991): Ring Shear Characteristics of Clays in Fractured-zone-landslide, Journal of Geotechnical Engineering, Japanese Society of Civil Engineering, No. 436/III-16, pp. 93-101 (in Japanese).

Table 1. Installation depths of earth pressure transducers and soil properties there.
Transducers at the underlined depth are used without specification of their depths.

BV	slip surface depth (m)	transducer depth (m)	distance from slip surface (m)	soil properties (color*)
BV4	10.8	3.25	+ 7.5	loose sandy (y/br)
		8.25	+ 2.5	stiff silty (br)
		13.25	2.5	loose sandy (y/gy)
		18.25	7.5	clayey (bl)
	8.2	0.75	+ 7.4	loose sandy (y/br)
		5.75	+ 2.4	loose silty (gy)
		10.75	2.6	loose silty (y/br)
		14.75	7.6	stiff silty (gy)
BV6	2.0	0.75	+ 1.2	loose silty (y/gr)
		4.25	2.3	stiff sandy (gr)
		9.25	7.3	stiff clayey (gy)
BV7	8.3	6.25	+ 2.0	loose silty (y/br)
		11.25	3.0	clayey (gr)
BV8	15.6	12.25	+ 3.3	stiff silty (y/gy)
		17.25	1.7	stiff clayey (y/gy)
BV9	2.6	4.25	1.7	loose sandy (y/br)

* Soil color was checked during drilling.
y; yellow, br; brown, gy; gray, bl; black, gr; green.

Table 2. Material properties for 2-D isoparametric elements.

Property	Material 1	Material 2	Material 3	Material 4	Material 5
total unit weight (tf/m^3)	1.9	2.1	2.1	2.1	2.4
Young's modulus (MPa)	27	55	140	280	1400
shear stiffness (MPa)	9.8	20	51	100	510
peak friction angle (°)	30	32	34	35	42
cohesion (kPa)	1.0	2.0	2.9	3.9	10

Table 3. Material properties for joint elements.

Property	Material 1	Material 2	Material 3
normal stiffness (MPa)	55	55	55
shear stiffness (MPa)	20	20	20
friction angle (°)	17	21	23
cohesion (kPa)	0.010	0.010	0.010

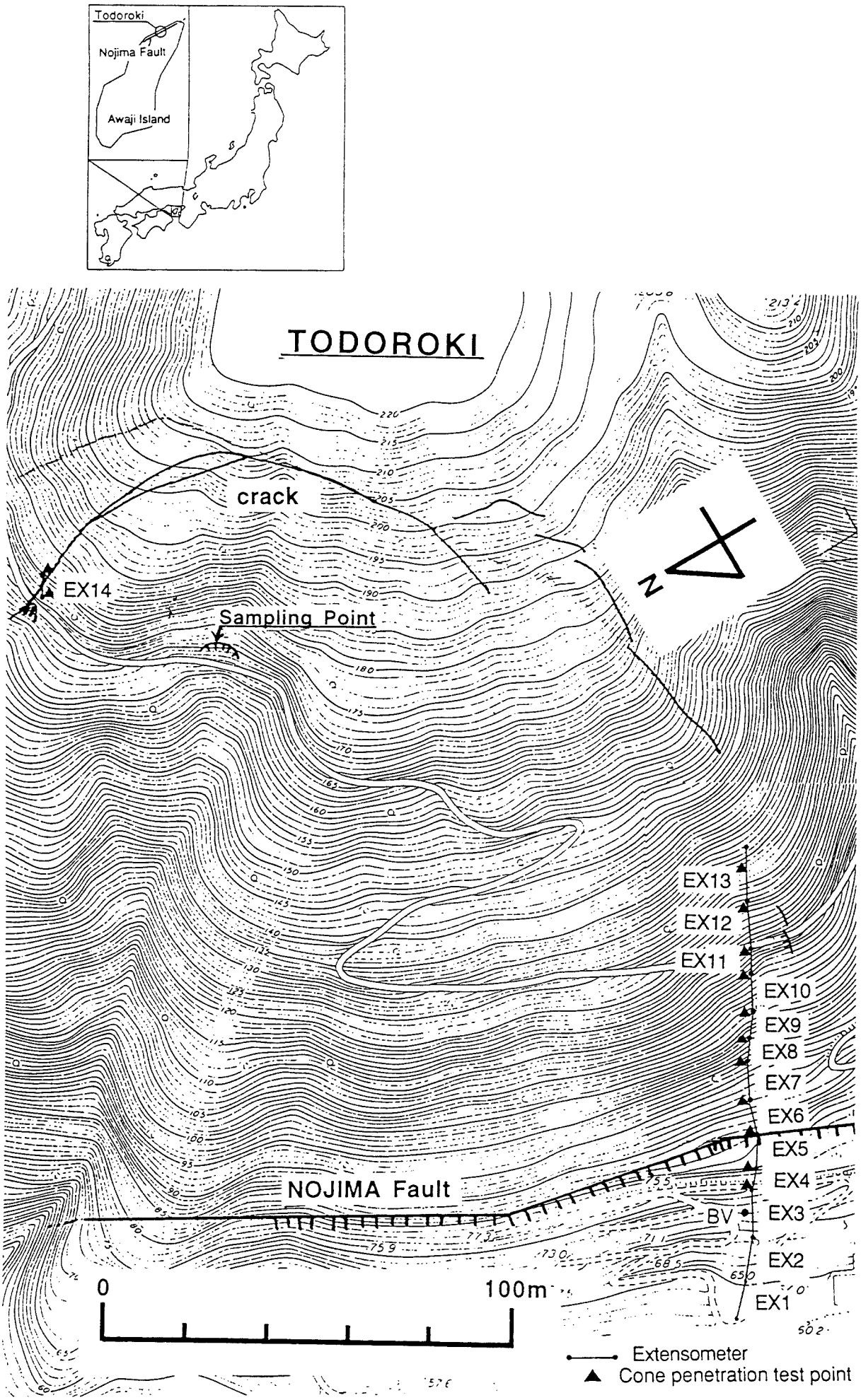

Fig. 1. Topography of the Todoroki landslide and arrangement of observation equipment.

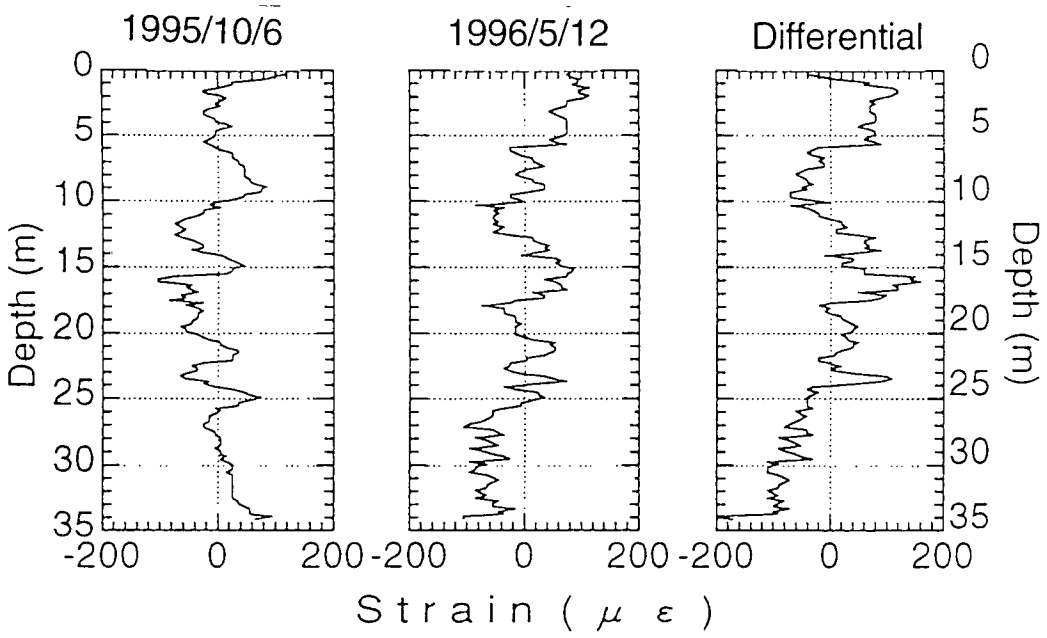

Fig. 2. Results of observation on insertion-type bending pipe at BV in Fig. 1.

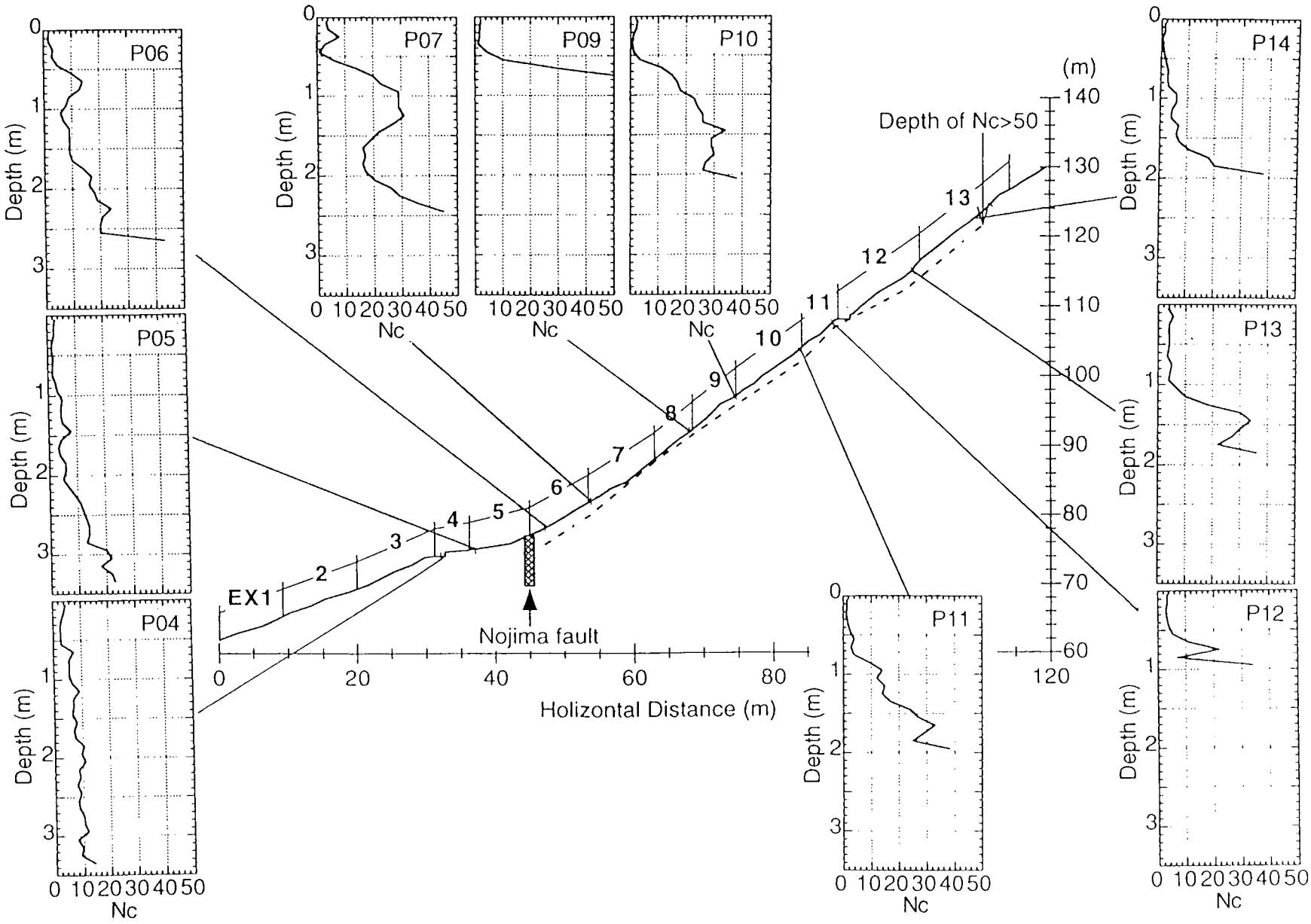

Fig. 3. Results of the portable cone penetration tests (dotted line in the cross section shows depth of layer of $Nc_{10} > 50$).

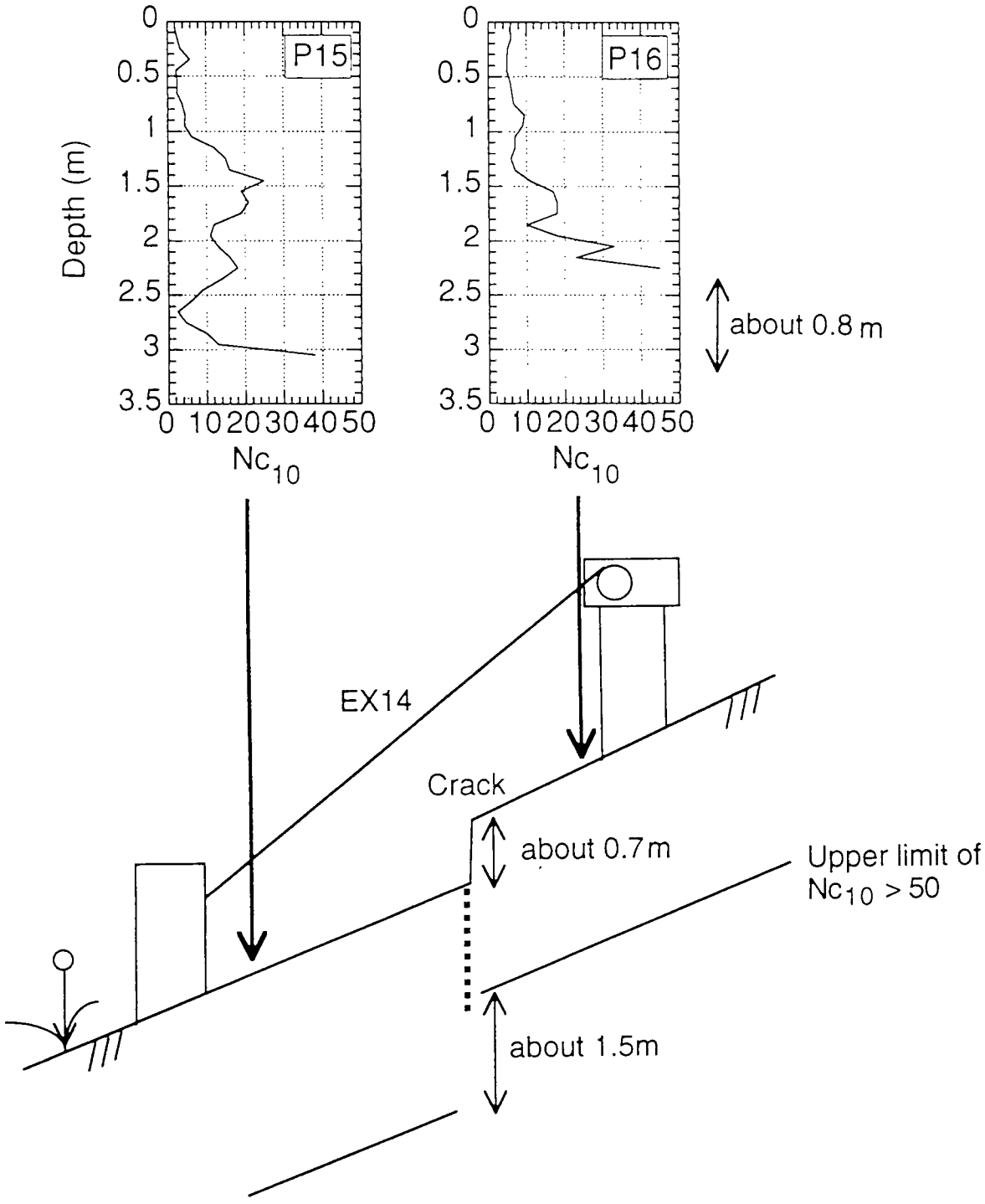

Fig. 4. Schematic figure of ground condition around the crack at EX 14.

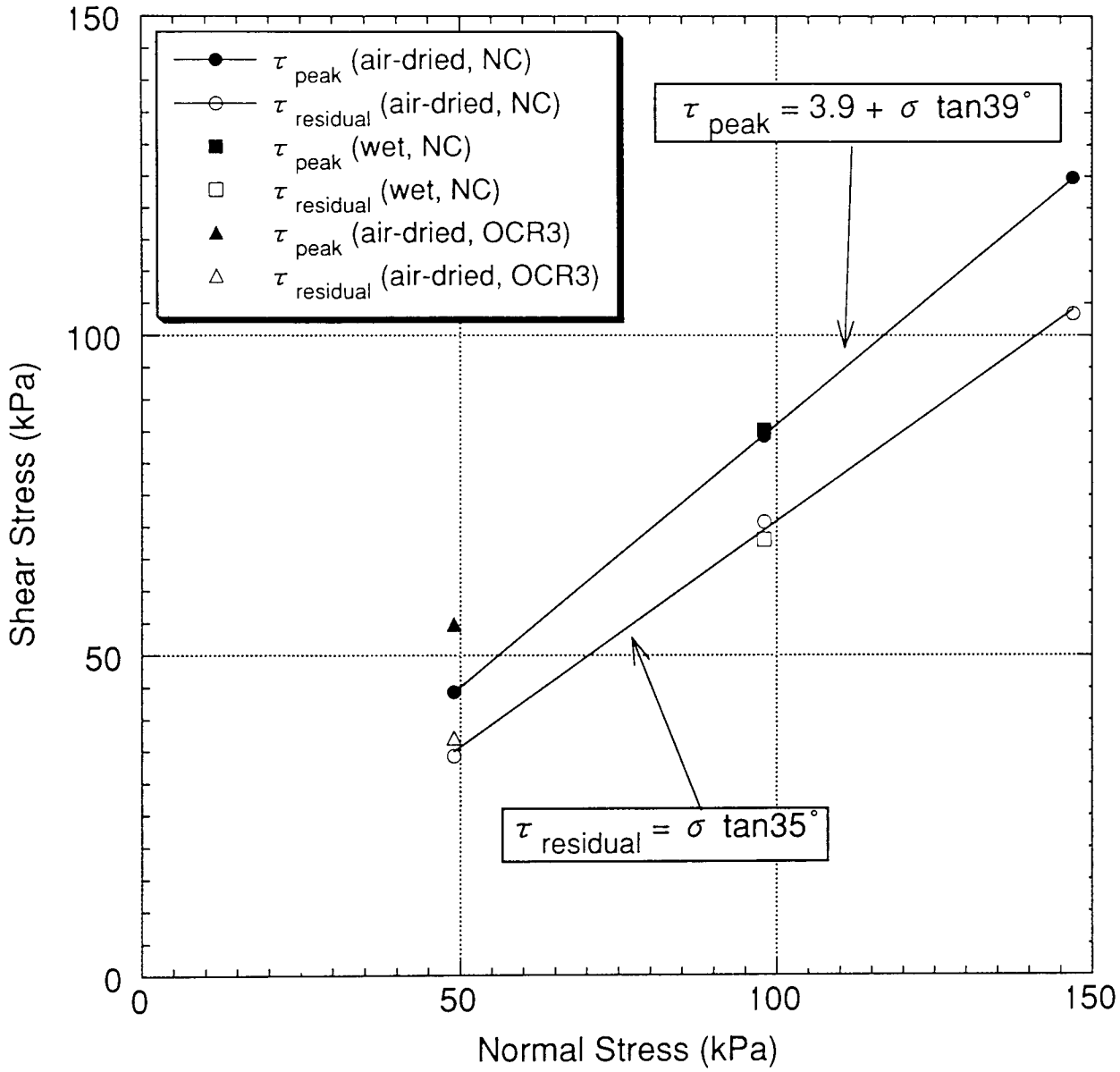

Fig. 5. Results of ring shear tests performed on specimen taken at "sampling point" in Fig. 1. Regression lines were calculated for result of tests on air-dried and NC specimen. Solid markes indicate peak shear stress and open ones indicate residual shear stress.

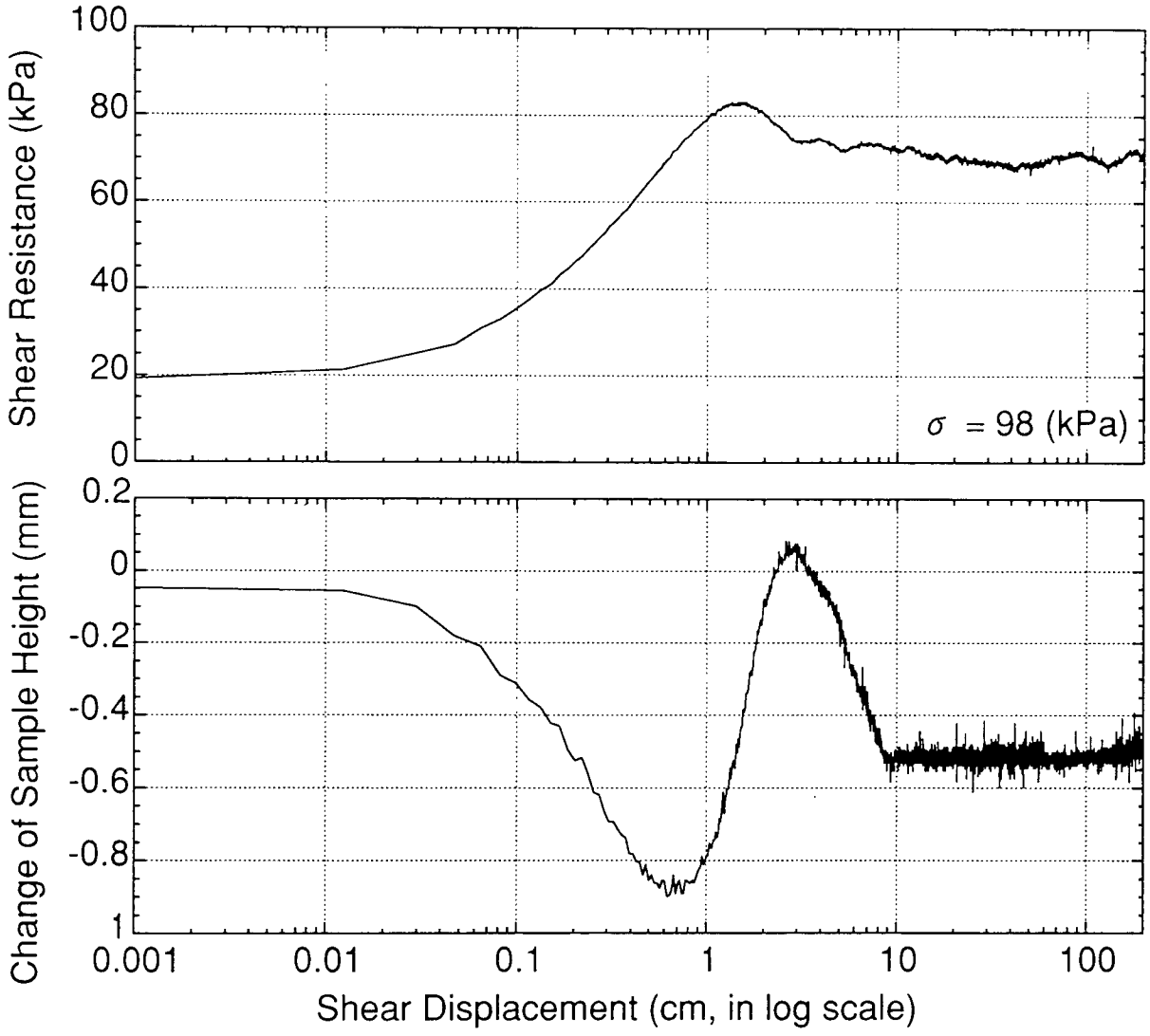

Fig. 6. Change of shear resistance and sample height with shear displacement during a ring shear test on air-dried normally consolidated specimen.

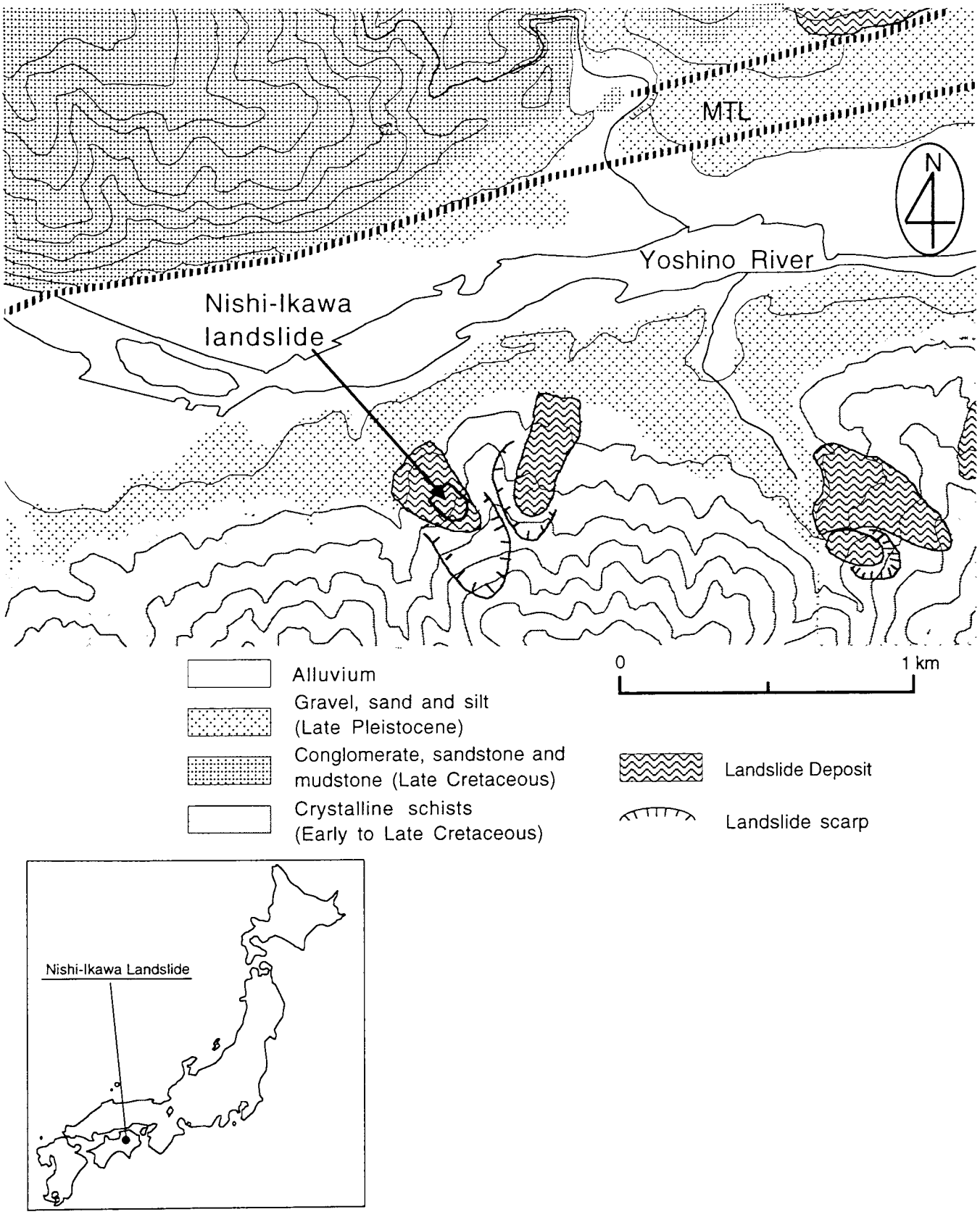

Fig. 7. Geological setting around the Nishi-Ikawa landslide (after Mizuno *et al.* (1993)).
The position of the Nishi-Ikawa landslide is added by the author in a deposit of ancient landslide.

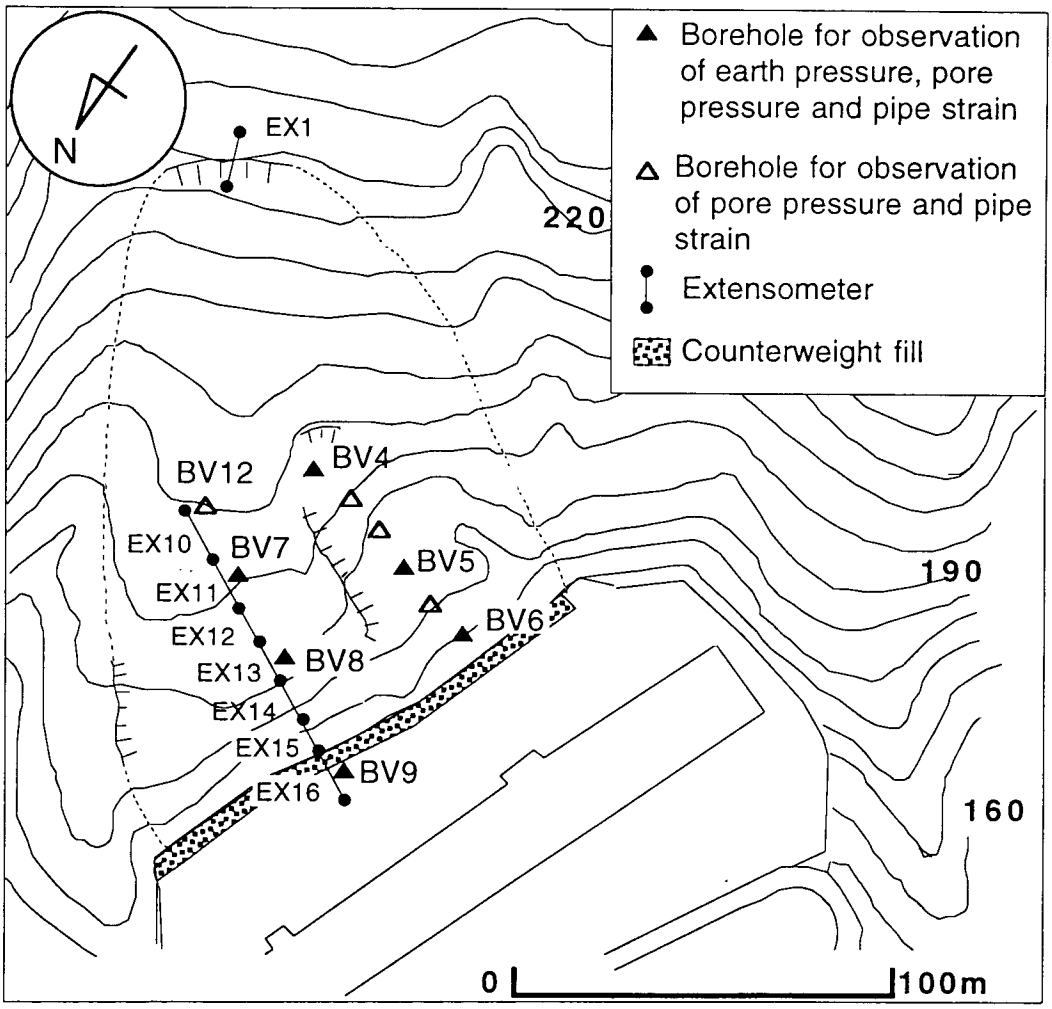

Fig. 8. Topography of the Nishi-Ikawa landslide and arrangement of observation equipment.

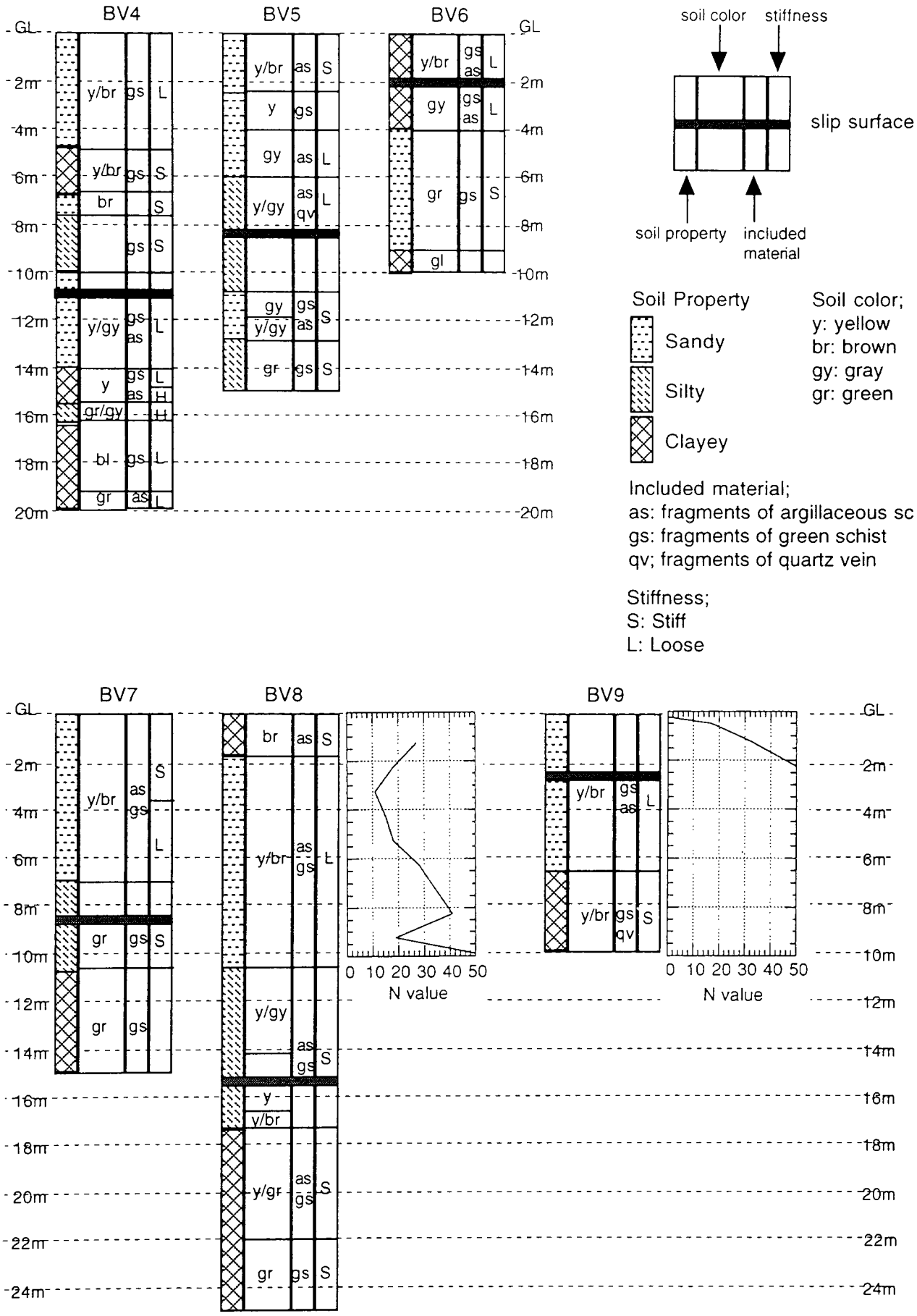

Fig. 9. Result of visual inspection of drilled cores and standard penetration tests in the Nishi-Ikawa landslide.

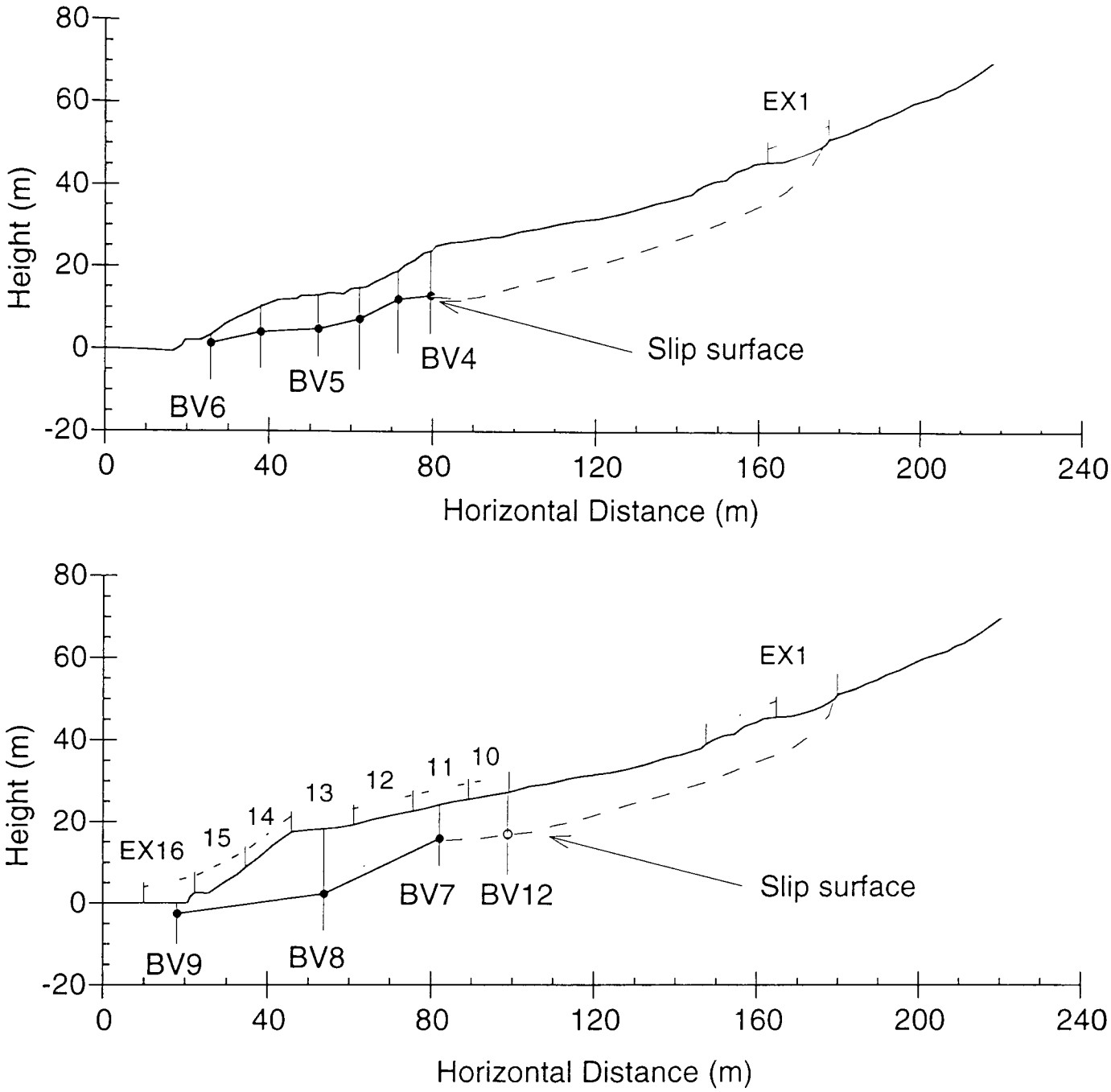

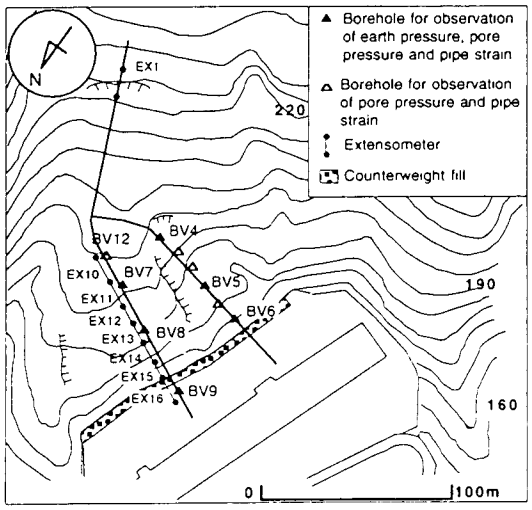

Fig. 10. Two cross sections along survey lines. Depth of slip surface has been confirmed by long-term observation. The head scarp is located in the span of EX 1.

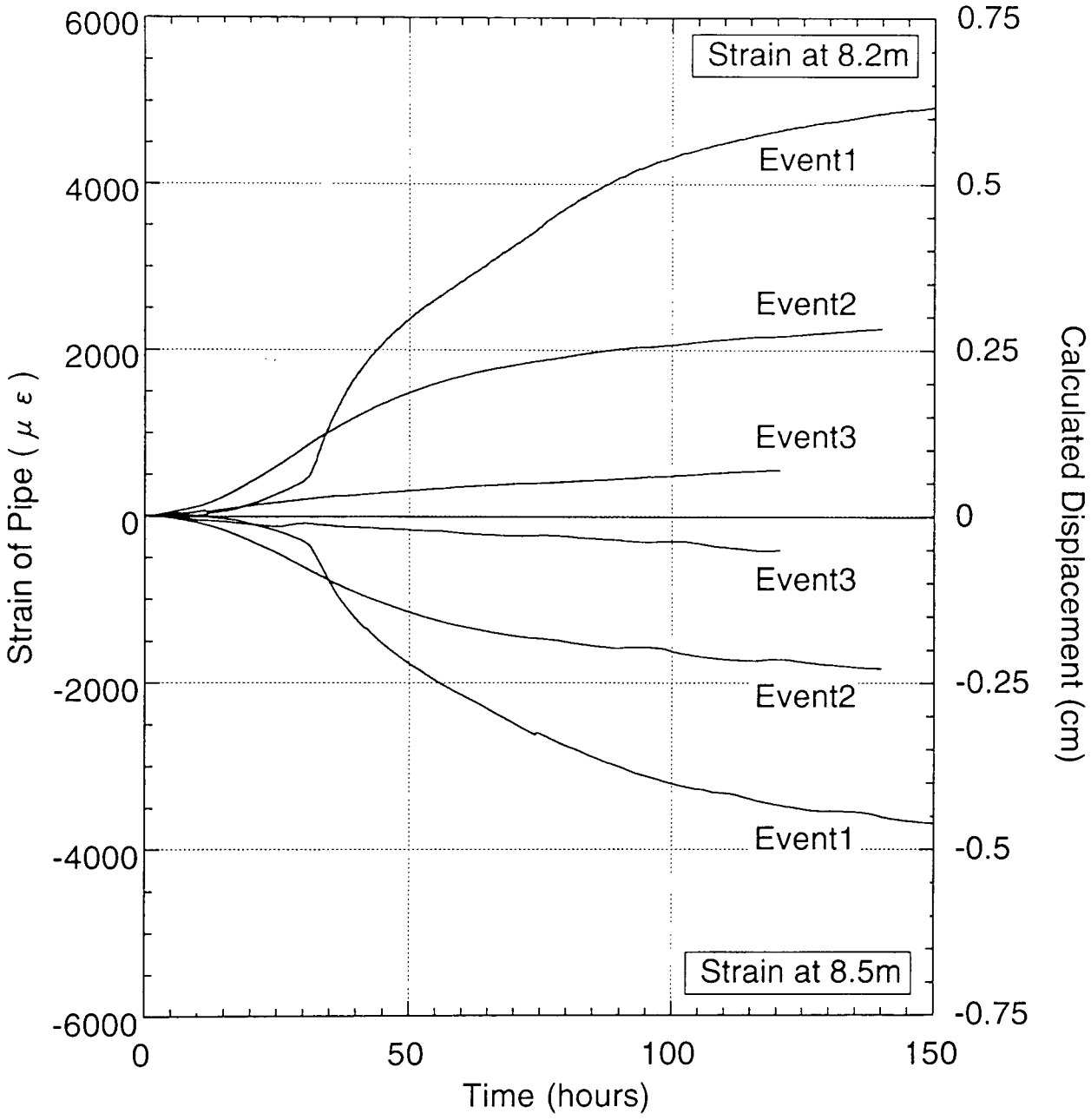

Fig. 11. Result of measurement of pipe strain near the slip surface in BV 7 for three events. Calculated displacement using relationship in Fig. 17 (stated later) is shown in the right axis.

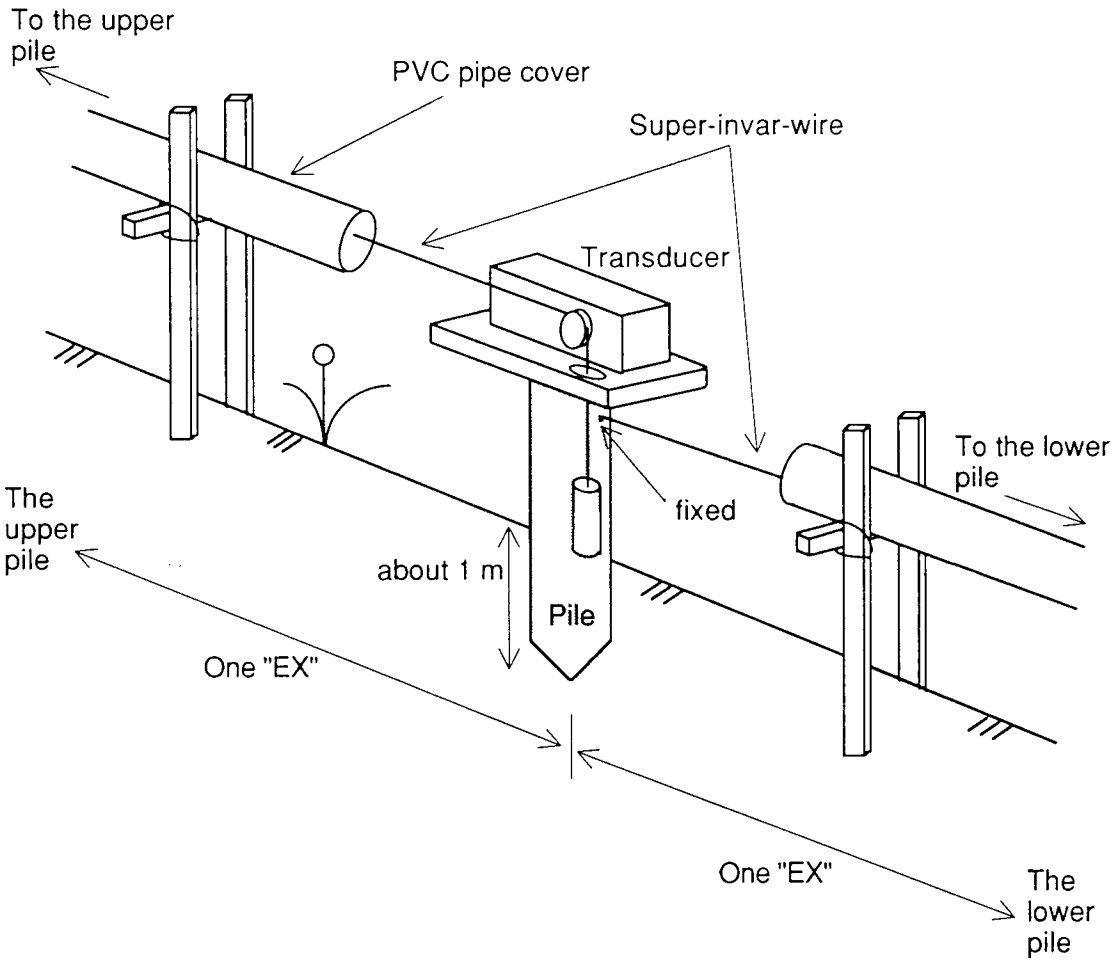

Fig. 12. Schematic structure of extensometers.

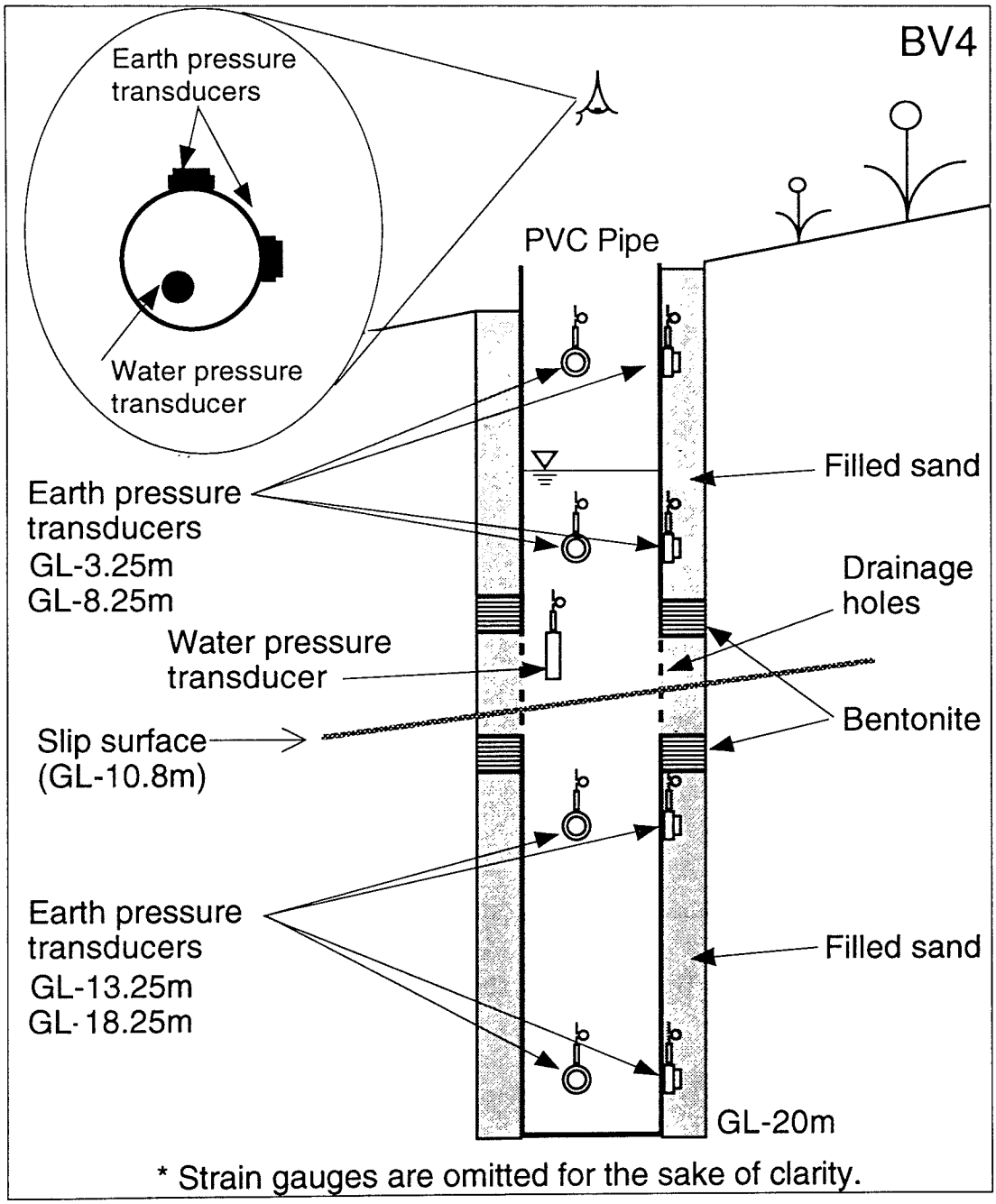

Fig. 13. Schematic structure of an observation borehole.

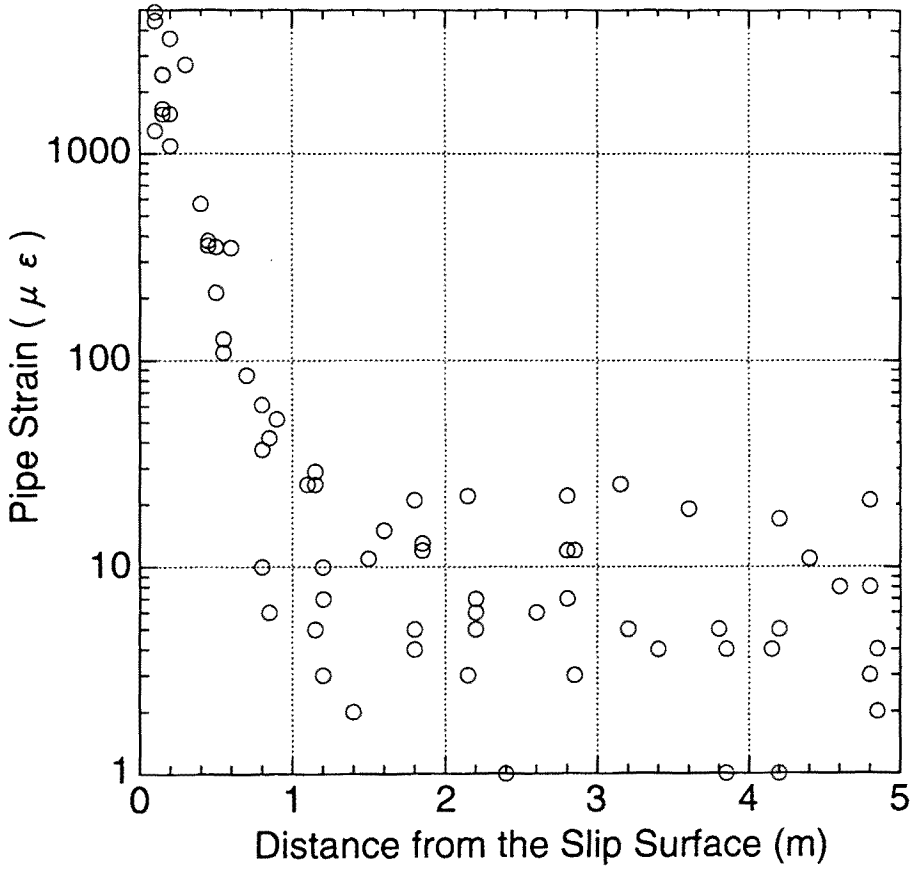

Fig. 14. Attenuation of the maximum variation of pipe strain with distance from the slip surface observed during Event 1 in the Nishi-Ikawa landslide.

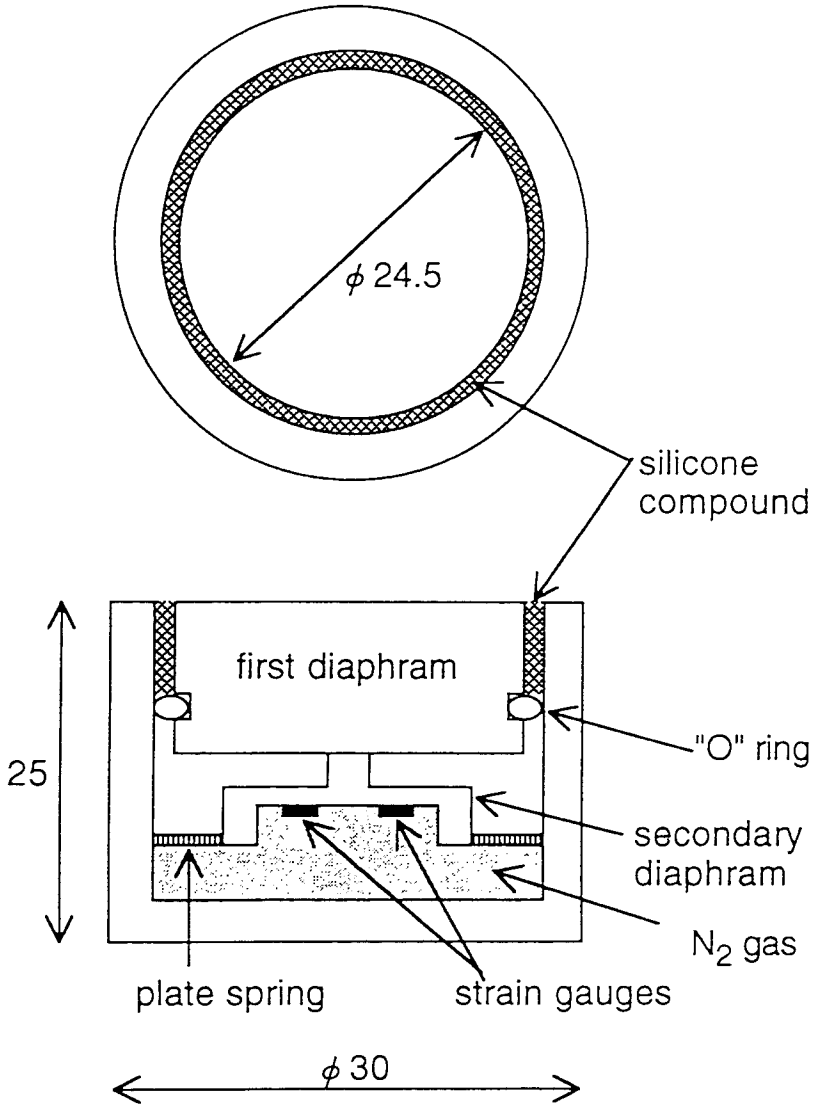

Fig. 15. Structure of the earth pressure transducer used (unit: mm).

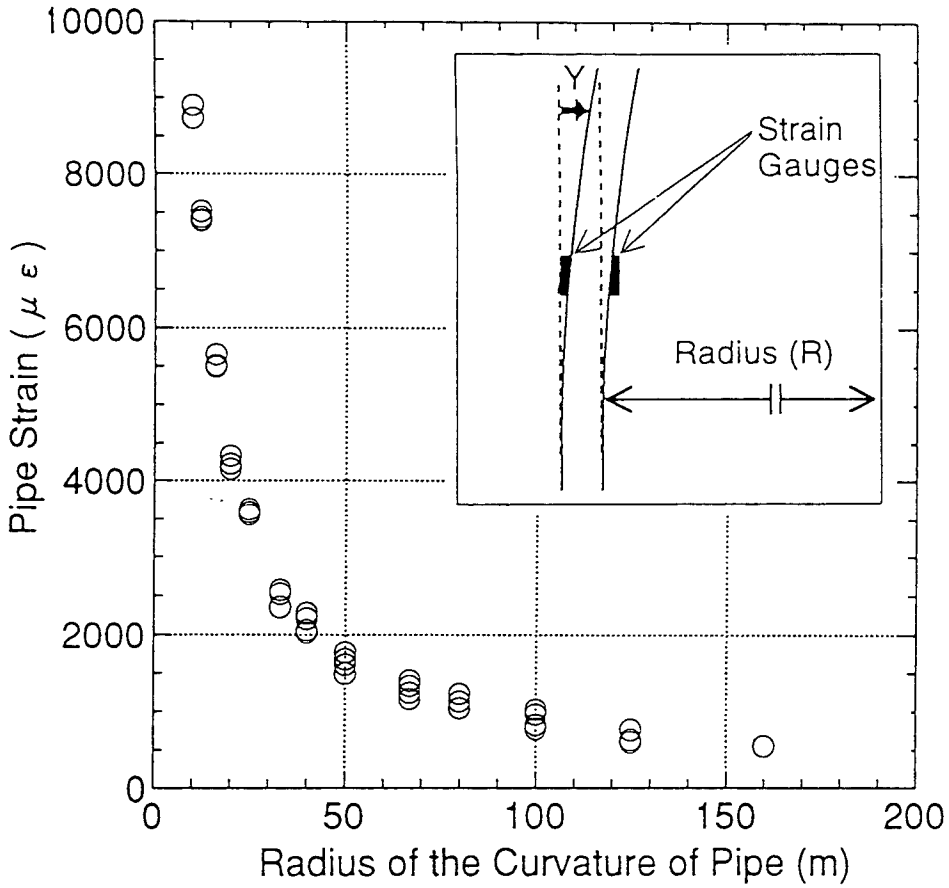

Fig. 16. Calibration test results for measurement of the strain on a pipe.

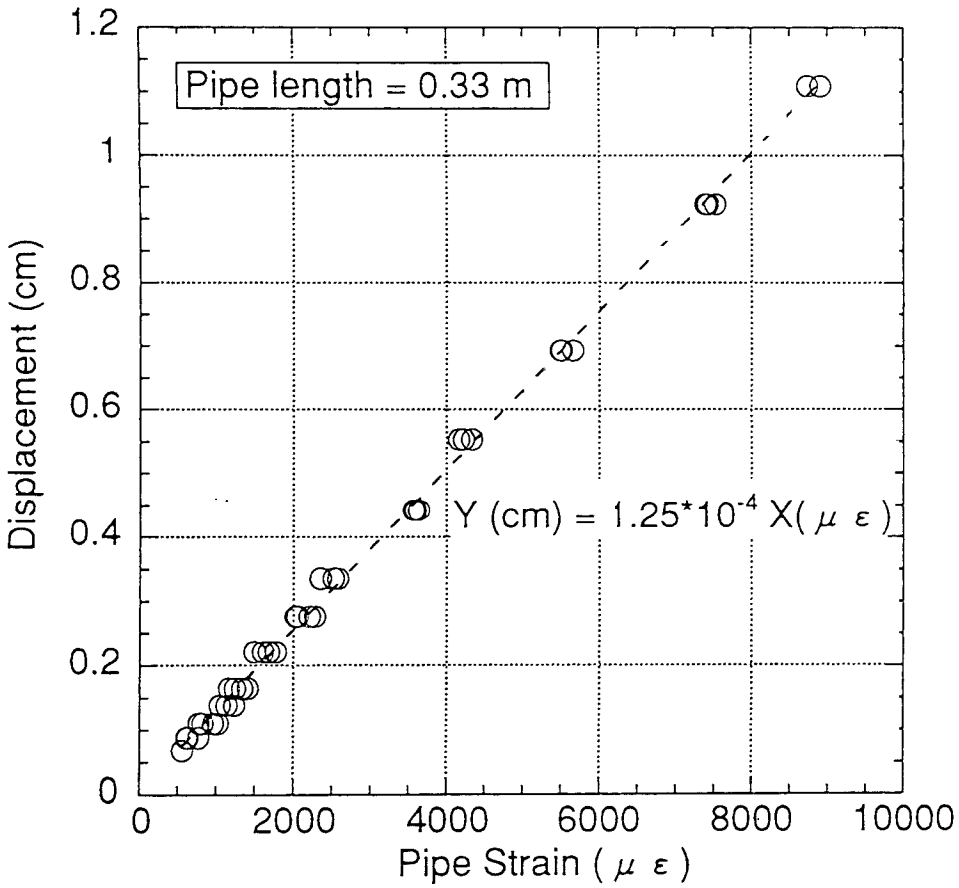

Fig. 17. Relationship between the output of the strain gauge and the relative displacement, calculated from Fig. 16.

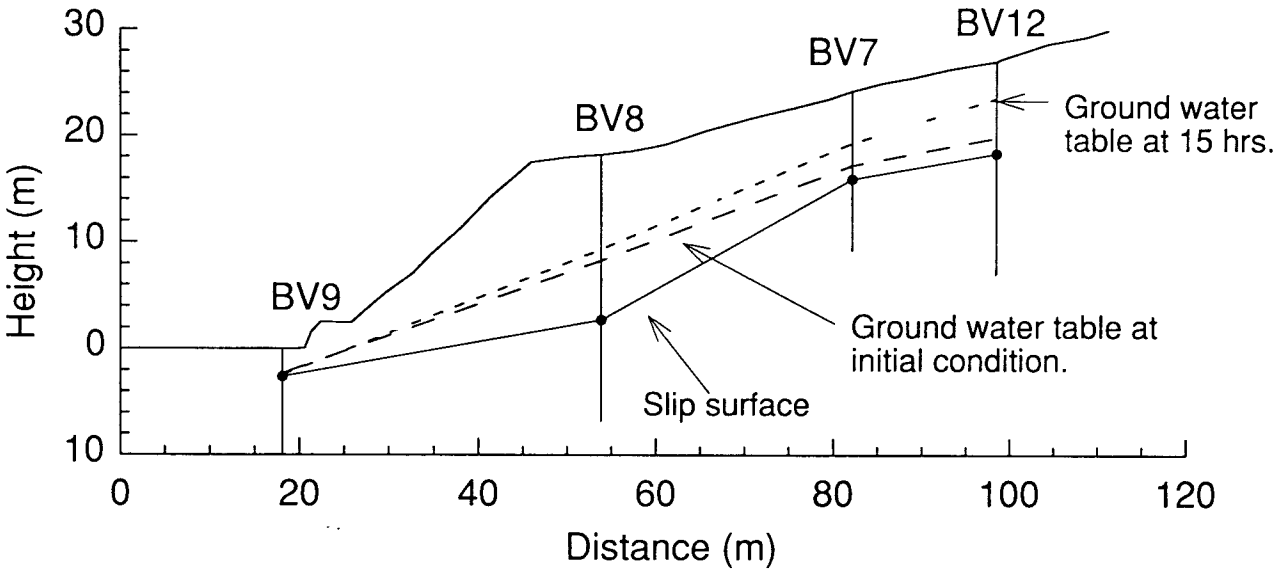

Fig. 18. Ground water table assumed for the FEM analysis.

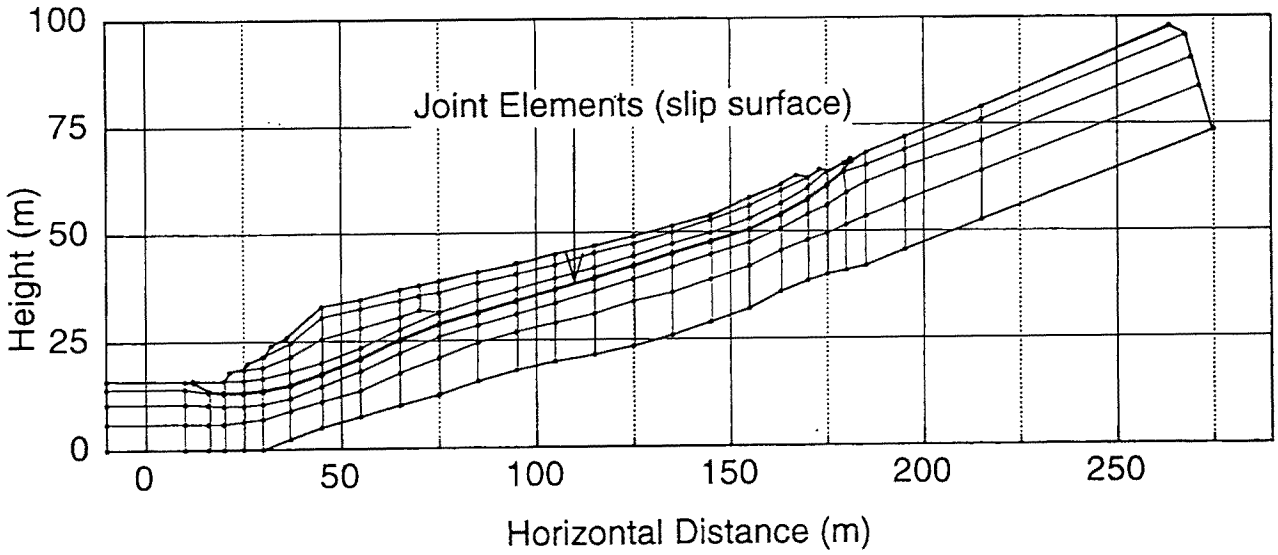

Fig. 19. FEM meshes for calculation (joint elements are expressed as thick line).

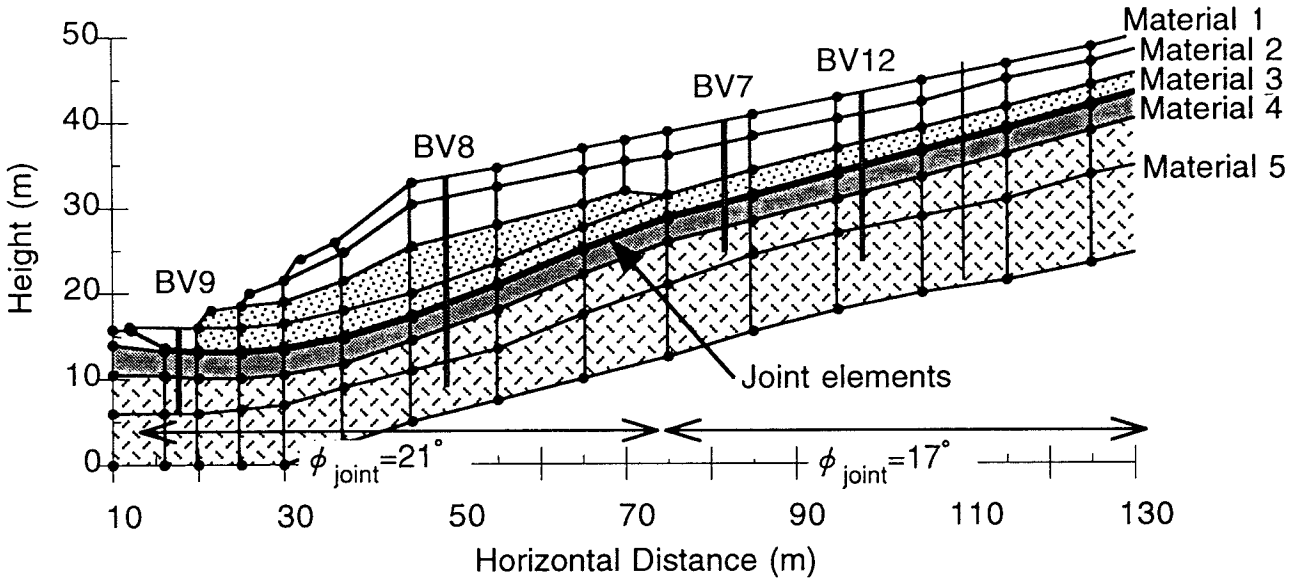

Fig. 20. Structure of model ground in the slope from BV 9 to BV 12.

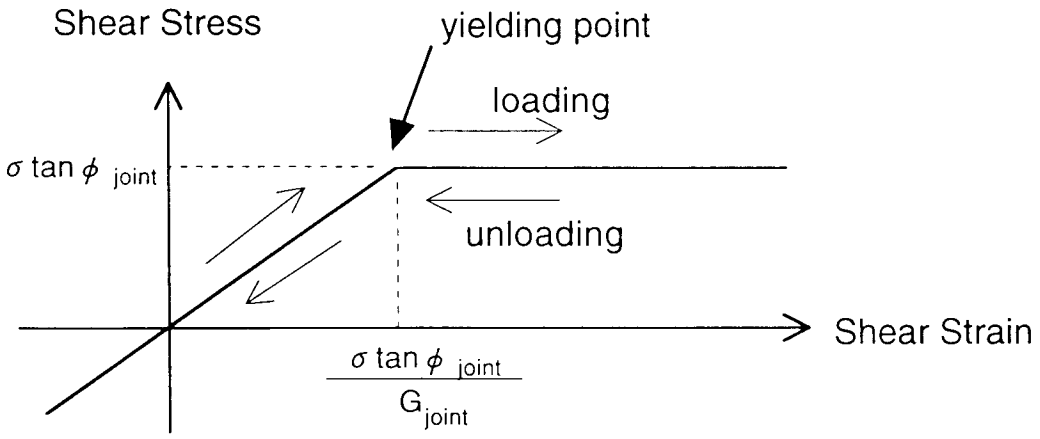

ϕ_{joint}: friction angle of joint
G_{joint}: Shear stiffness of joint

Fig. 21. Shear behavior of joint element under constant effective stress.

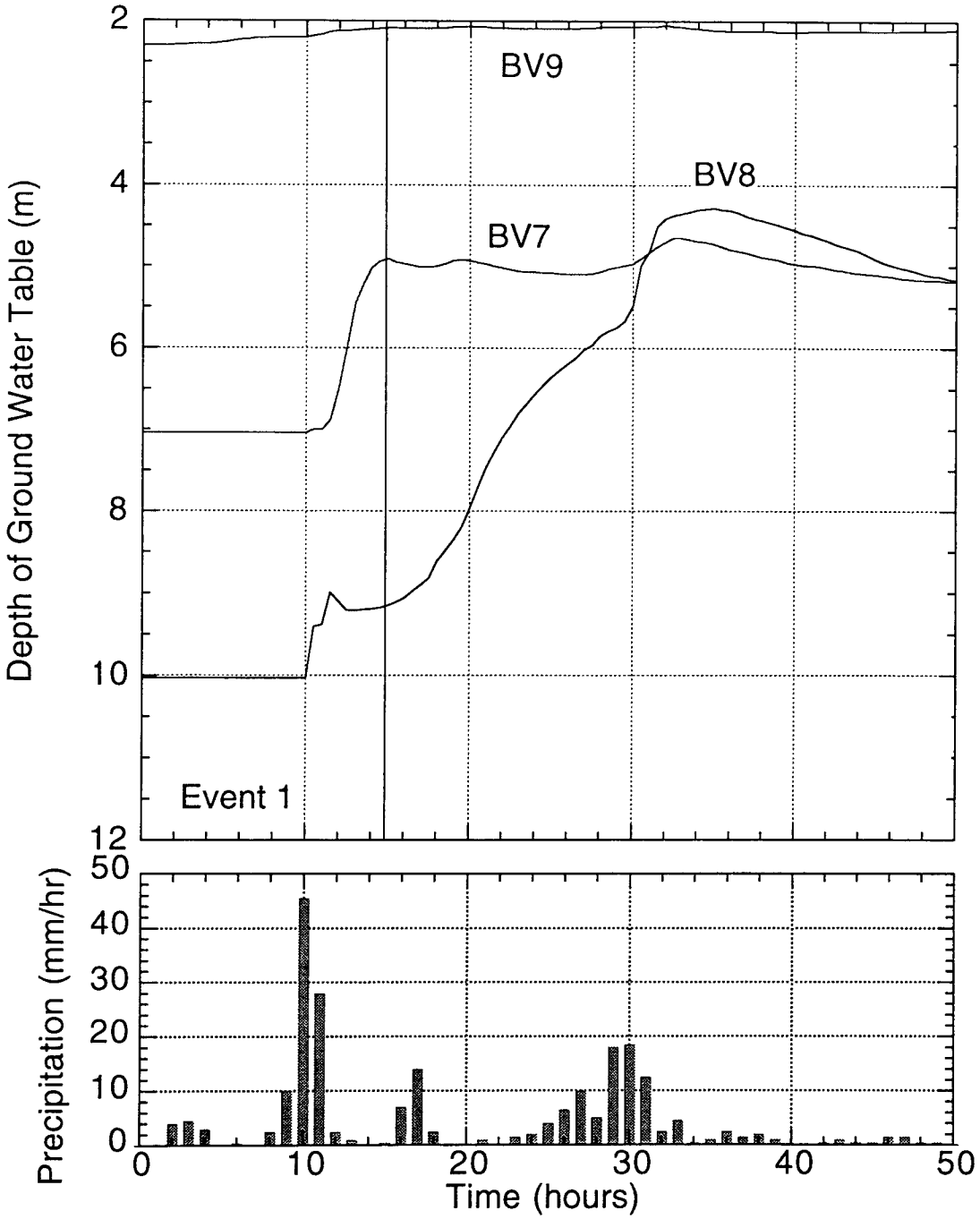

Fig. 22. Depth of ground water table used for the FEM analysis calculated from observed pore pressure at the slip surface.

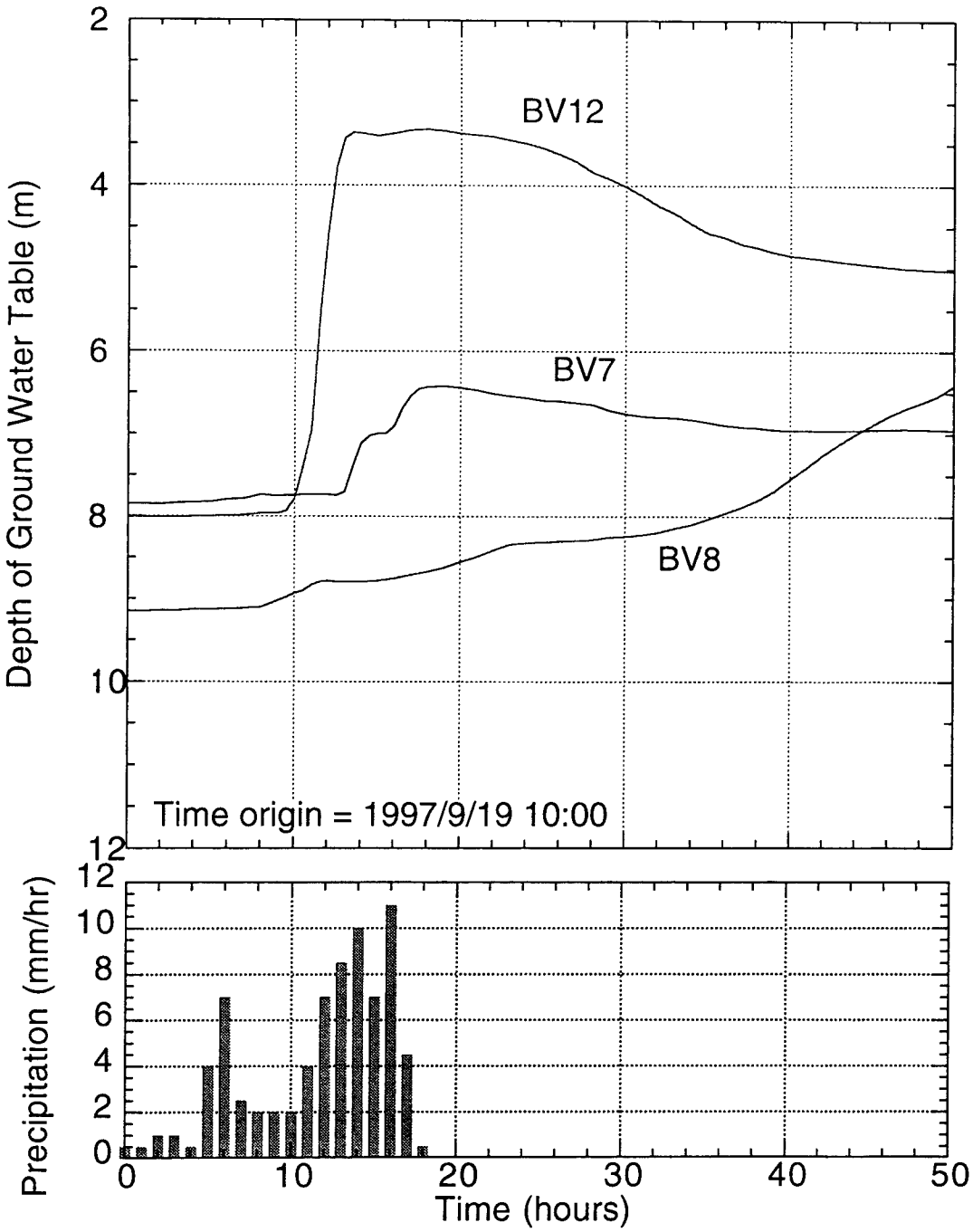

Fig. 23. Depth of ground water table observed in September 1997, after installation of BV 12.

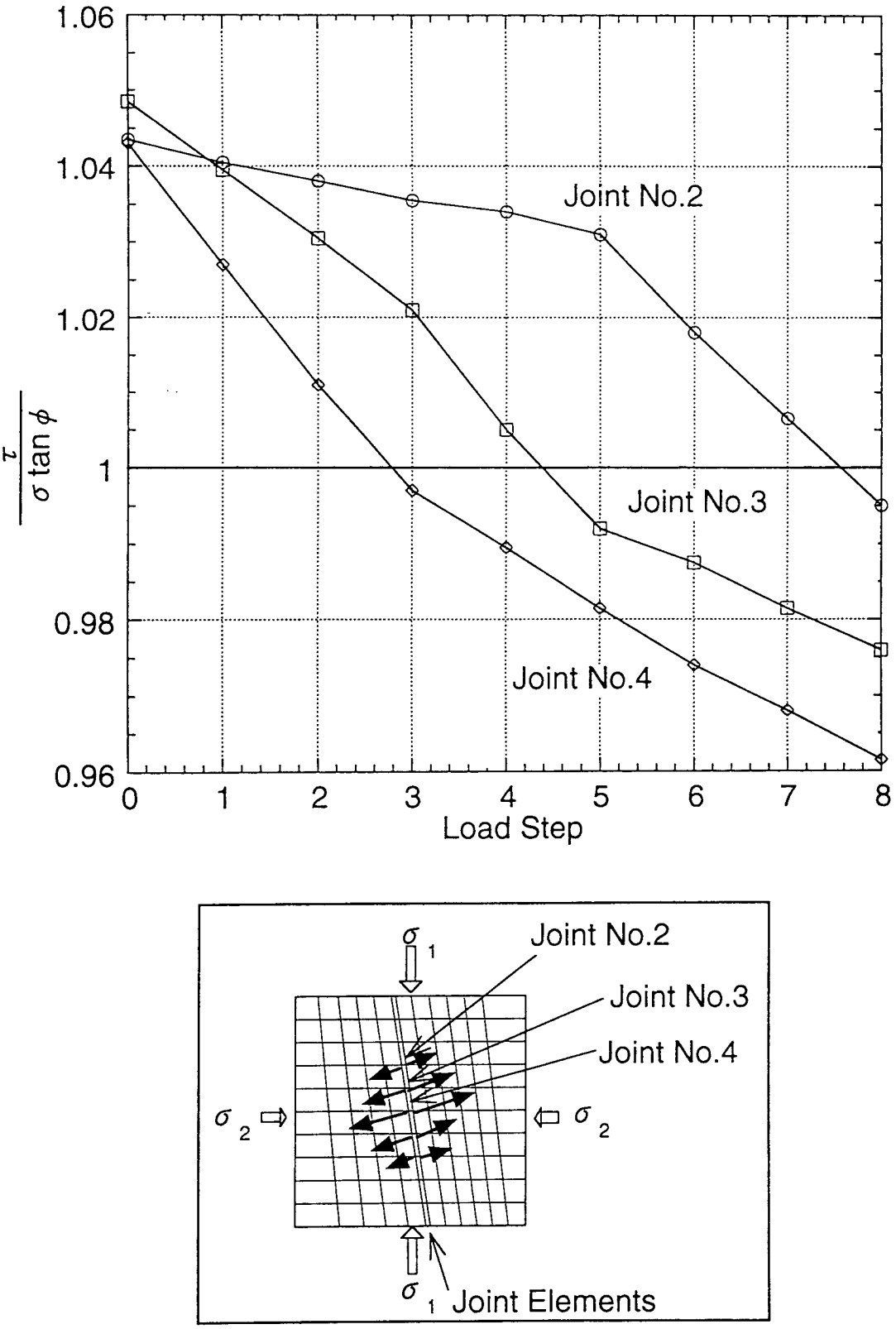

Fig. 24. Result of preliminary test, lower figure shows structure of soil and applied force, upper diagram shows decrease in LSF with load step.

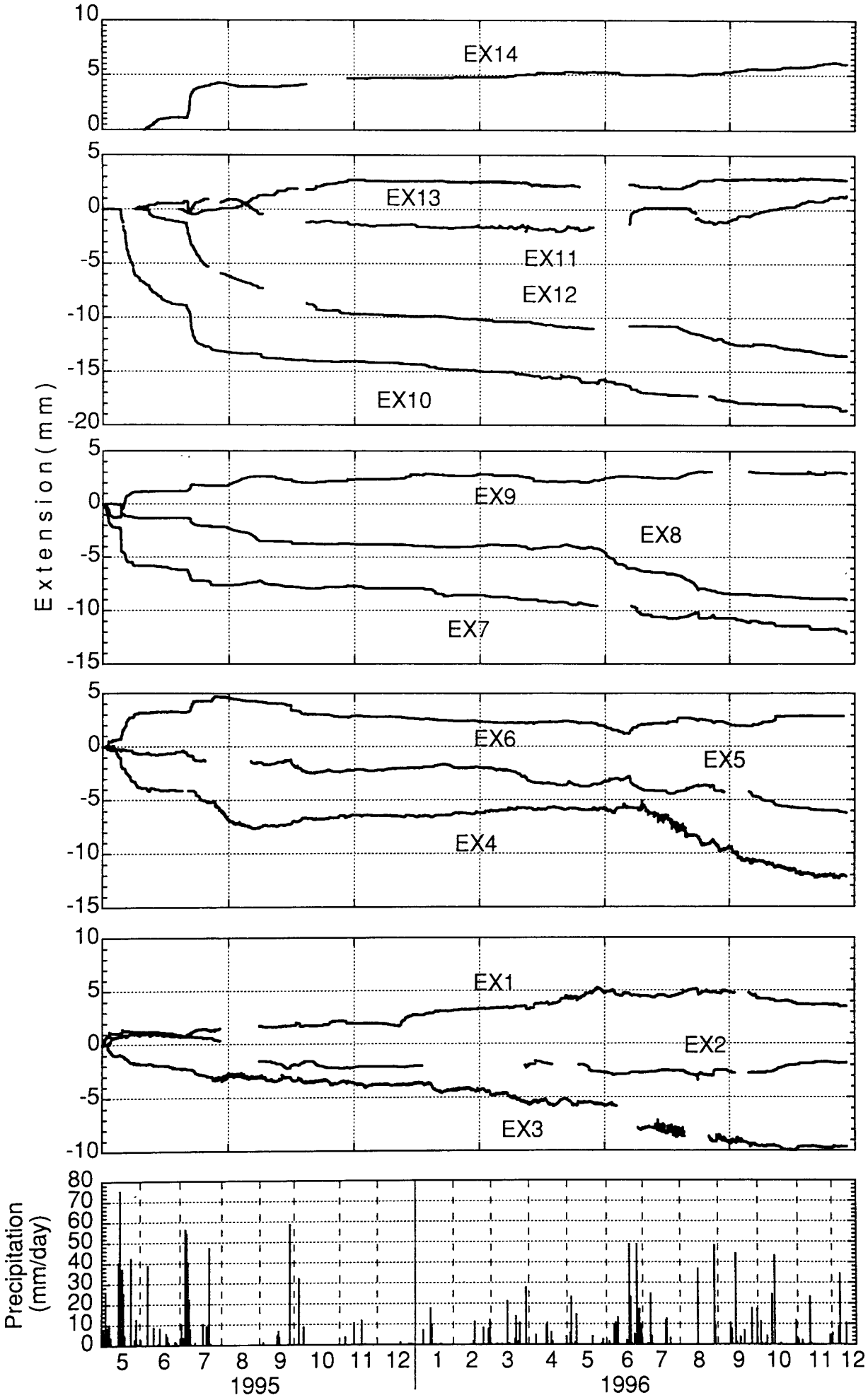

Fig. 25. Result of measurements of extensometers in the Todoroki landslide from 1995/4/28 to 1996/12/11.

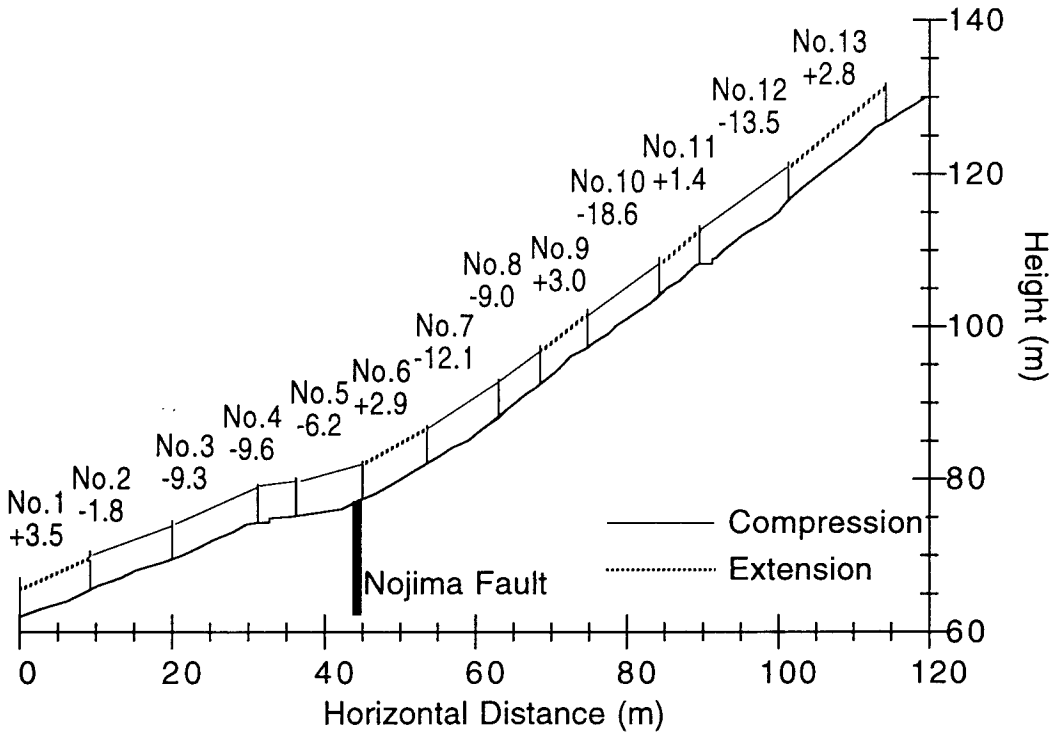

Fig. 26. Distribution of extensive / compressive surface strain.

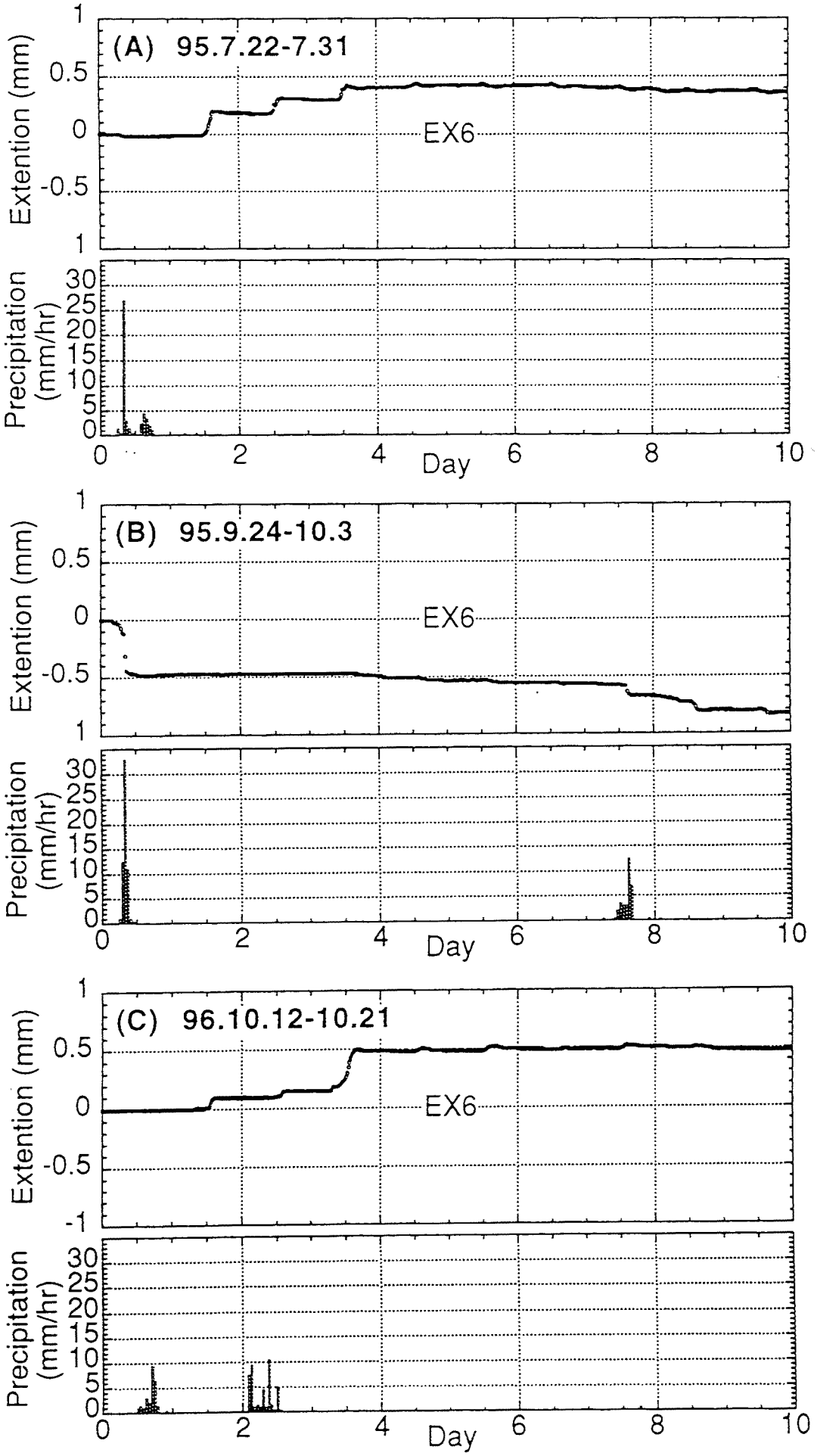

Fig. 27. Variation in EX 6 in three distinct events.

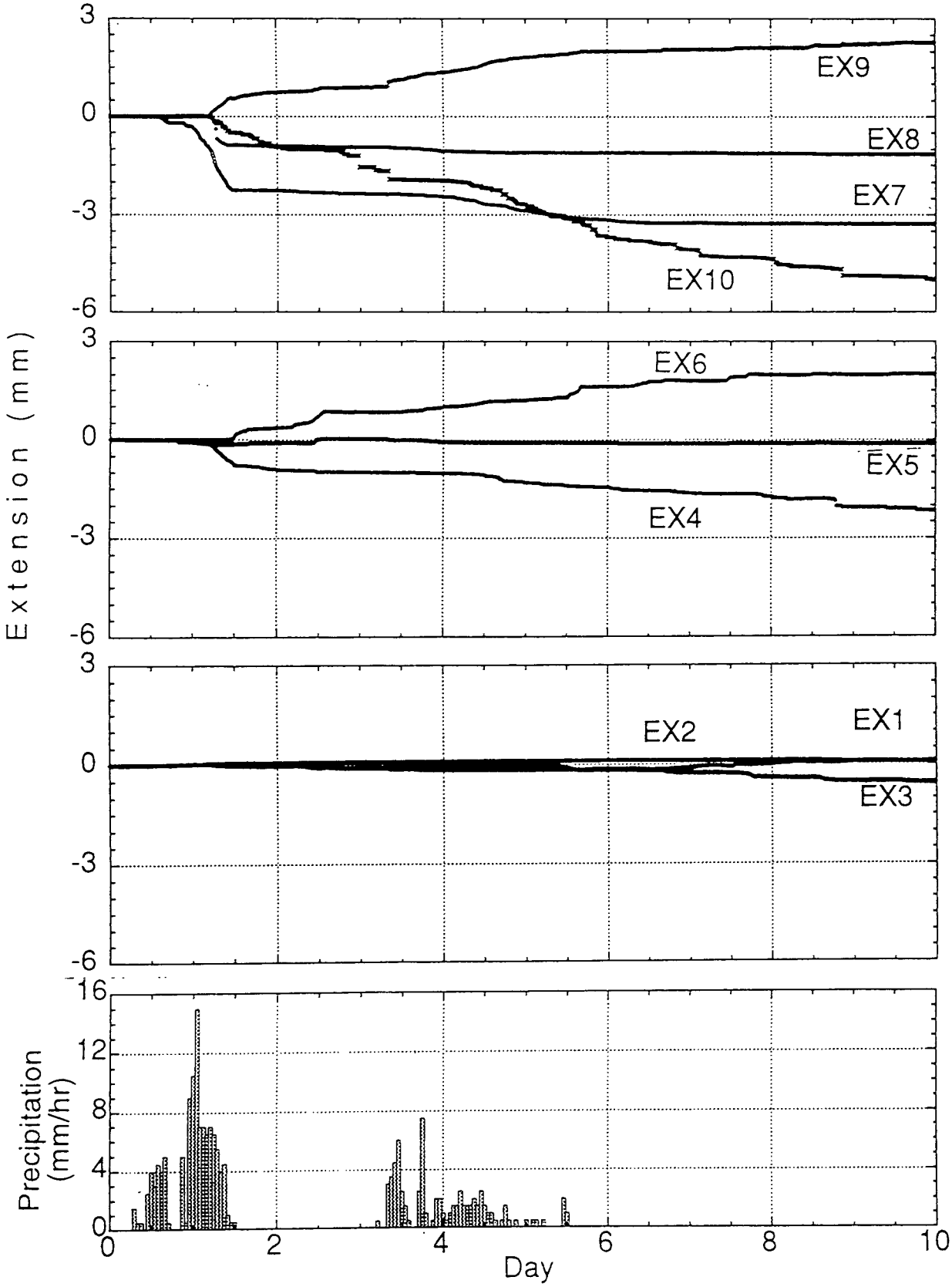

Fig. 28. Variations in EXs in the period of 1995/5/11-20.

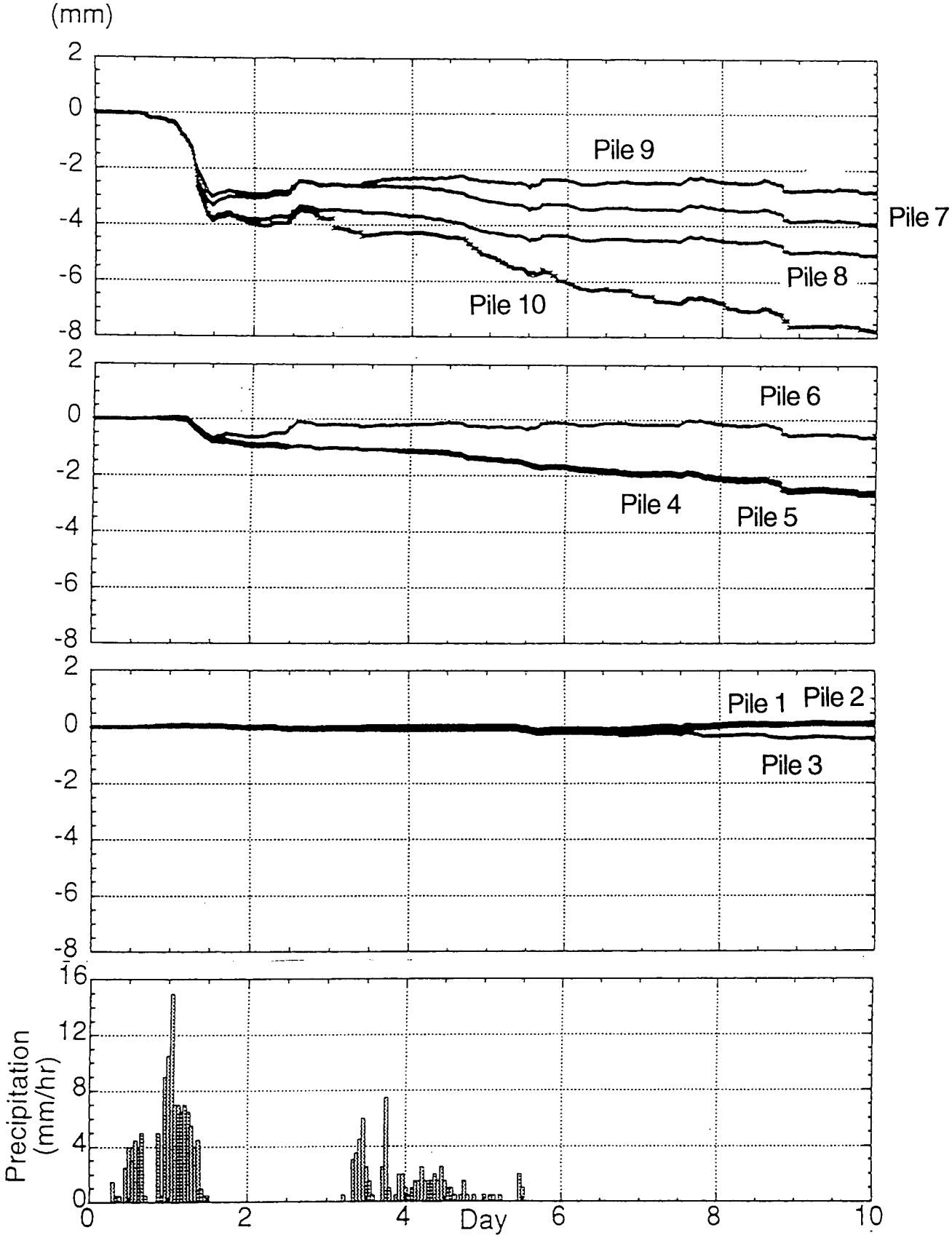

Fig. 29. Variation in the distance from the bottom end of survey line to each pile calculated from Fig. 28.

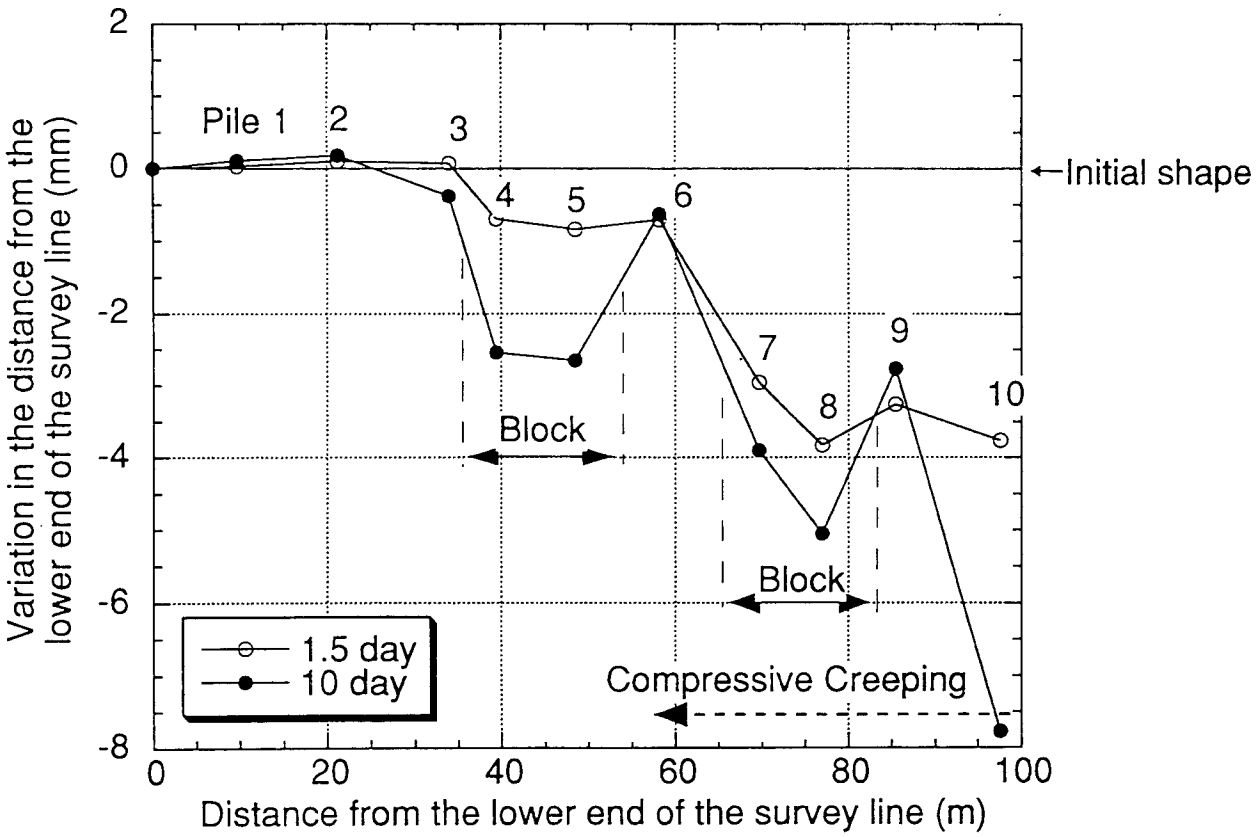

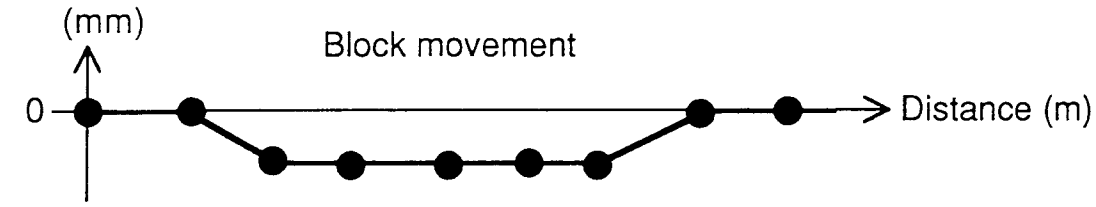

Variation in the distance from the lower end of the survey line

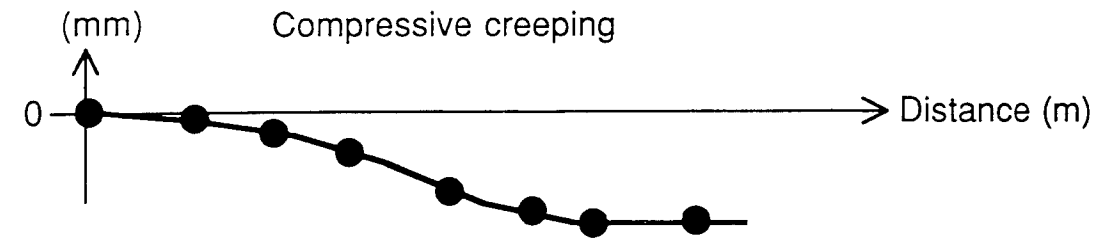

Variation in the distance from the lower end of the survey line

Fig. 30. Distribution of change in the distance from the bottom end of survey line to each pile at 1.5 (days) and at 10 (days) and definition of "block movement" and "compressive creeping"

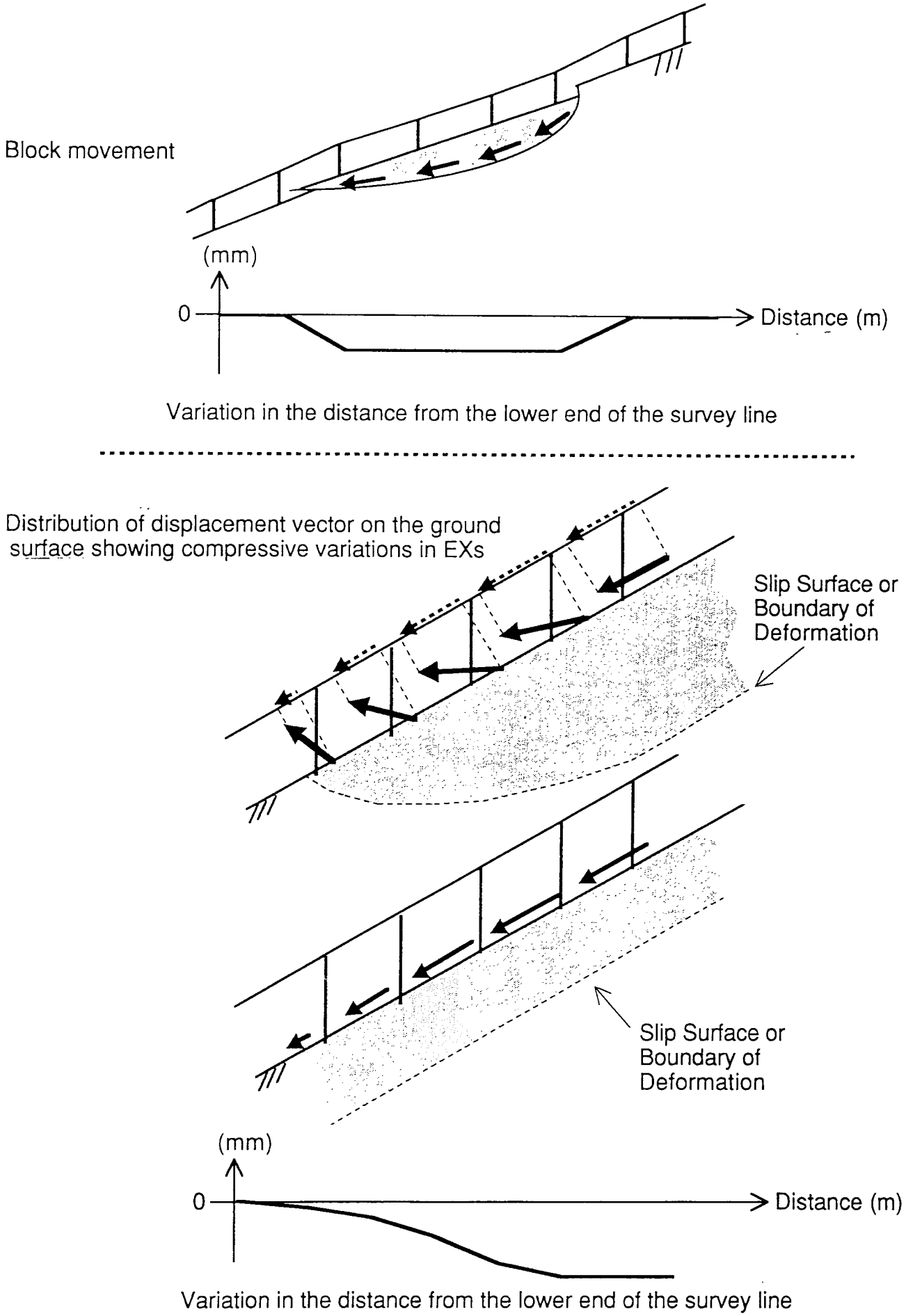

Fig. 31. Models of slope movement and their results in variation in the distance from the lower end of the survey line, the upper is represent block movement and the lower two represent compressive creeping.

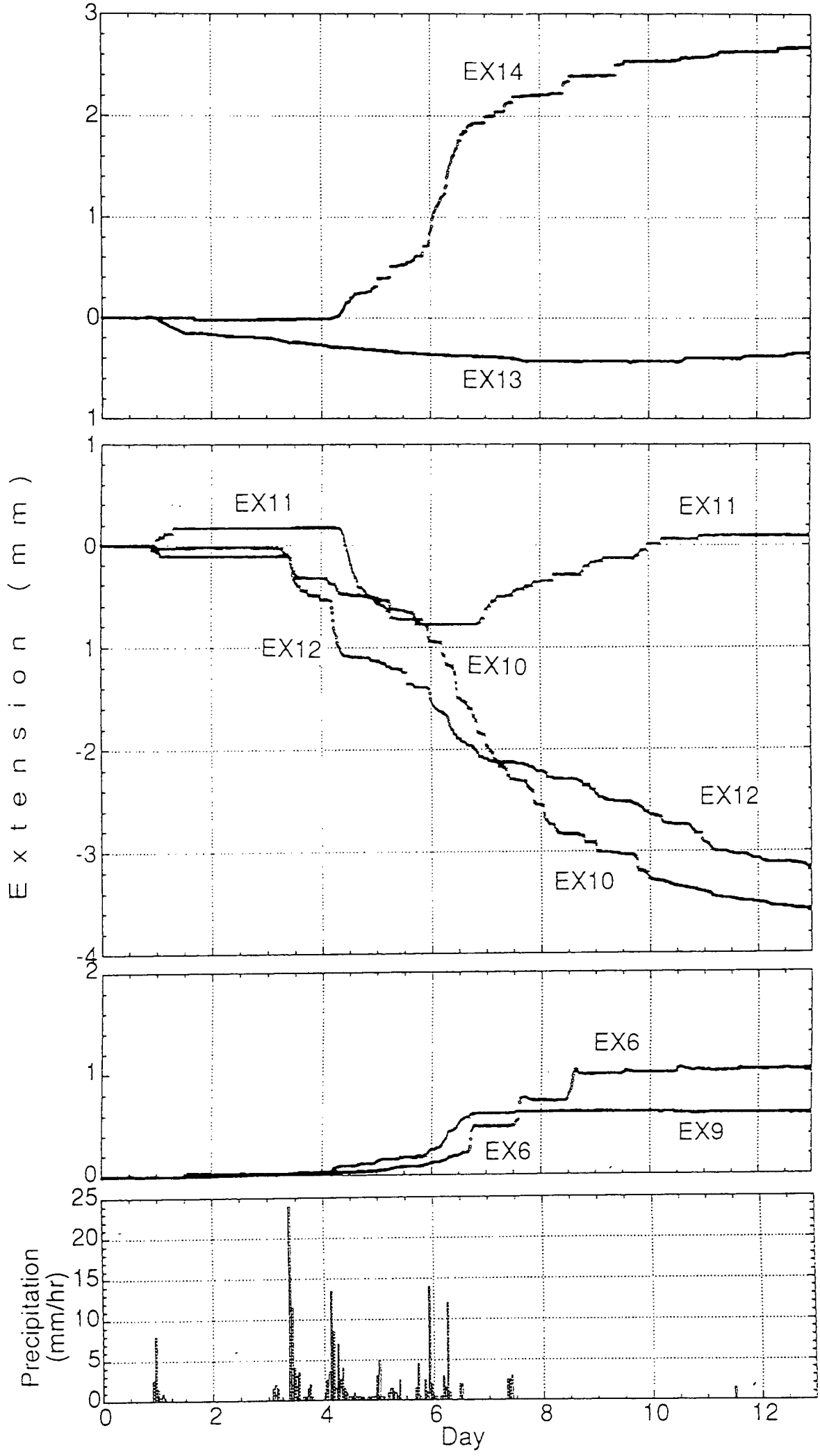

Fig. 32. Variations in EXs in upper part of the survey line in the period of 1995/6/30- 7/14.

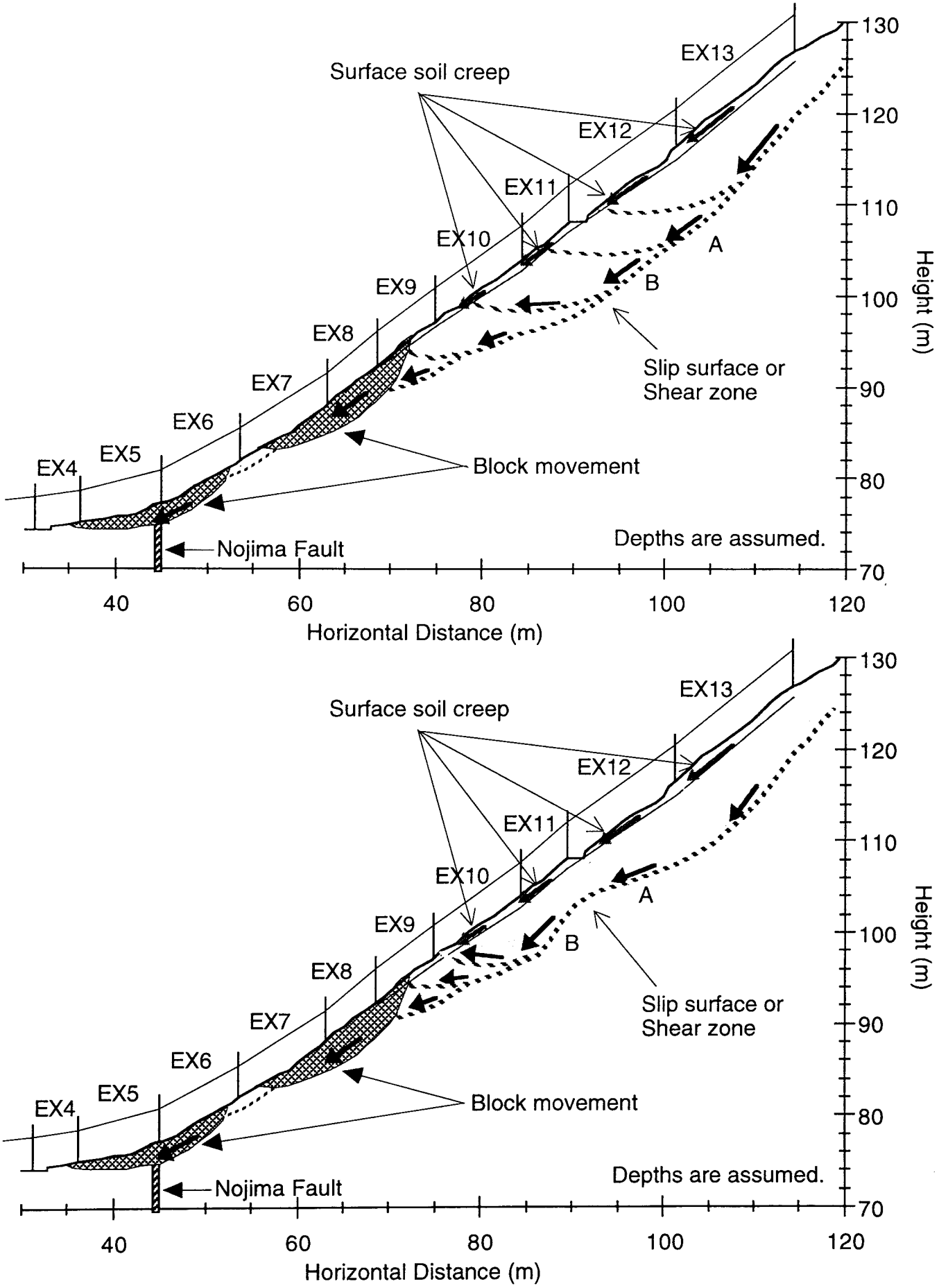

Fig. 33. Two possible models of the Todoroki landslide. The upper model explains propagation of active area observed in EX 11 as a result of relative movement of two blocks. The lower explains it as a result of shape of slip surface.

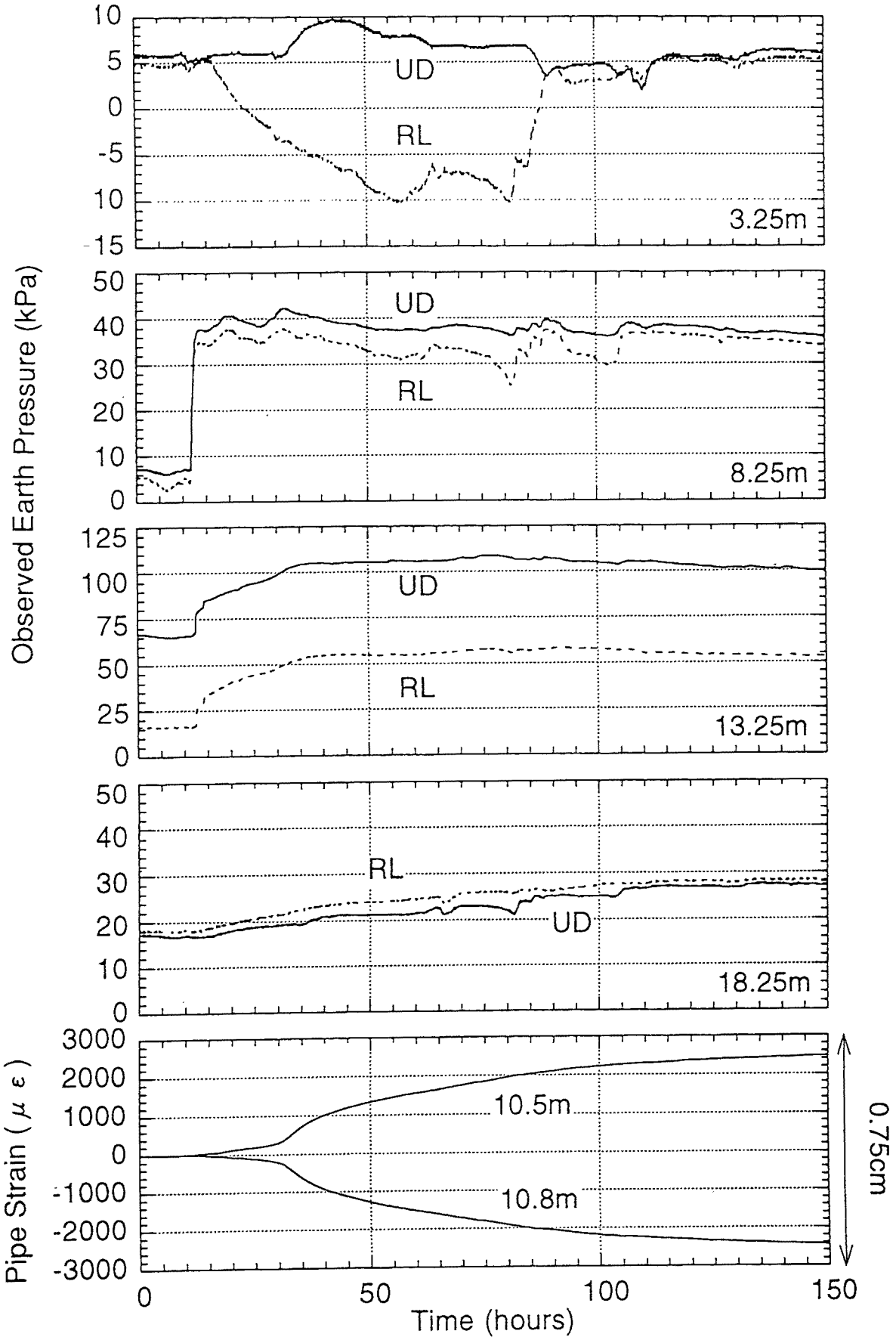

Fig. 34. Earth pressure in BV 4 (upper 4 diagrams) and pipe strain at the slip surface in BV 4 (bottom diagram) during Event 1.

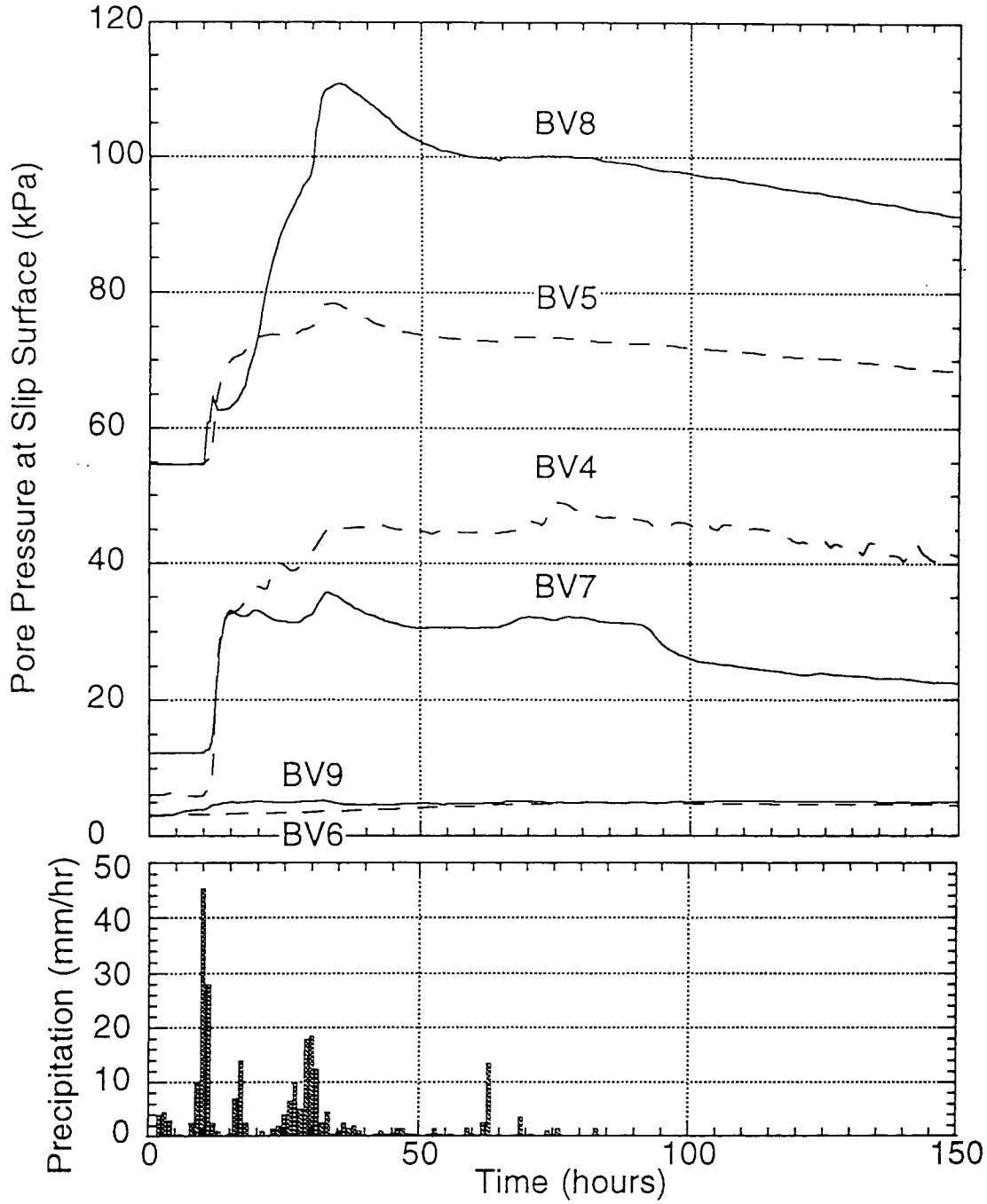

Fig. 35. Pore water pressures at the slip surface during Event 1 and hourly precipitation.

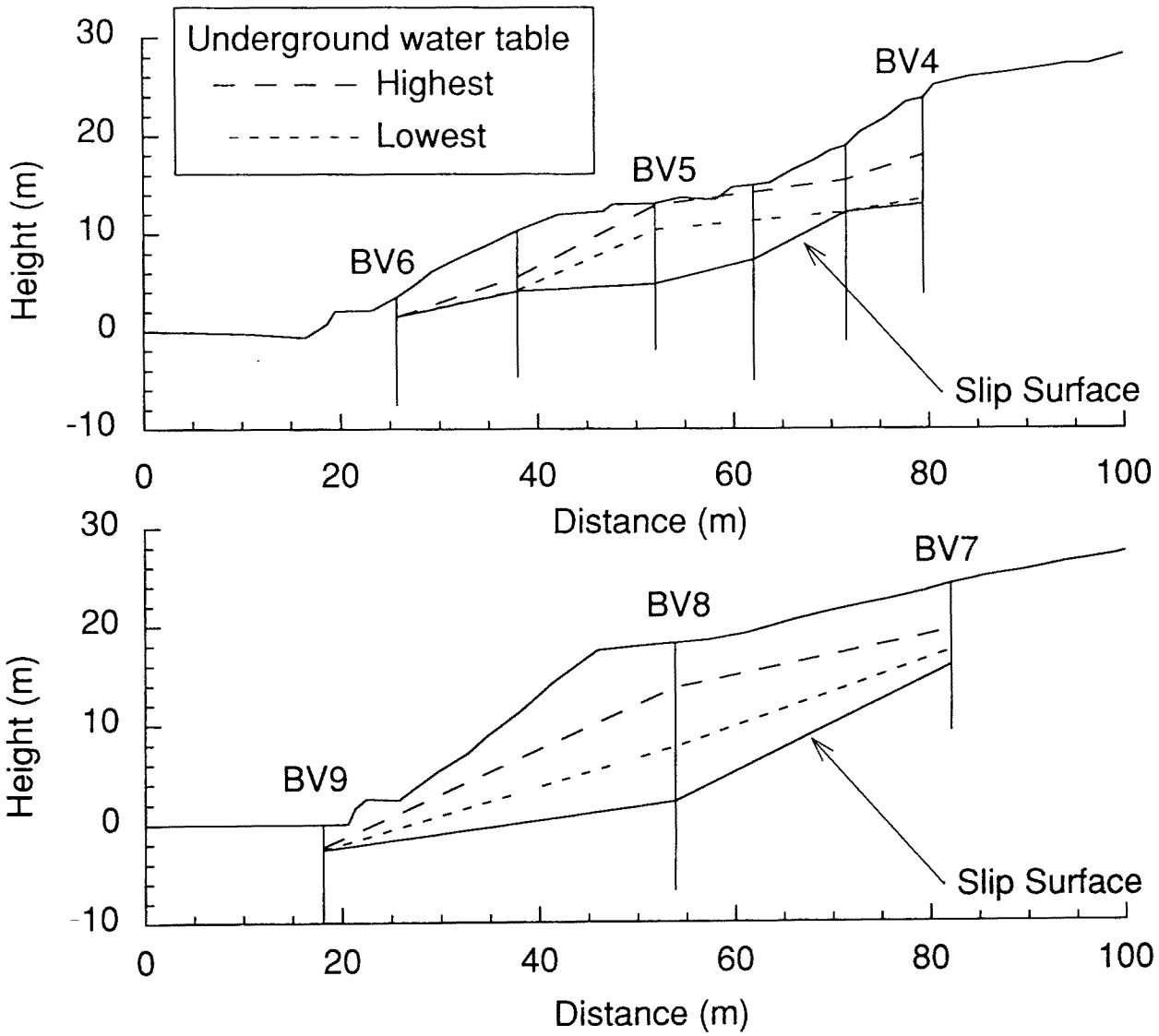

Fig. 36. Calculated highest and lowest ground water table during Event 1.

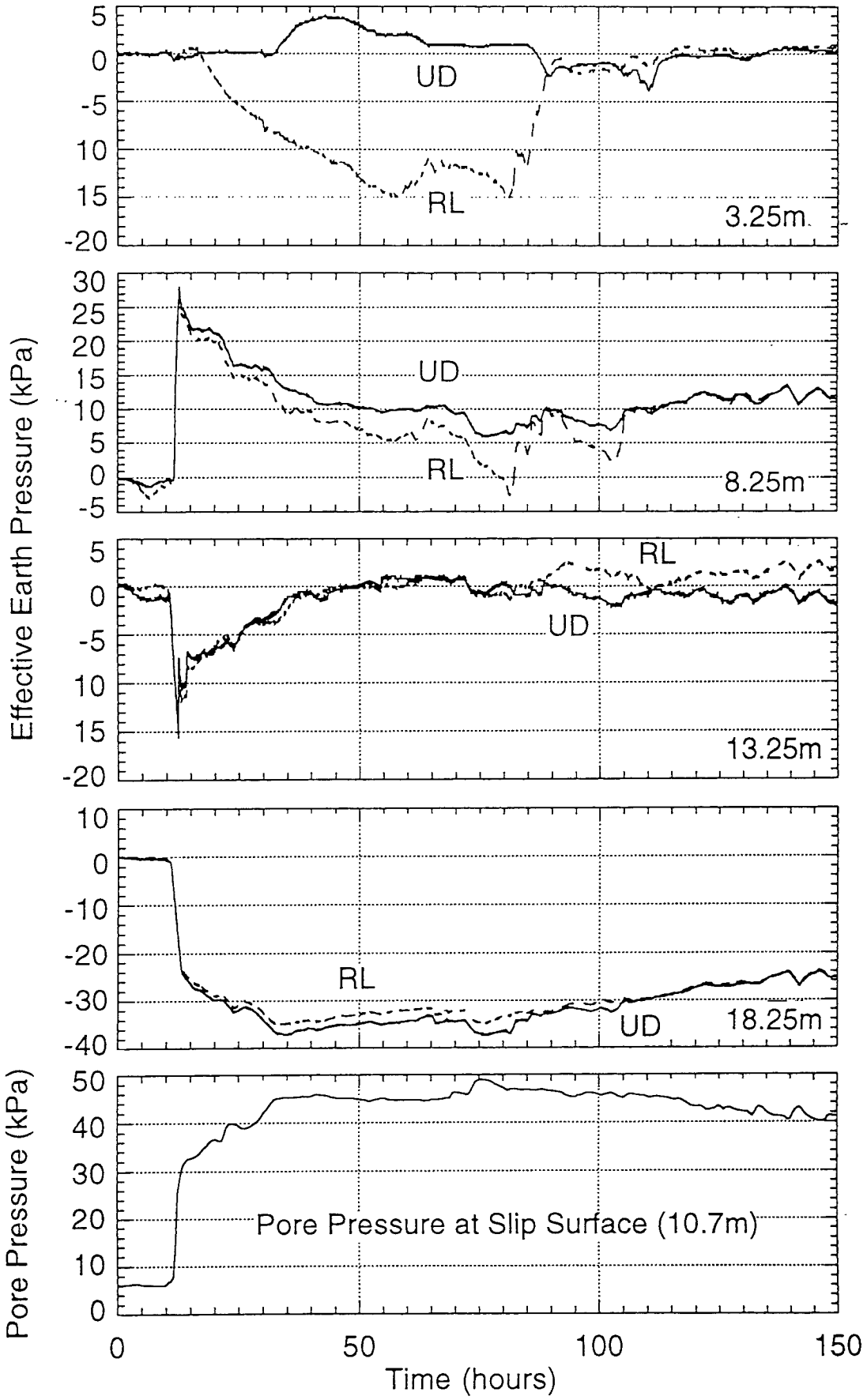

Fig. 37. Effective earth pressure (upper 4 diagrams) and pore water pressure at the slip surface in BV 4 (bottom diagram) during Event 1.

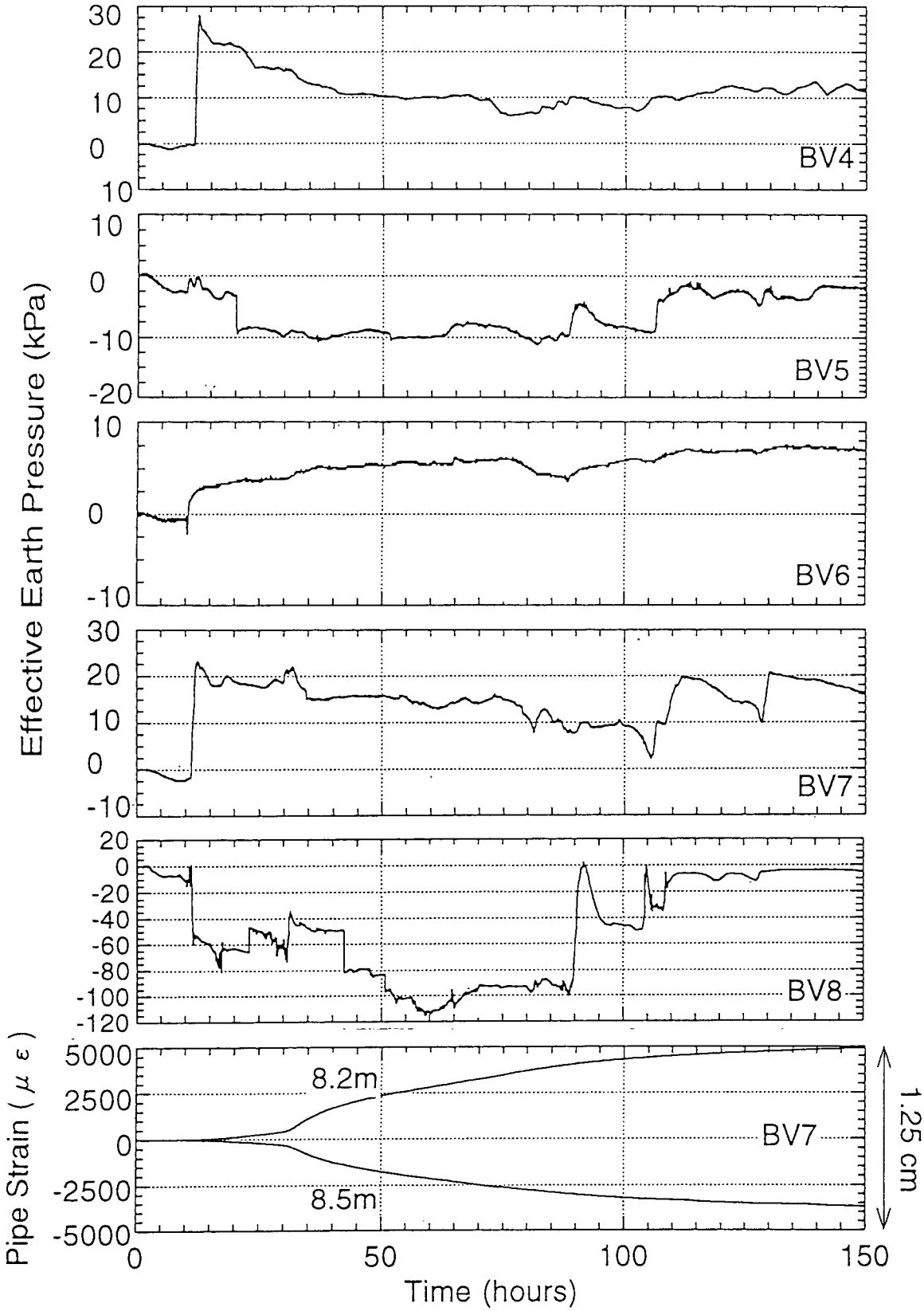

Fig. 38. Variations in the effective earth pressure in the UD direction at the nearest depth above the slip surface in each borehole during Event 1 (upper five diagrams) and pipe strain at the slip surface in BV 7 (bottom diagram).

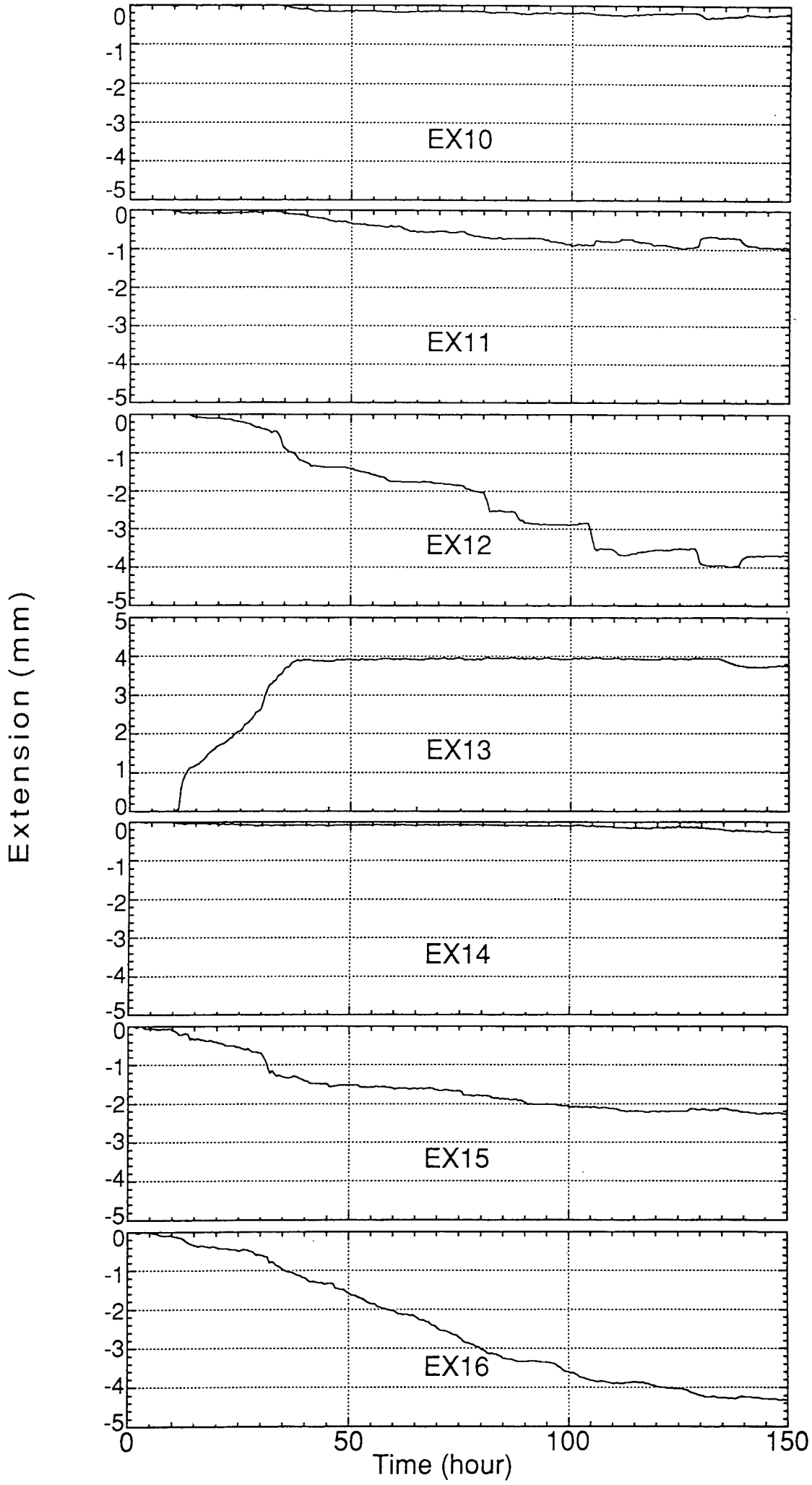

Fig. 39. Results of measurement on EXs during Event 1.

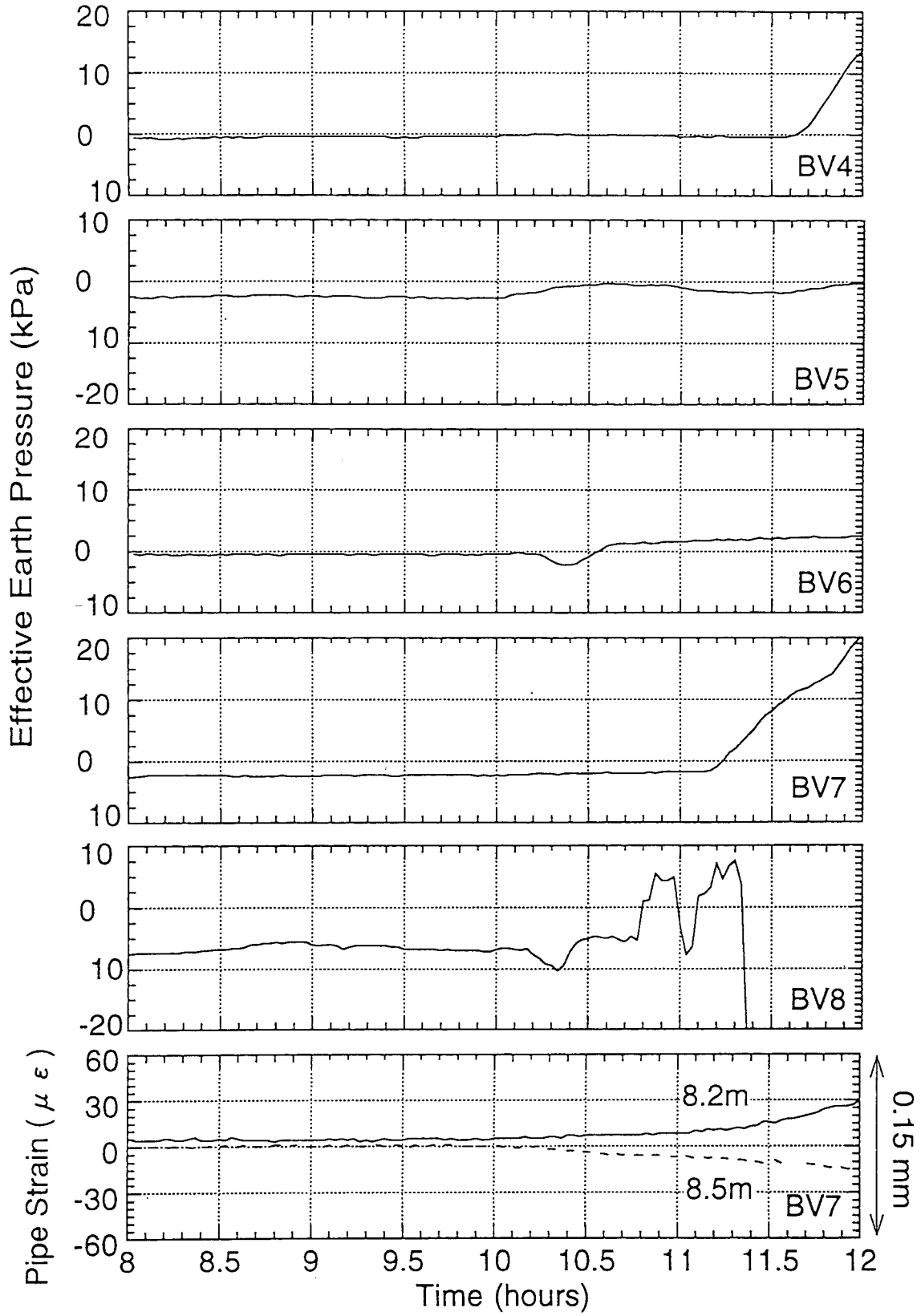

Fig. 40. Variations in the effective earth pressure in the UD direction at the nearest depth above the slip surface at the onset of landslide movement (upper five diagrams) and pipe strain at the slip surface in BV 7 (bottom diagram) during Event 1.

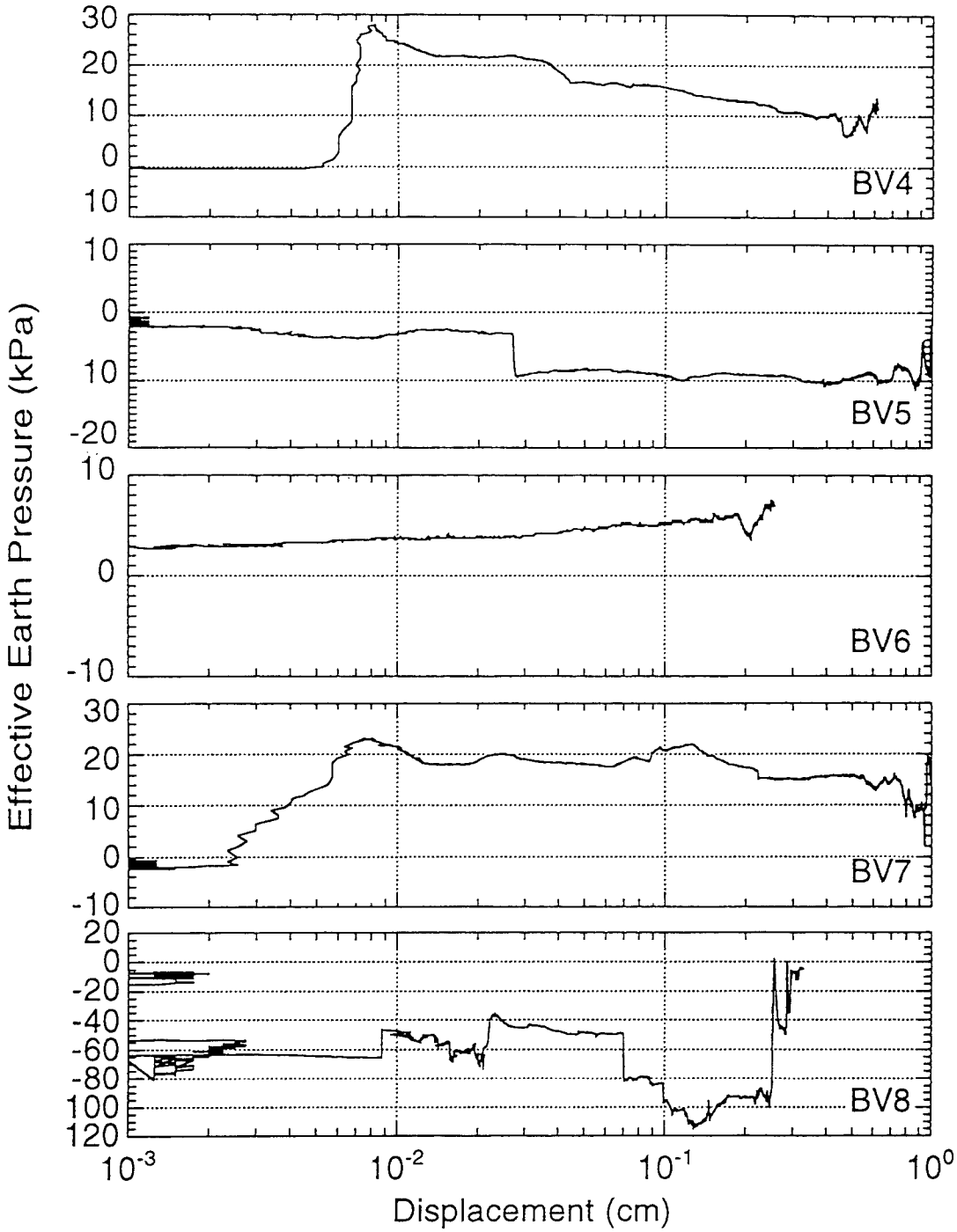

Fig. 41. Relationship between the relative displacement at the slip surface and the effective earth pressure at the nearest depth above the slip surface during Event 1.

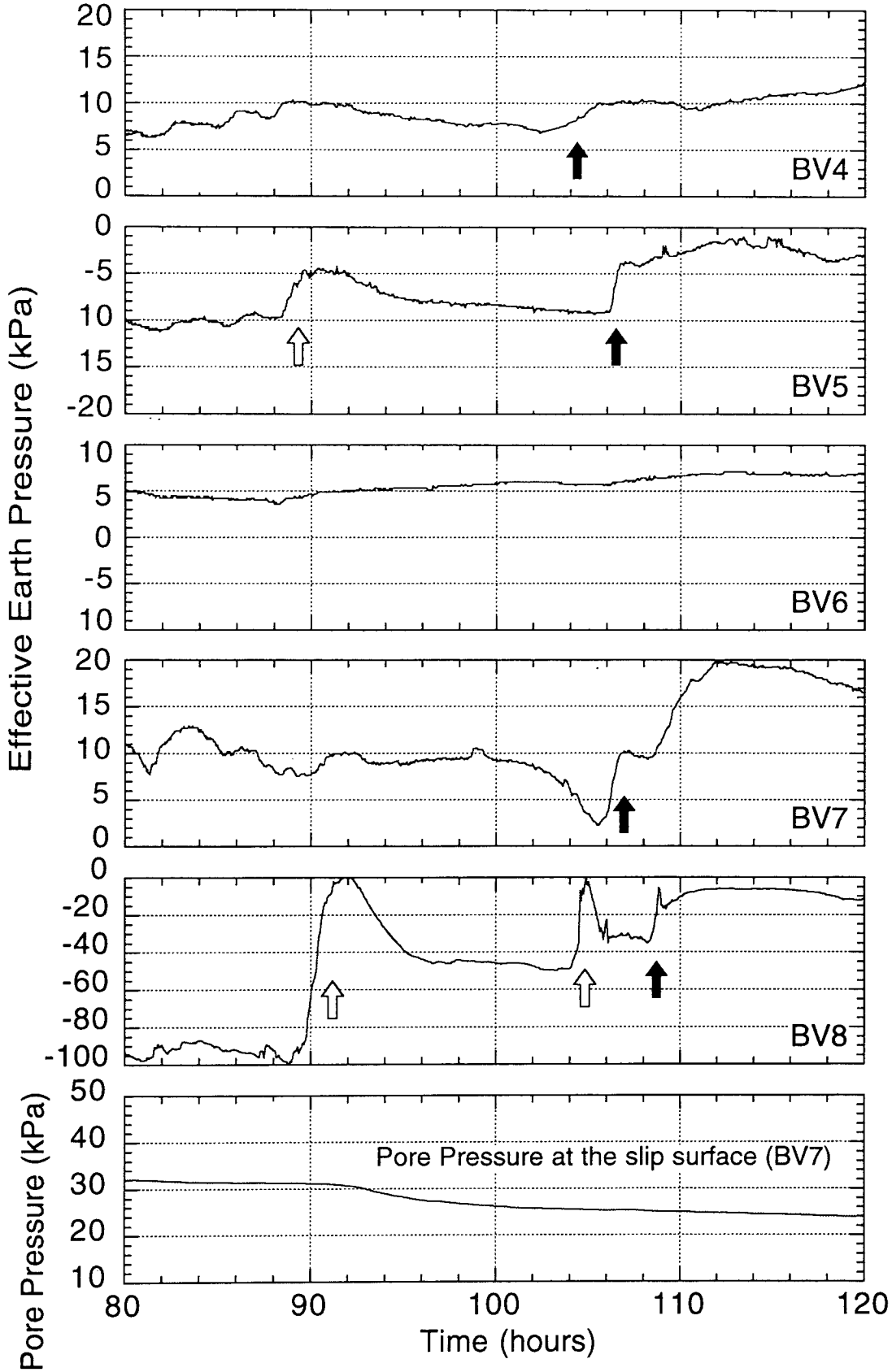

Fig. 42. Variation in the effective earth pressure in the UD direction at the nearest depth above the slip surface and pore pressure at the slip surface in BV 7 at the end of Event 1.

⇧ : "Hesitant behavior" ⬆ : "Stopping phase"

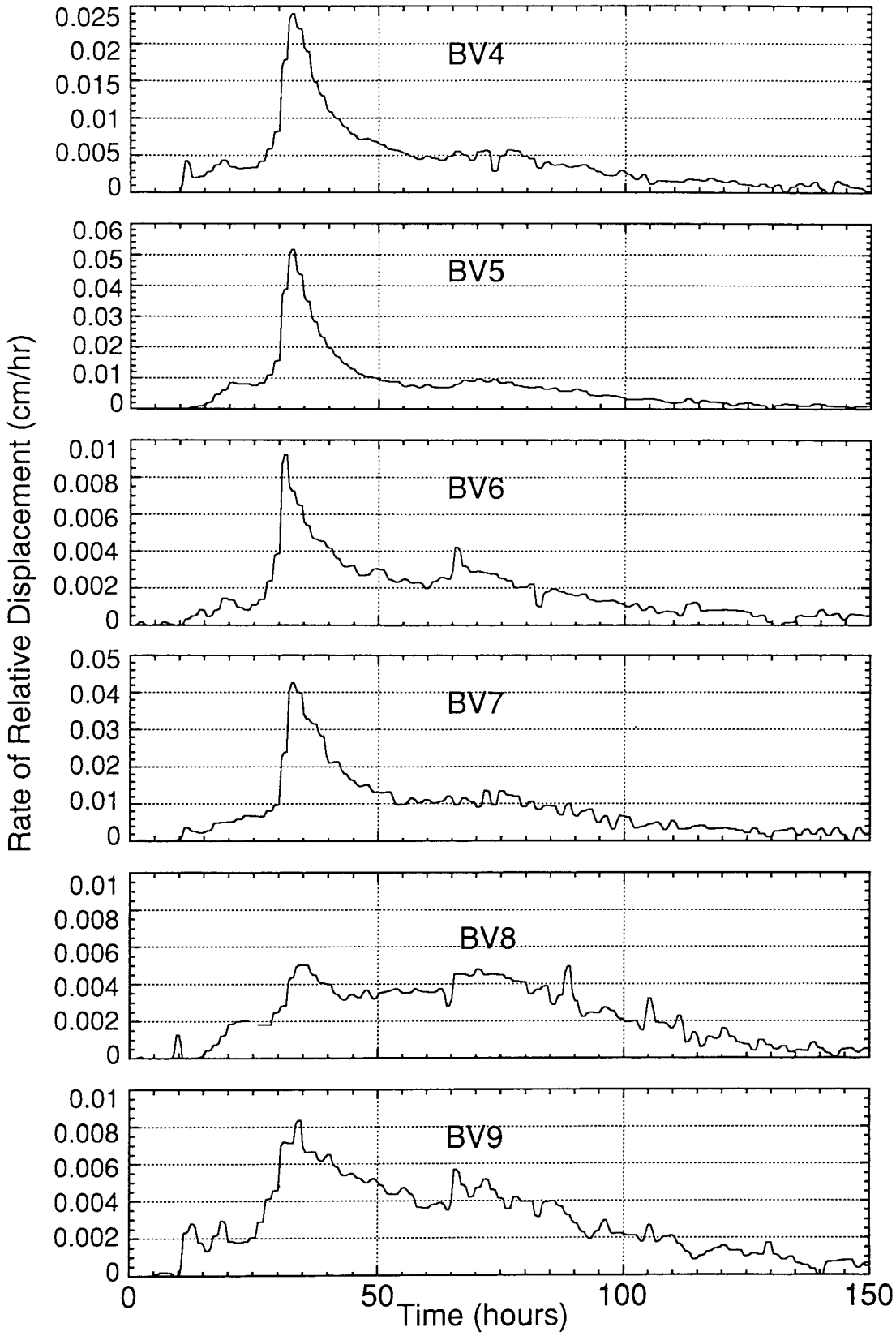

Fig. 43. Variation in rate of relative displacement at the slip surface during Event 1.

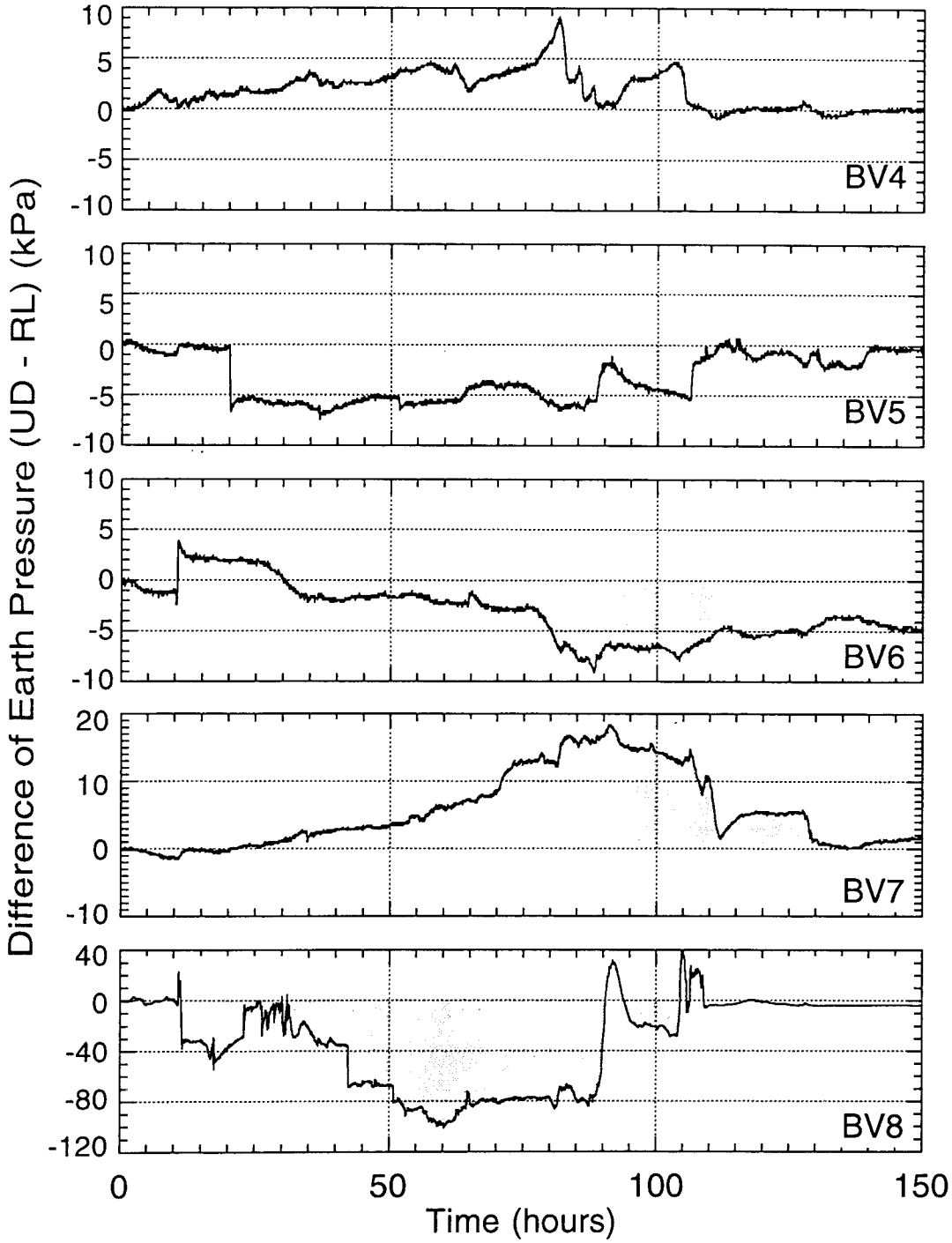

Fig. 44. Variation in difference between earth pressure in the UD and RL directions during Event 1 (UD - RL). Hatched area indicates anistropic variation.

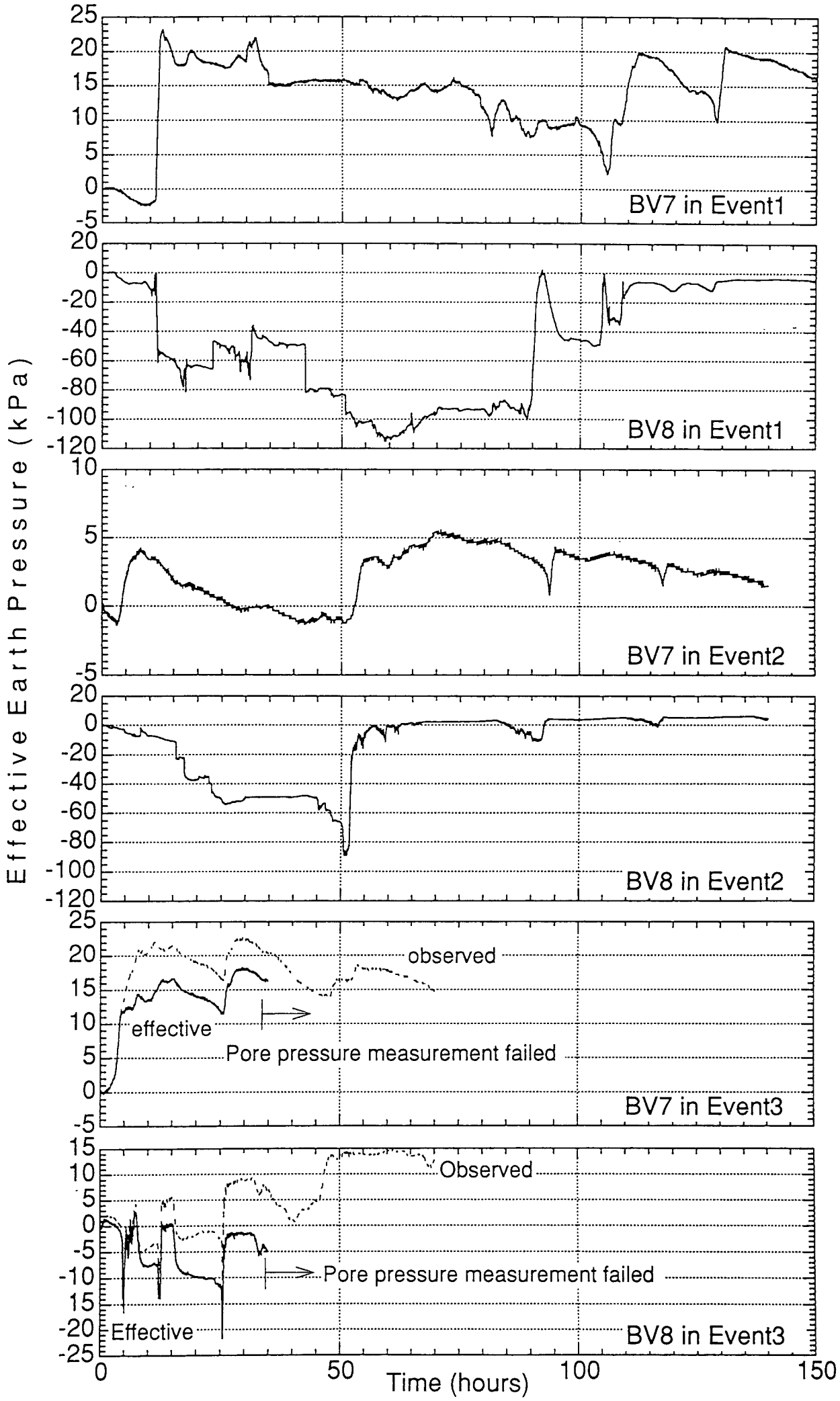

Fig. 45. Variations in the effective earth pressure in BV 7 and 8 during three events.

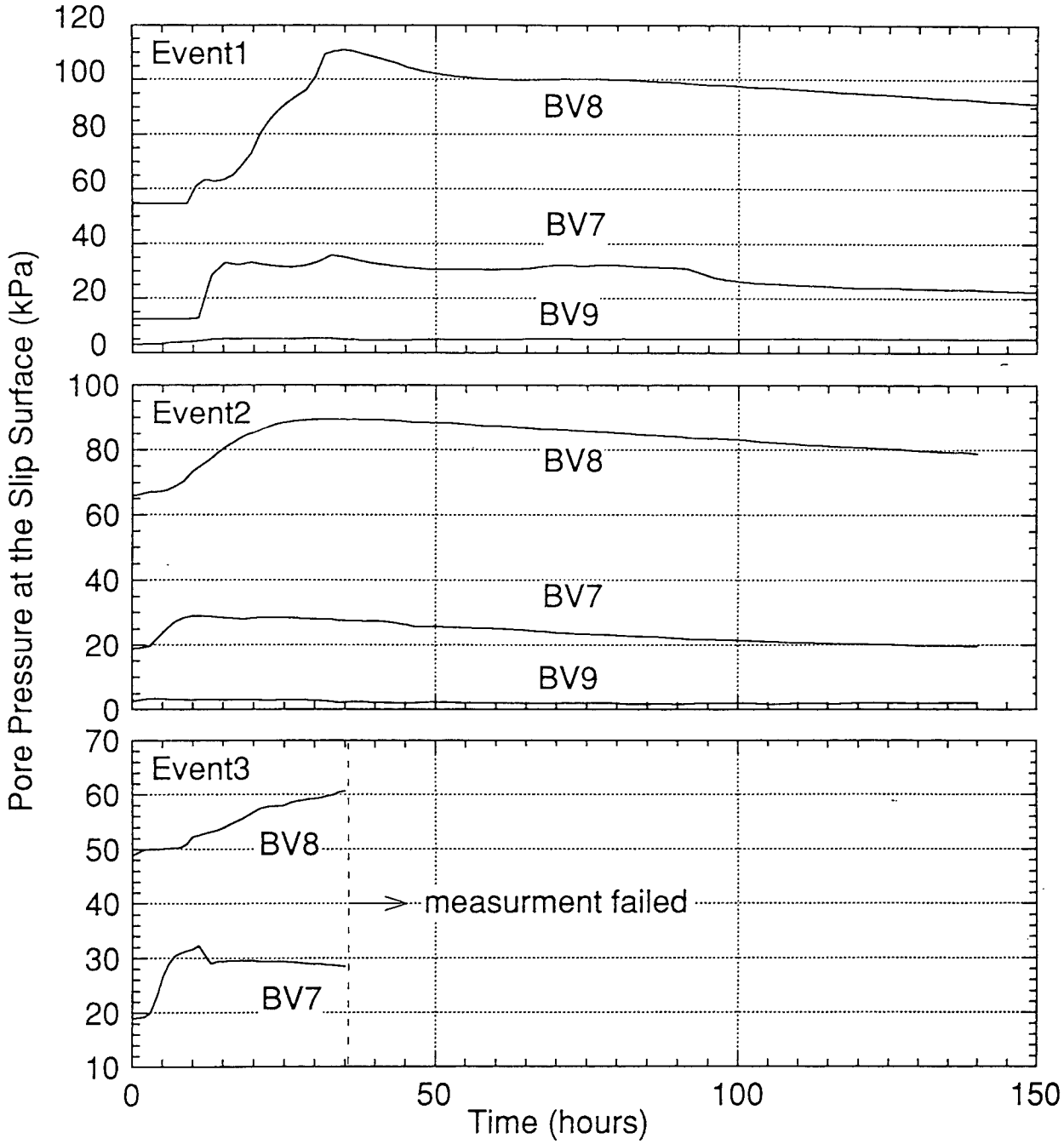

Fig. 46. Pore pressures at the slip surface observed during three events.

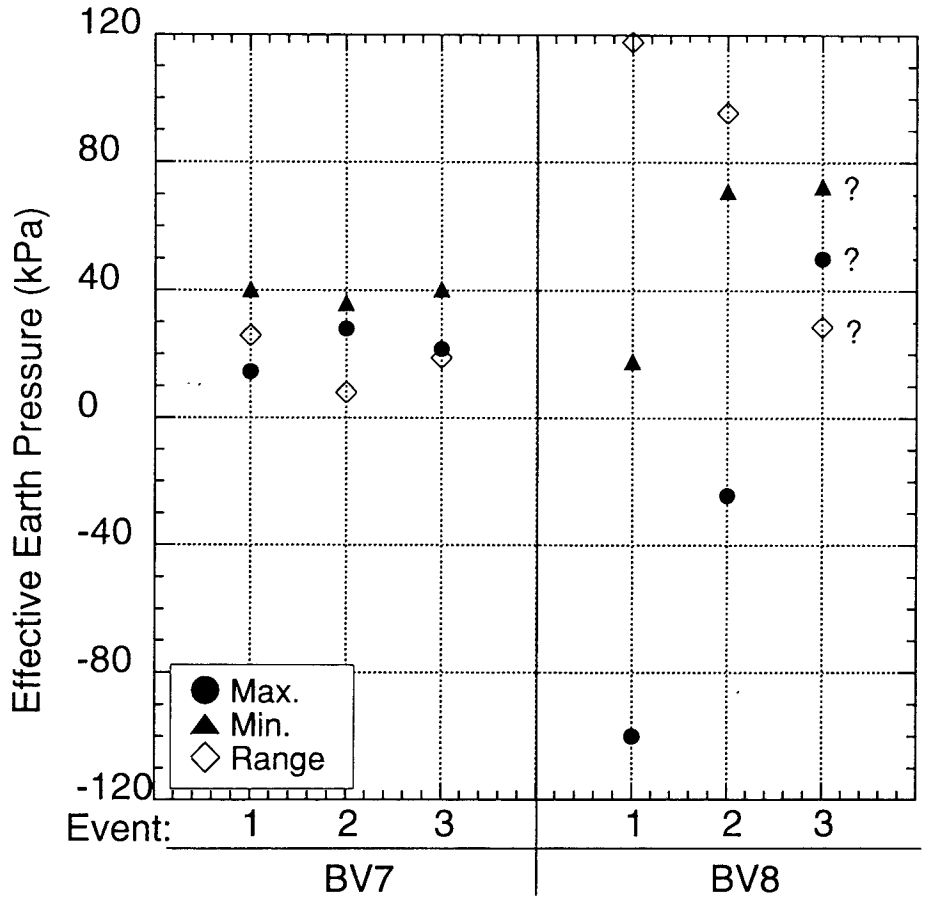

Fig. 47. The maximum and minimum values and the range of variation (the maximum - the minimum value) in the effective earth pressure in BV 7 and 8 for three events.
Pore pressure measurement partially failed in BV 8 during Event 3 (see Fig. 46). Values plotted with "?" were obtained for period when pore pressure was measured (0 to 35 (hrs)).

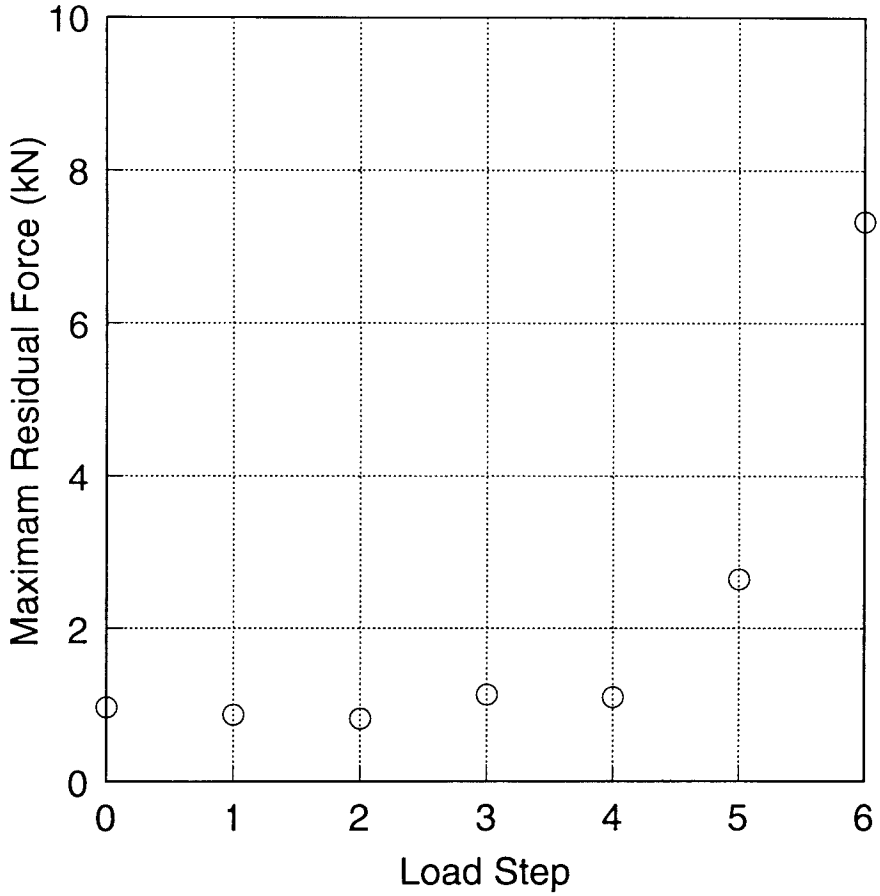

Fig. 48. Increase of the maximum residual force with load step.

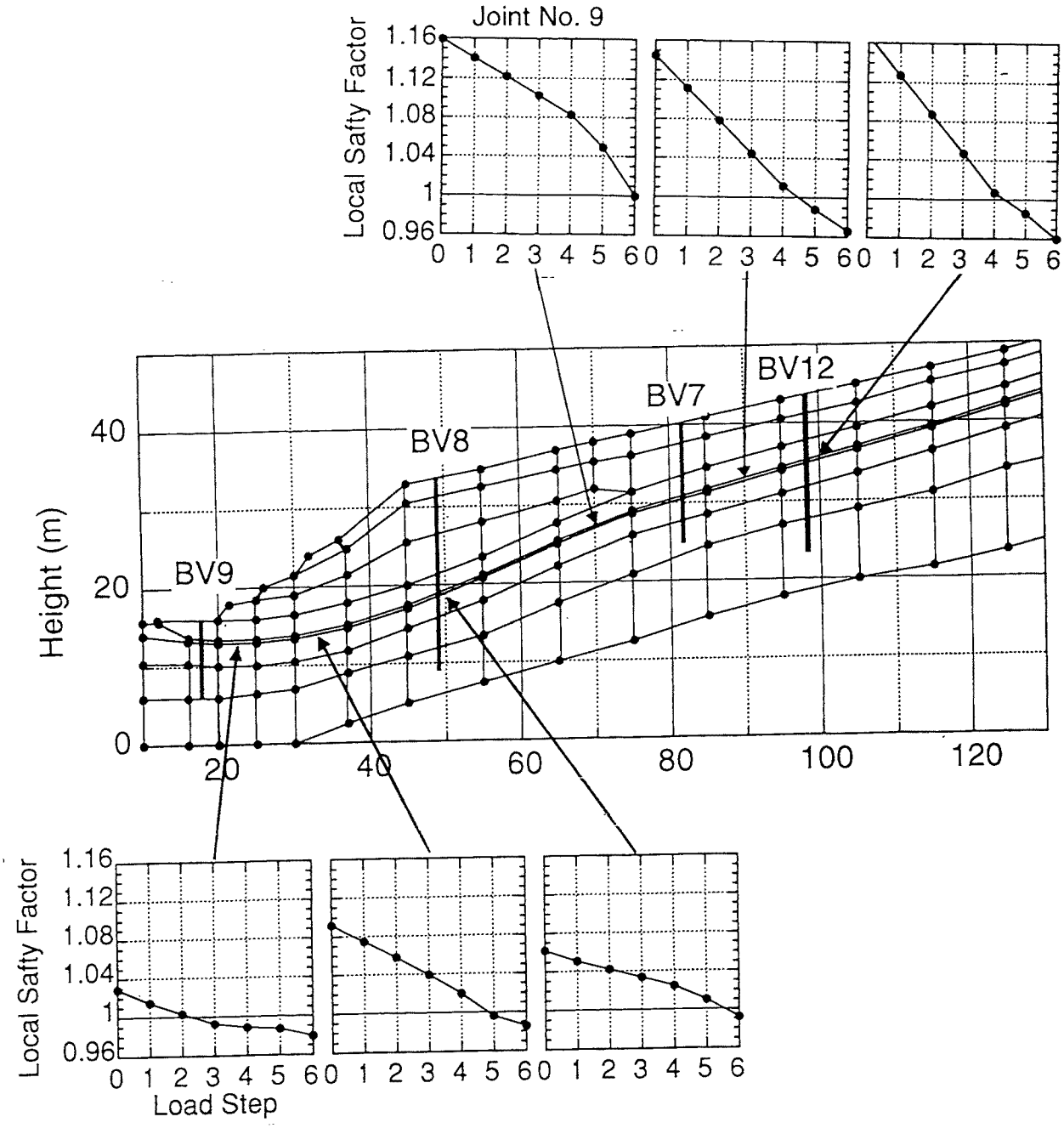

Fig. 49. Distribution of LSF and its variation with load step.

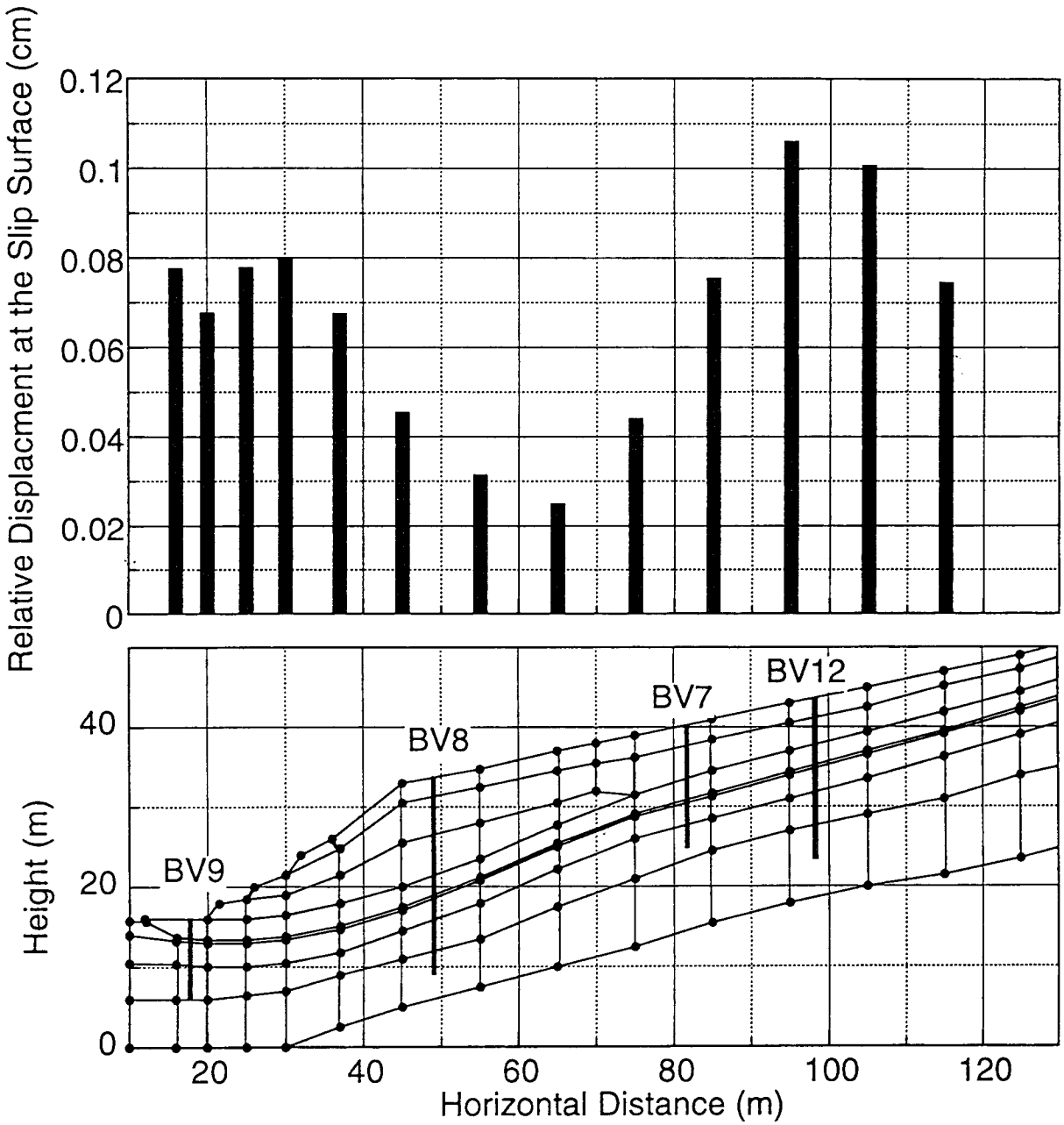

Fig. 50. Distribution of relative displacement at joint elements.

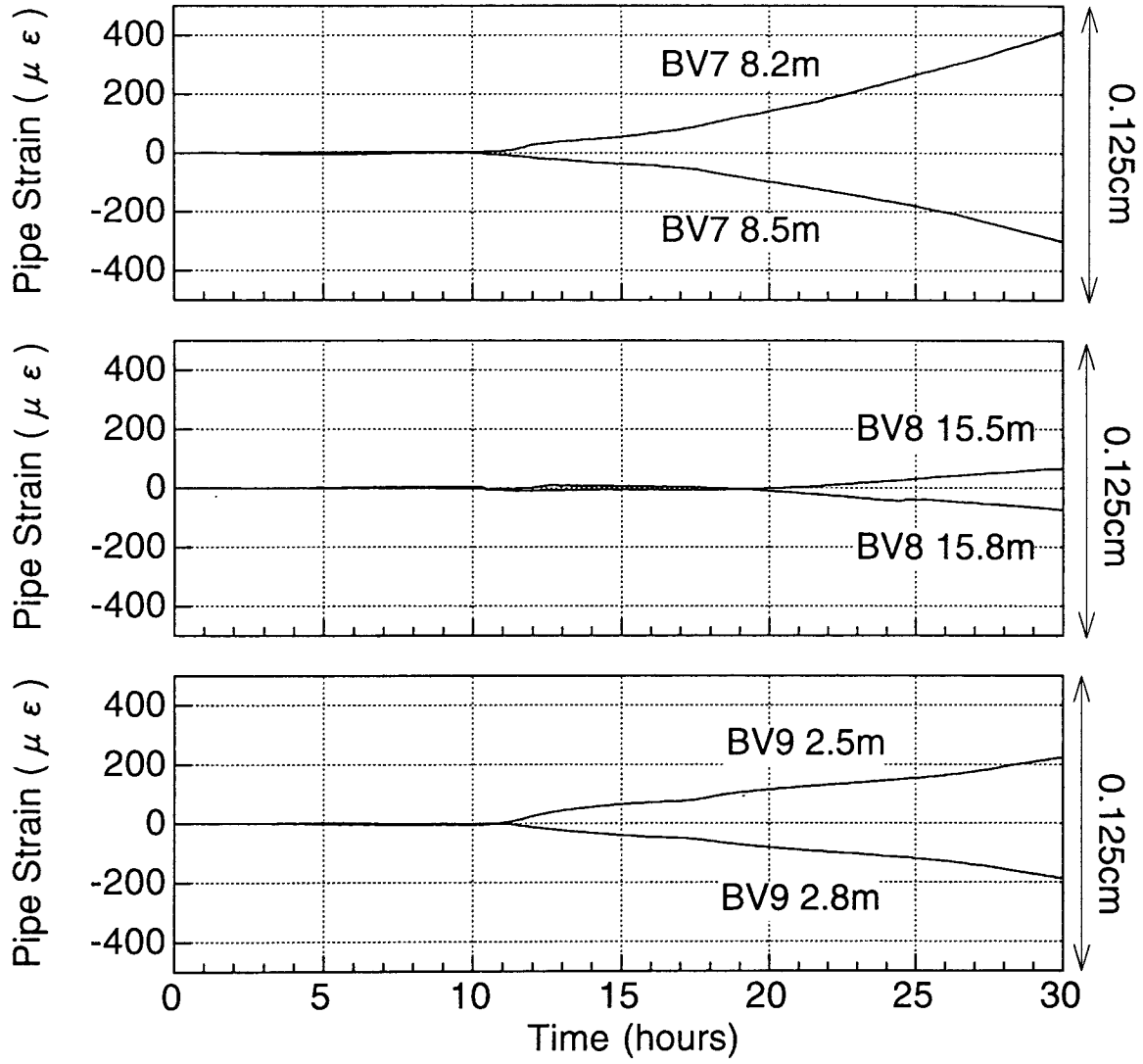

Fig. 51. Pipe strain just above and blow the slip surface in BV 7 to 9 during the initial period of Event 1.

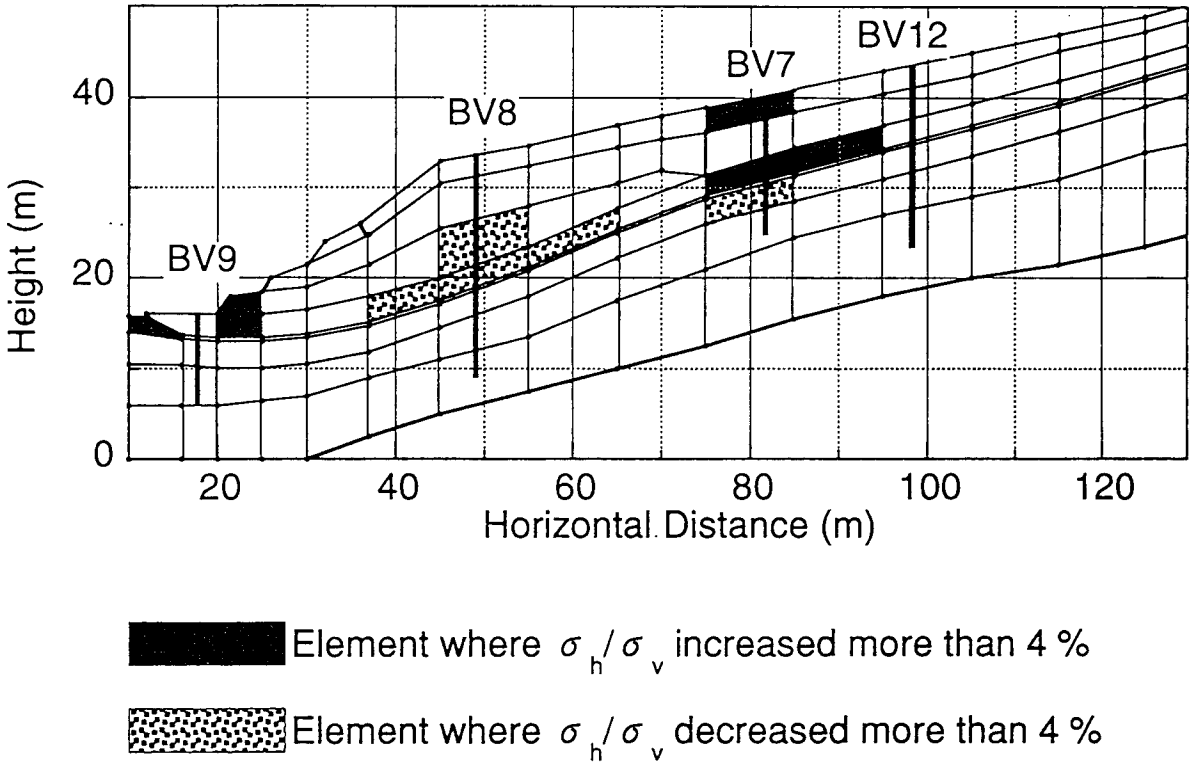

Fig. 52. Distribution of difference in the earth pressure coefficients between at the initial condition and at the end of analysis.

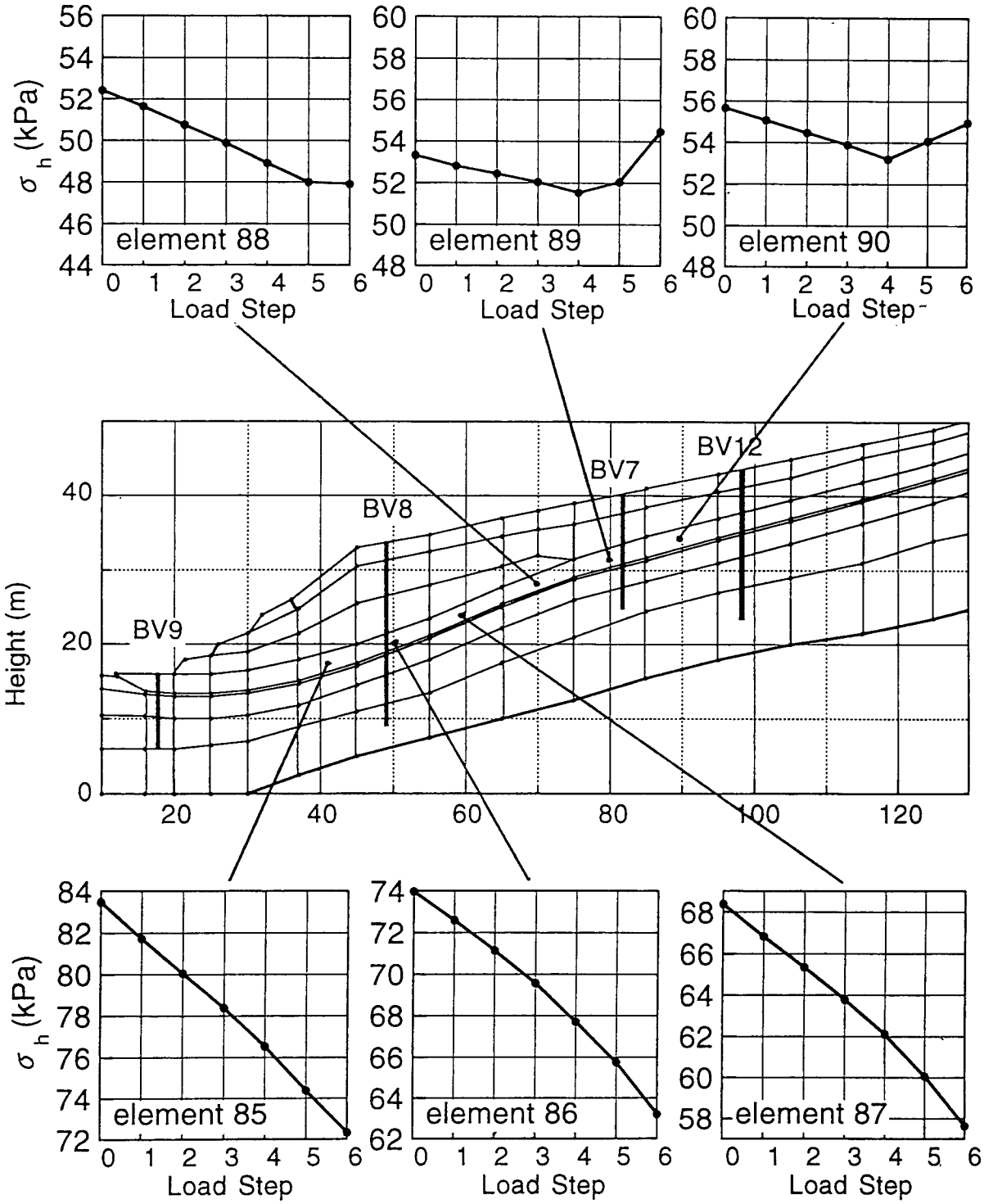

Fig. 53. Variation in the horizontal earth pressure with load step of FEM analysis.

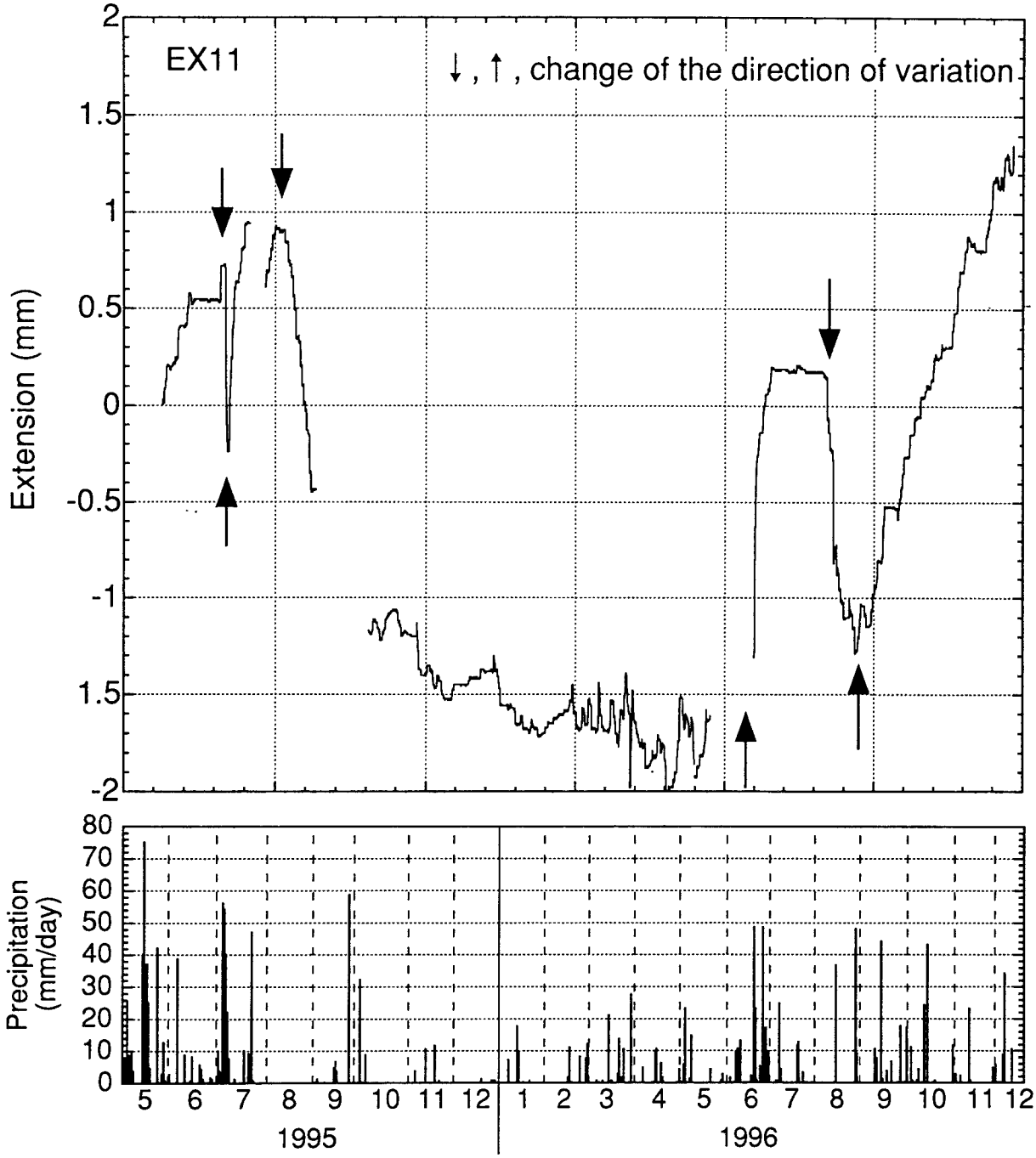

Fig. 54. Change of the direction of variation in EX 11 in the Todoroki landslide.

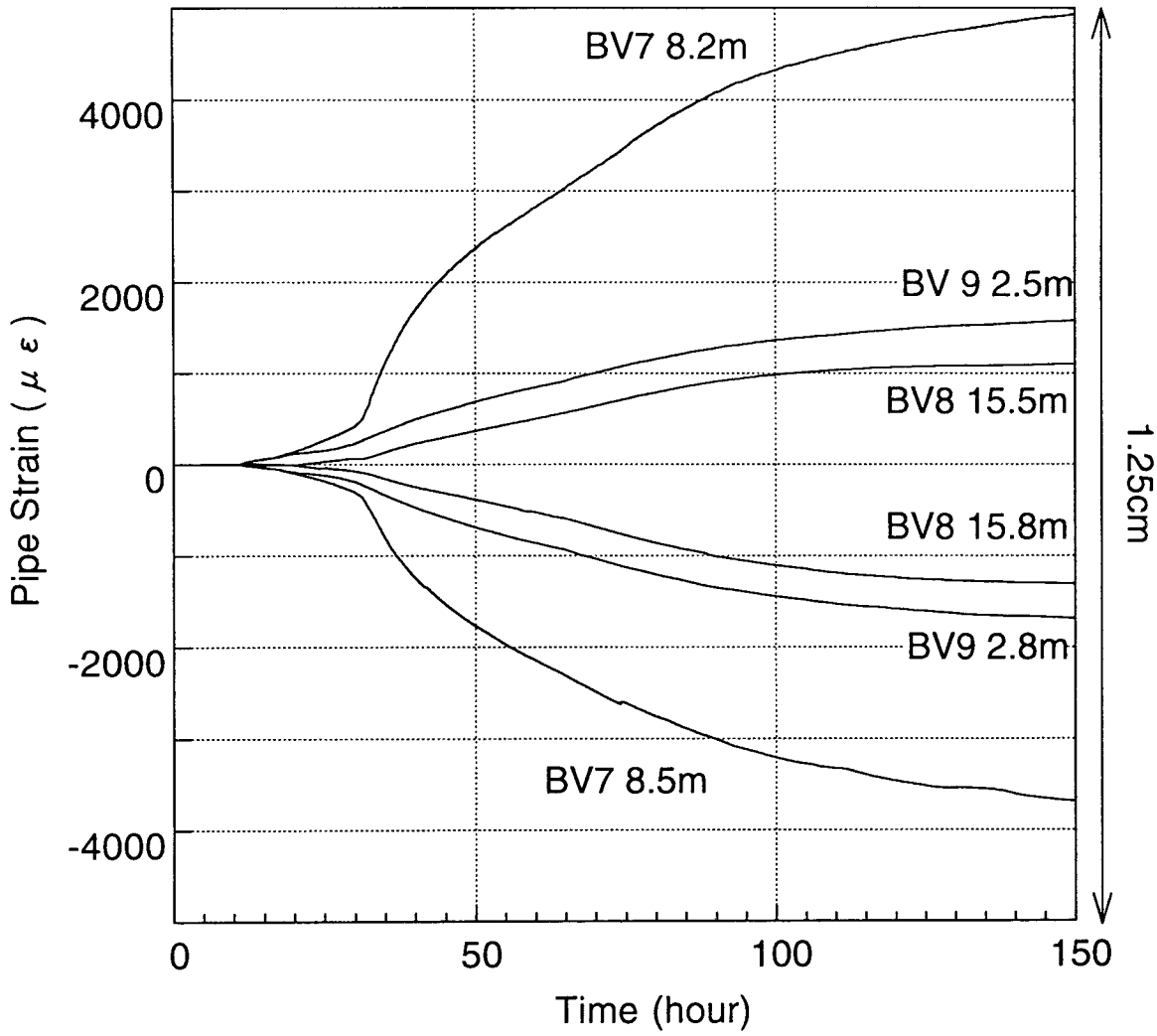

Fig. 55. Pipe strain at the slip surface observed during Event 1.

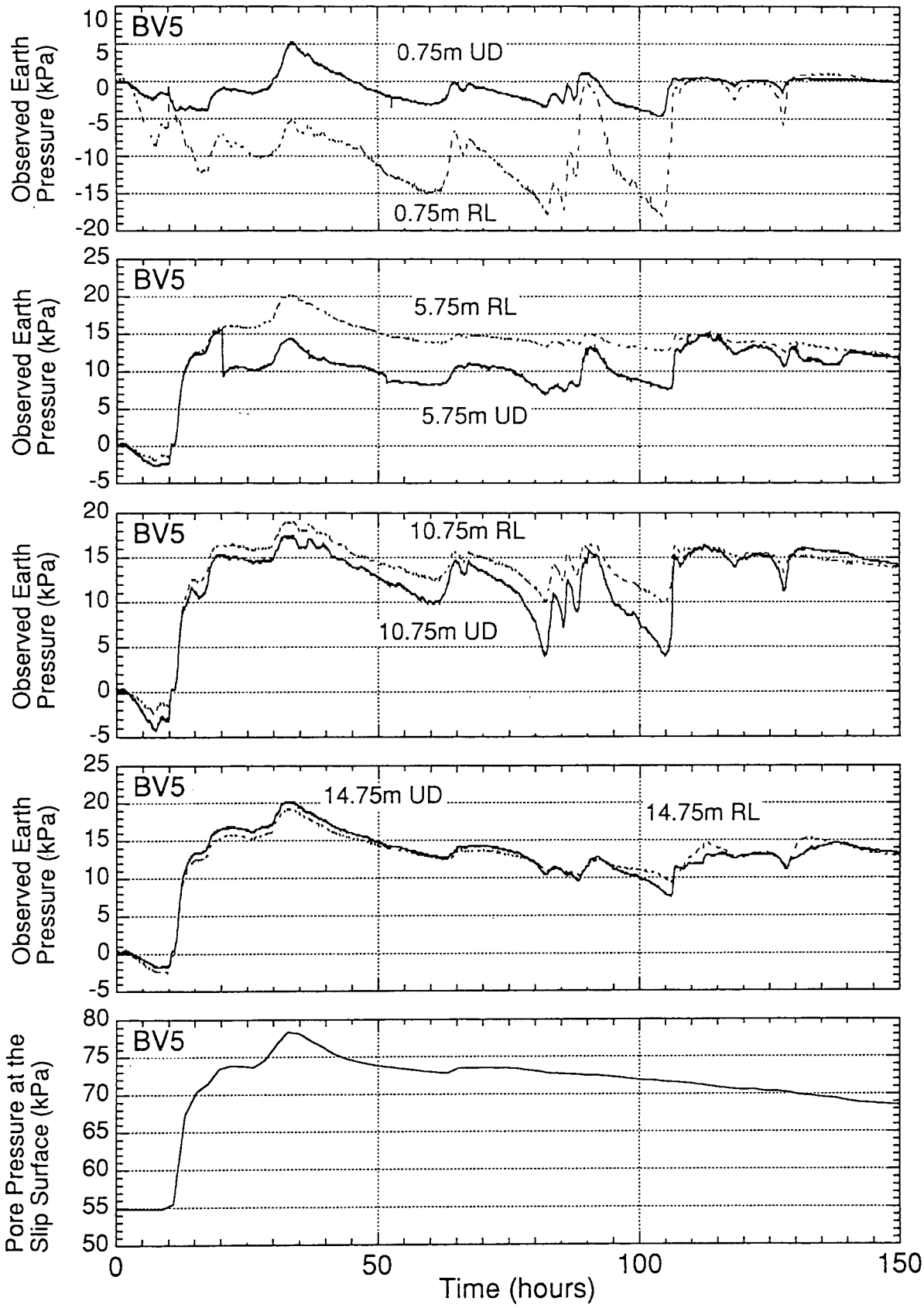

Appendix 1 (four pages): Observed earth pressures for BV 5 to 9 in Event 1 and pore pressure at the slip surface (those for BV 4 are shown in Fig. 34).

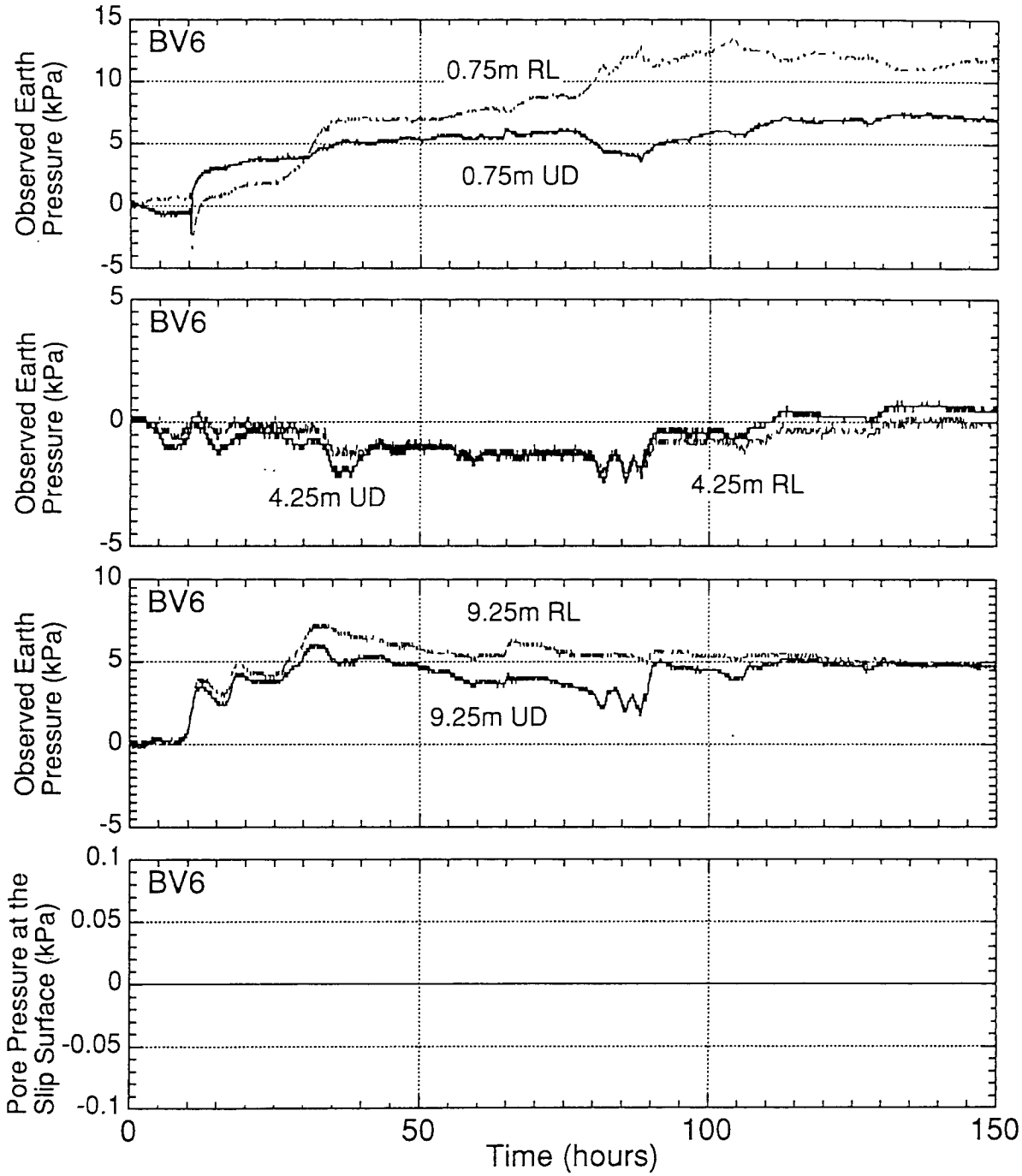
BV6
0.75m RL
0.75m UD
Observed Earth Pressure (kPa)
15
10
5
0
-5
BV6
4.25m UD
4.25m RL
Observed Earth Pressure (kPa)
5
0
-5
BV6
9.25m RL
9.25m UD
Observed Earth Pressure (kPa)
10
5
0
-5
BV6
Pore Pressure at the Slip Surface (kPa)
0.1
0.05
0
-0.05
-0.1
0
50
100
150
Time (hours)

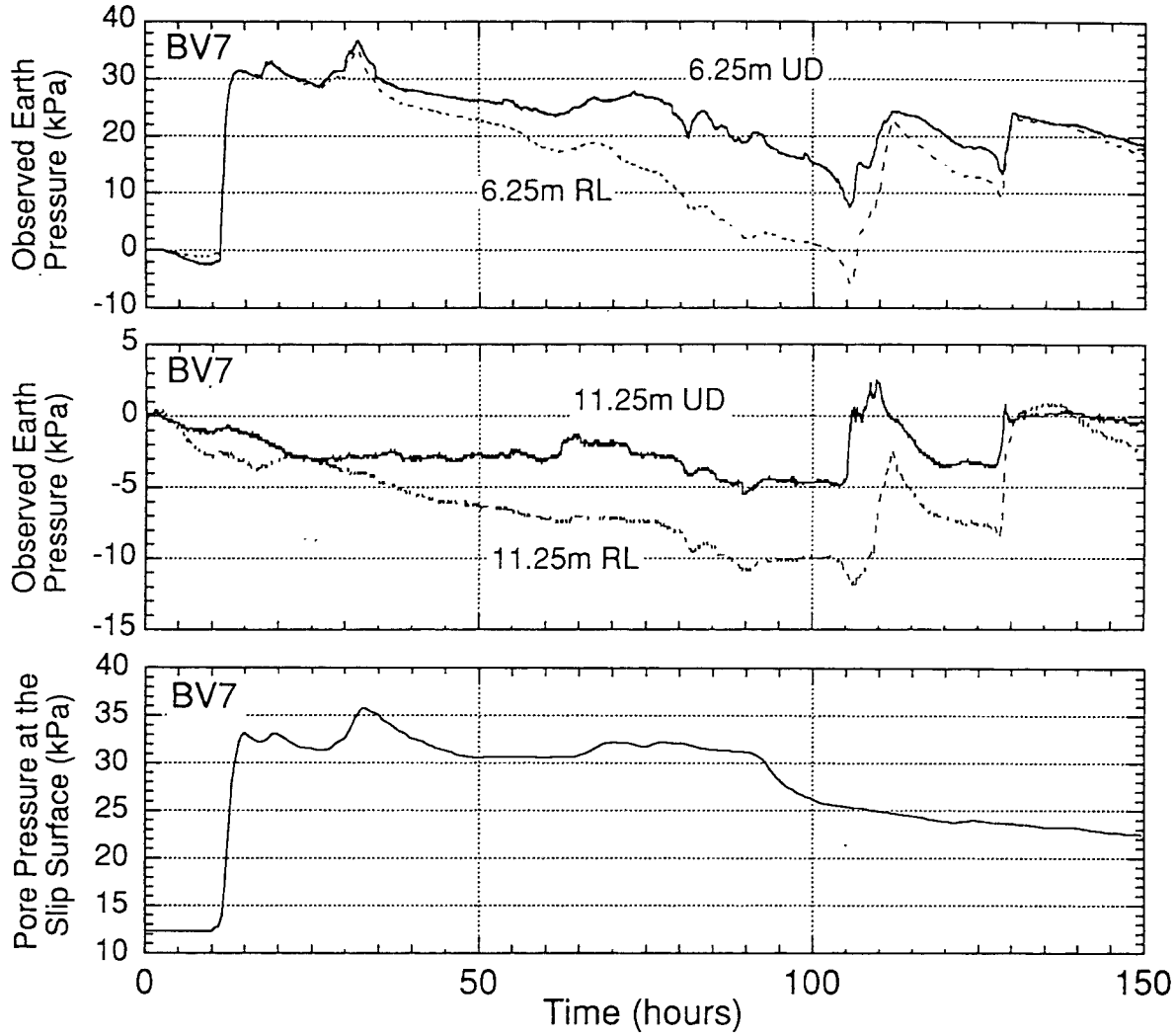
BV7
6.25m UD
6.25m RL
Observed Earth Pressure (kPa)
40
30
20
10
0
-10
BV7
11.25m UD
11.25m RL
Observed Earth Pressure (kPa)
5
0
-5
-10
-15
BV7
Pore Pressure at the Slip Surface (kPa)
40
35
30
25
20
15
10
0
50
100
150
Time (hours)

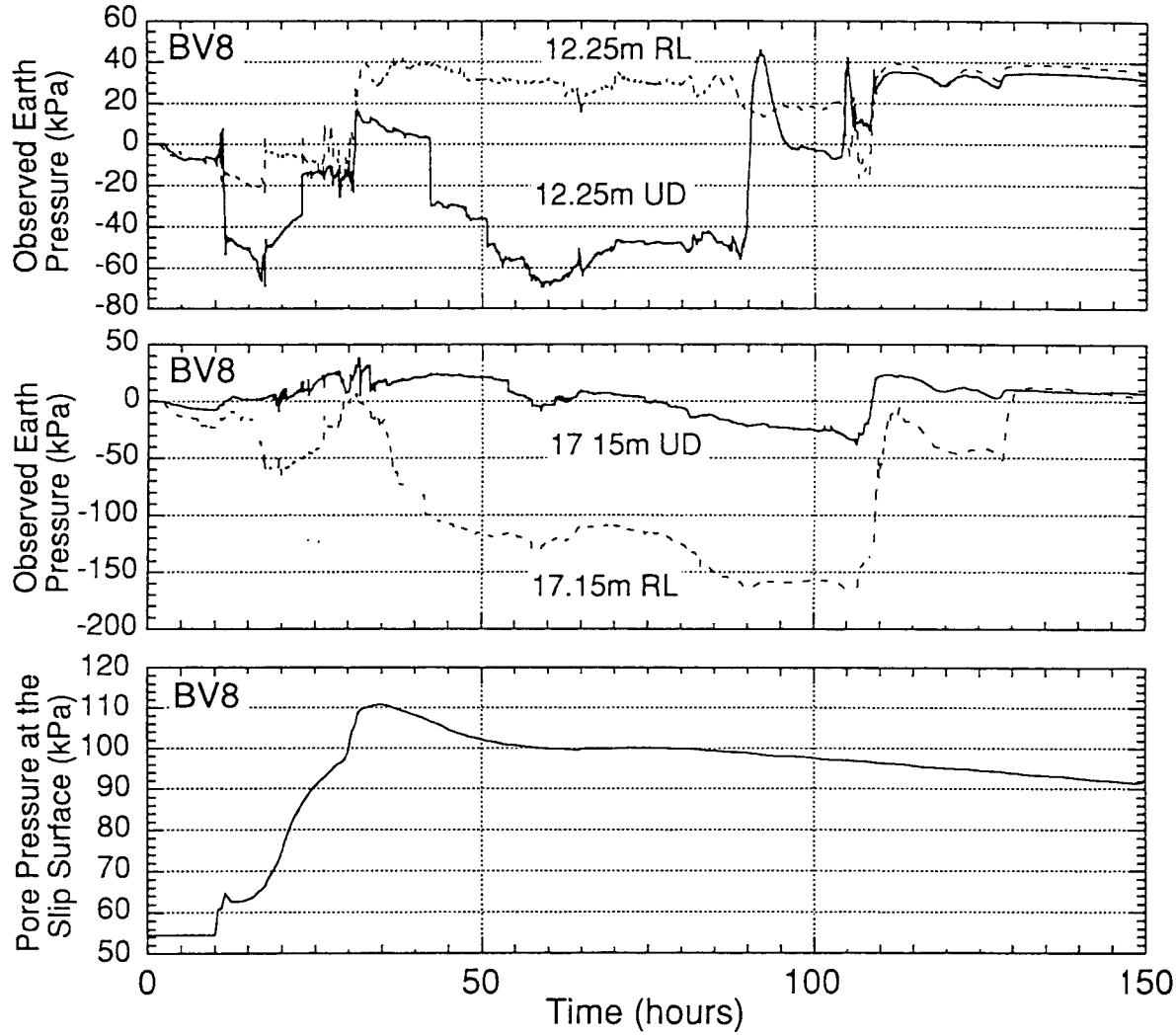
BV8
12.25m RL
12.25m UD
Observed Earth Pressure (kPa)
60
40
20
0
-20
-40
-60
-80
BV8
17 15m UD
17.15m RL
Observed Earth Pressure (kPa)
50
0
-50
-100
-150
-200
BV8
Pore Pressure at the Slip Surface (kPa)
120
110
100
90
80
70
60
50
0
50
100
150
Time (hours)

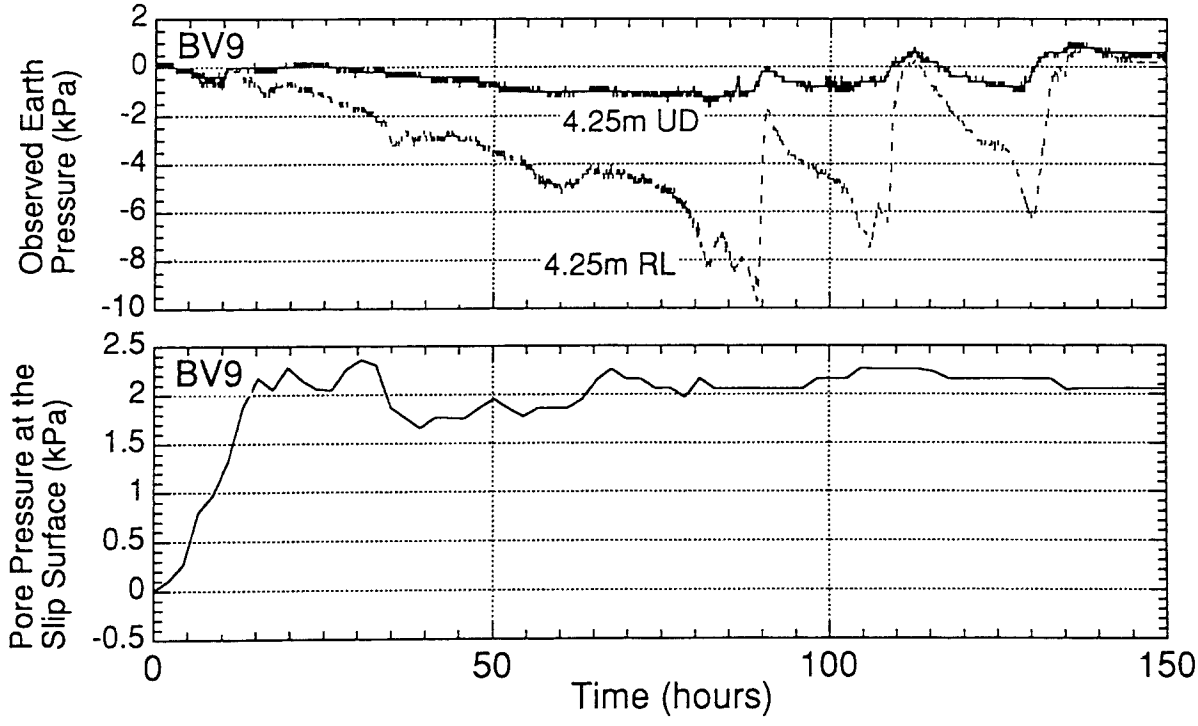
BV9
4.25m UD
4.25m RL
Observed Earth Pressure (kPa)
2
0
-2
-4
-6
-8
-10
BV9
Pore Pressure at the Slip Surface (kPa)
2.5
2
1.5
1
0.5
0
-0.5
0
50
100
150
Time (hours)

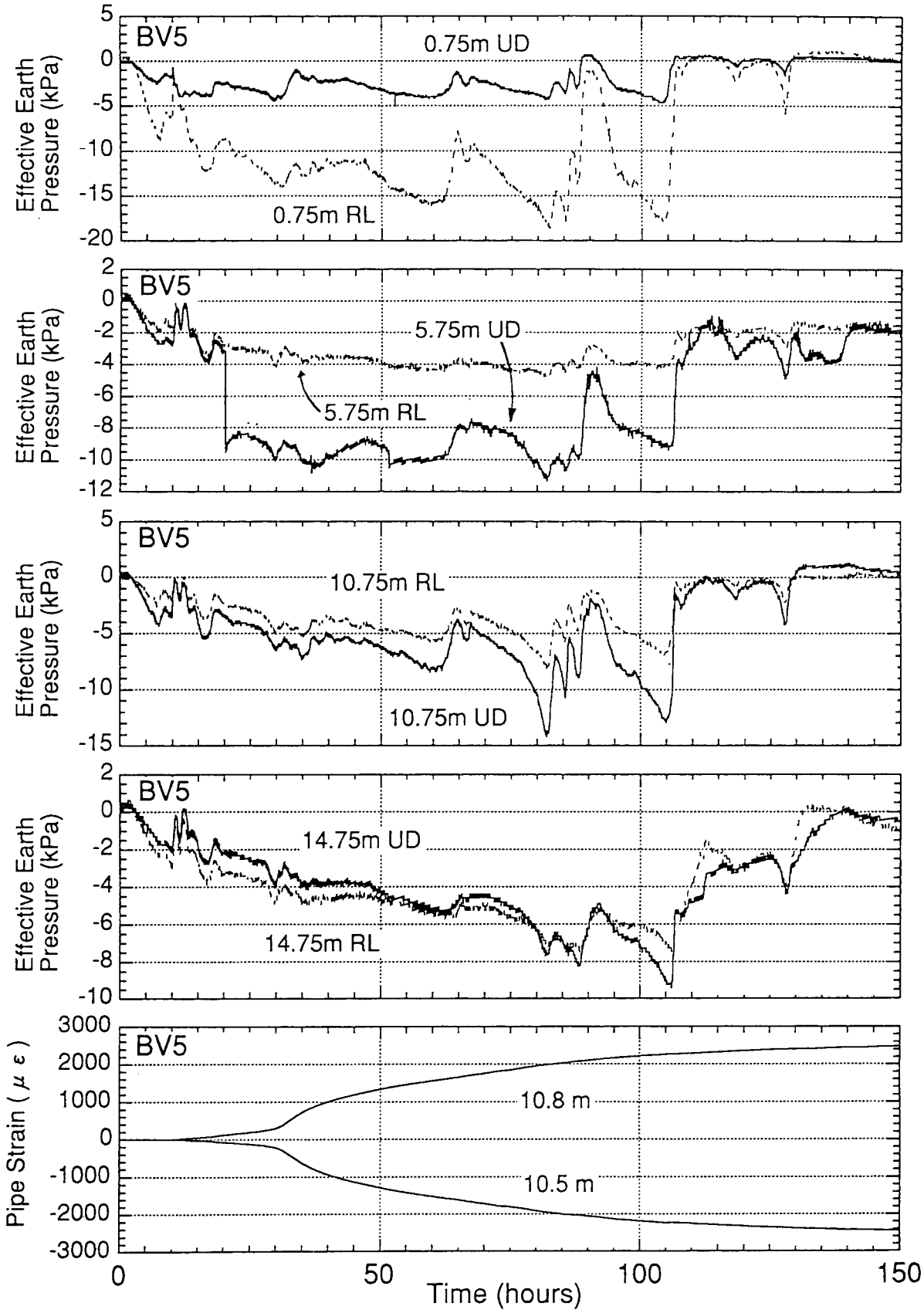

Appendix 2 (four pages): Calculated effective earth pressures for BV 5 to 9 in Event 1 and pipe strains at the slip surface (those for BV 4 are shown in Fig. 34).

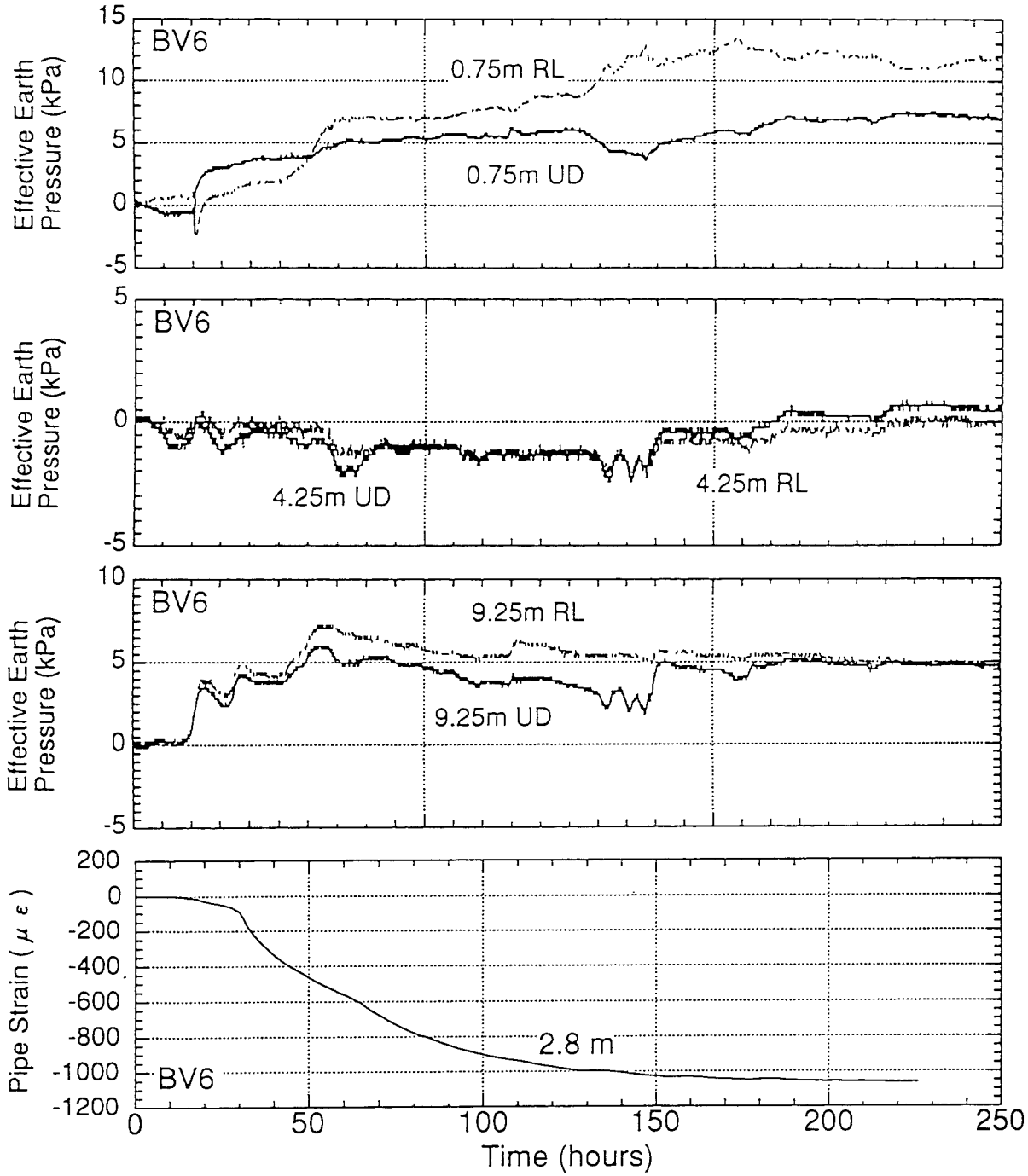
BV6
0.75m RL
0.75m UD
Effective Earth Pressure (kPa)
15
10
5
0
-5
BV6
4.25m UD
4.25m RL
Effective Earth Pressure (kPa)
5
0
-5
BV6
9.25m RL
9.25m UD
Effective Earth Pressure (kPa)
10
5
0
-5
BV6
2.8 m
Pipe Strain (μ ε)
200
0
-200
-400
-600
-800
-1000
-1200
0
50
100
150
200
250
Time (hours)

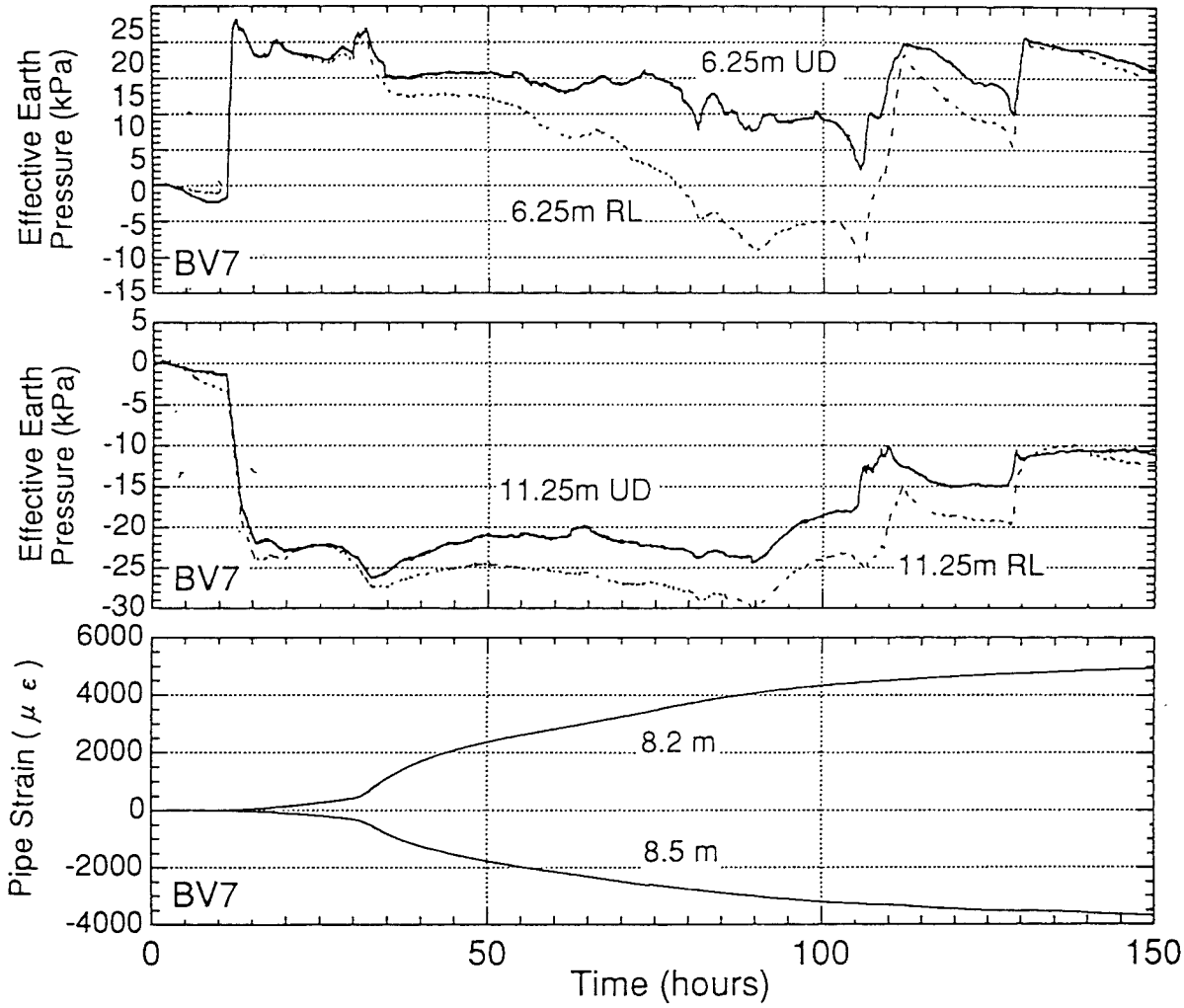
Effective Earth Pressure (kPa)
25
20
15
10
5
0
-5
-10
-15
6.25m UD
6.25m RL
BV7
Effective Earth Pressure (kPa)
5
0
-5
-10
-15
-20
-25
-30
11.25m UD
11.25m RL
BV7
Pipe Strain (μ ε)
6000
4000
2000
0
-2000
-4000
8.2 m
8.5 m
BV7
0
50
100
150
Time (hours)

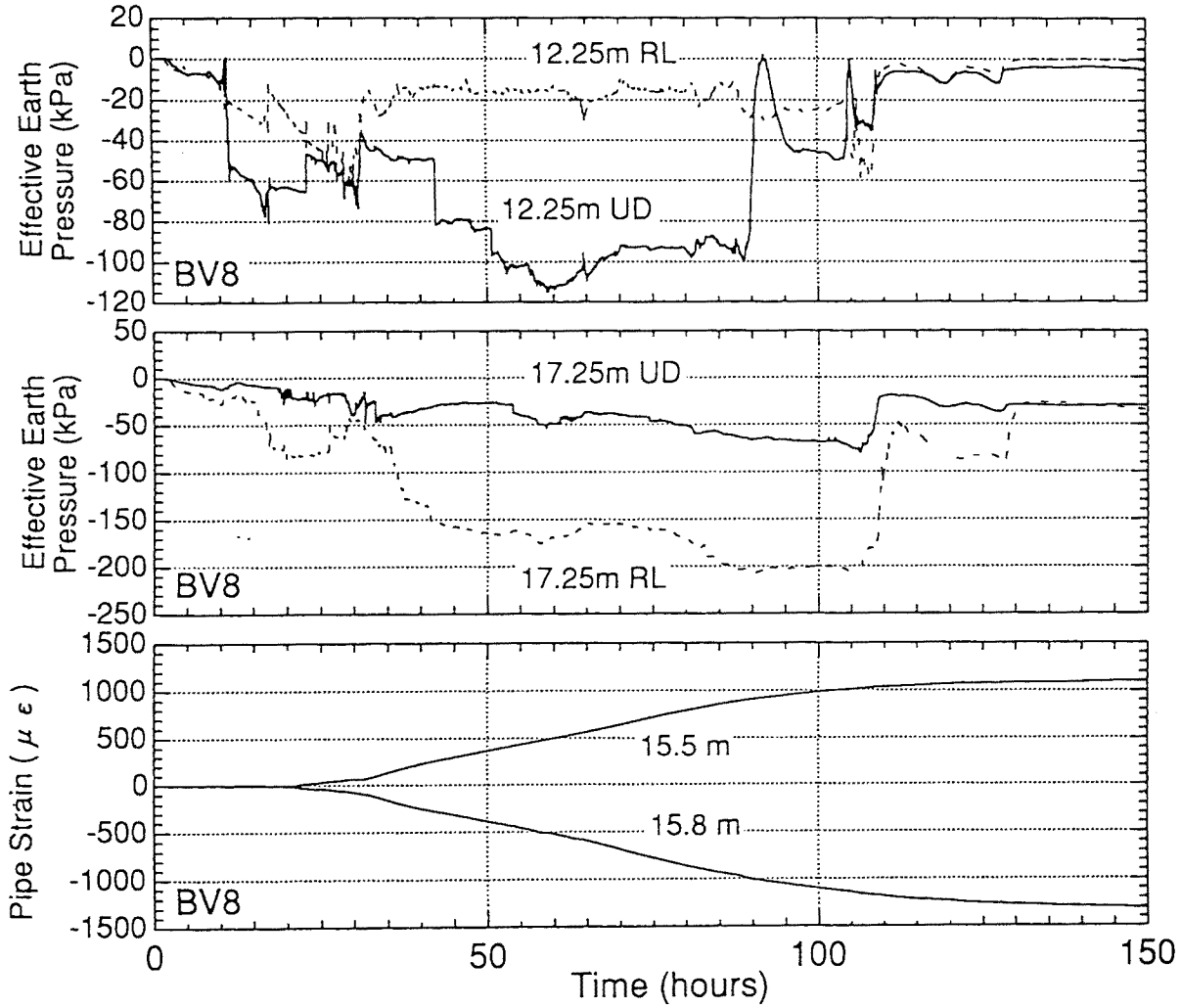
Effective Earth Pressure (kPa)
20
0
-20
-40
-60
-80
-100
-120
12.25m RL
12.25m UD
BV8
Effective Earth Pressure (kPa)
50
0
-50
-100
-150
-200
-250
17.25m UD
17.25m RL
BV8
Pipe Strain (μ ε)
1500
1000
500
0
-500
-1000
-1500
15.5 m
15.8 m
BV8
0
50
100
150
Time (hours)

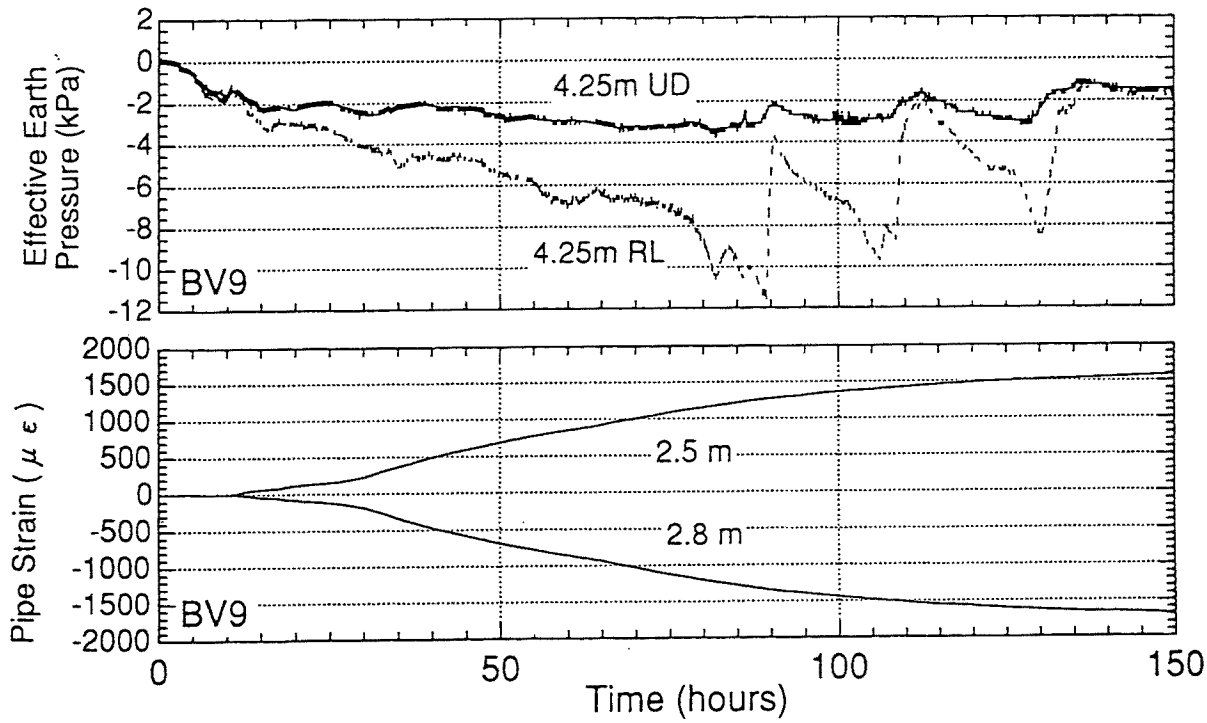
Effective Earth Pressure (kPa)
2
0
-2
-4
-6
-8
-10
-12
4.25m UD
4.25m RL
BV9
Pipe Strain (μ ε)
2000
1500
1000
500
0
-500
-1000
-1500
-2000
2.5 m
2.8 m
BV9
0
50
100
150
Time (hours)